U.S. DEPARTMENT OF THE INTERIOR

GEOLOGICAL SURVEY

PROGRESS OF STUDIES ON THE IMPACT OF HURRICANE HUGO ON THE COASTAL RESOURCES OF PUERTO RICO

edited by

William C. Schwab[1] and Rafael W. Rodriguez[2]

U. S. Geological Survey Open-File Report 92-717

(1992)

[1] U. S. Geological Survey, Woods Hole Massachusetts

[2] U. S. Geological Survey, San Juan, Puerto Rico

TABLE OF CONTENTS

Any use of trade names or companies is for descriptive purposes only and does not imply endorsement by the U.S. Geological Survey.

EXECUTIVE SUMMARY

Hurricane Hugo struck the Commonwealth of Puerto Rico on September 18, 1989, causing extensive damage to the coast of Puerto Rico. The U.S. Geological Survey (USGS), Office of Energy and Marine Geology, Atlantic Branch of Marine Geology is coordinating studies of the impact of major storm events on the coastal resources of Puerto Rico. Field studies were conducted to assess the effects of Hugo on three critical coastal resources: beaches, offshore sand deposits, and coral reefs. These studies are being conducted, when possible, in selected areas where sufficient data on pre-storm conditions exist to compare to post-storm observations. The four studies are:

1. Shoreline Erosion/Beach Recovery — This investigation was designed to quantify the changes in shoreline location along selected portions of the north and east coast of Puerto Rico using aerial photographs taken before and after the storm and to document the impact of Hugo on recreational beaches, particularly in the San Juan area, where baseline data is available from years of beach-profile measurements made prior to the storm.

2. Offshore Sand Deposit — This investigation was implemented to document the impact of HUGO on Escollo de Arenas, a 90 million m^3 offshore sand deposit off Vieques Island, that was observed to have been modified during a post-storm aerial reconnaissance survey.

3. Insular Shelf Mapping — This investigation was designed to document the effect of major storm events on the insular shelf in order to assess movement of the nearshore sand supply and the fate of sand eroded from the shoreline. The investigation used a segment of the northern insular shelf off the town of Luquillo as the study area.

4. Coral Reefs — This study was designed to document the effect of Hugo on coral reefs which are sources of carbonate sand production, buffers to storm-wave induced coastal erosion, sites of high biologic productivity, and a tourist attraction. The investigation concentrated on reef complexes around the island of Culebra, off the northeast coast of Puerto Rico.

Key results to date are:

Shoreline/erosion beach recovery

* Long-term accretionary trends have occurred within embayments between headlands in the San Juan area (areas were there are few or no engineering structures impinging the littoral zone), whereas quasi-stable to slightly erosional trends have occurred at headlands. Thus, there is an apparent possible long-term trend of shoreline straightening through headland erosion and embayment infilling.

* During the passage of Hurricane Hugo, damage to beaches occurred as a result of elevated water levels through a combination of storm surge, wave setup, and wave

swash. The typical beach profile change was one of a general flattening coincident with erosion of the upper beach combined with deposition on the lower beach; the net effect of Hugo on the sandy beaches appeared to be one of beach face erosion with eroded sediment transported both seaward and landward away from the beachface. In general, the effects of Hurricane Hugo on the sandy beaches in the San Juan area had been an erosional perturbation in the seasonal cycle.

* Post-Hugo changes to the beach profile have included a return to approximately pre-Hugo conditions in many natural localities. However, where engineering structures were extensively damaged because they extend too far seaward, beach recovery has been hindered.

Offshore Sand Deposits

* Preliminary analysis of aerial photographs suggested that the largest known offshore sand and gravel deposit, the Escollo de Arenas, located off Vieques Island, was severely affected by Hugo. However, analysis of closely spaced high-resolution seismic-reflection profiles, sediment cores, and grab samples show that large-scale changes affecting the volume and overall geographic extent of the sand and gravel deposit did not occur.

* Less than 4 percent of the original volume of the Escollo de Arenas deposit was lost during Hugo.

Insular Shelf Mapping

* Detailed sea-floor mapping was conducted over the insular shelf offshore of the town of Luquillo using high-resolution sidescan-sonar, seismic-reflection, photography, and bottom sampling techniques after the passage of Hurricane Hugo.

* Sea-floor structures and textural/compositional sedimentologic trends suggest that regional oceanographic processes result in a net cross-shelf, offshore sediment transport direction during storms such as Hurricane Hugo. However, east-west trending eolianite ridges that outcrop on the sea floor act as natural dams, blocking material removed from the shoreface and form sand deposits up to 20 m thick along the inner boundary of the eolianite ridges.

* Sand eroded from the beach front appears to move offshore. Offshore pathways can be documented using sidescan-sonar imaging techniques.

Coral Reefs

* Divers examined and photographed reefs around Culebra Island affected by Hurricane Hugo, drilled deep cores to determine the geologic history of reefs and took cores from individual living corals to study growth rate and evaluate the effect of Hugo and previous storms.

* Reefs on the east and southeast (windward) side of Culebra Island were devastated by Hugo, whereas only minor damage to the coral reefs along the west (lee) side of

Culebra was found.

* In spite of the devastation, the reefs on the east side of Culebra are showing signs of a healthy regrowth.

INTRODUCTION

William C. Schwab
(U.S. Geological Survey, Woods Hole,Massachusetts)

The U.S. Geological Survey (USGS), in cooperation with Duke University, is conducting studies in Puerto Rico designed to assess the impact of major storm events on coastal resources and coastal environments. Hurricane Hugo struck the Commonwealth of Puerto Rico on September 18, 1989, causing extensive damage along the coast. Preliminary studies of coastal erosion began immediately after Hugo whereas more comprehensive studies were initiated in October, 1990, upon the acquisition of necessary funding. Objectives of the studies are to: 1) document and assess the impact and subsequent recovery of selected critical coastal resources of Puerto Rico affected by Hugo, and 2) develop a better understanding of the impact of infrequent major storm events, such as hurricanes, on the coast of Puerto Rico.

The shallow marine shelf surrounding Puerto Rico has an area of about 3,500 km^2 within the 200 m isobath, or nearly two-thirds that of the land area of the Commonwealth. On an island where more than 85 percent of the population lives within 7 km of the sea and is dependent on the tourism that its beaches and coral reefs attract, it is necessary that high-quality scientific data be available to help formulate public policy regarding residential and commercial rebuilding along the coast, beach replenishment, and future utilization of marine resources. Offshore mineral resources, especially sand, gravel, and limestone for construction and beach replenishment, are of major importance because of their potential for low-cost development and because suitable onshore sources have been depleted. Prior to the investigations described in this report, it was generally unknown where the sand eroded from the coast by Hugo (or other major storms) had gone, if the material was recoverable, if the damages to the coast and offshore coral reefs are permanent or likely to recover on their own, or what effect Hugo has had on previously identified offshore sand reservoirs.

A limited series of field studies were conducted following Hugo to assess the effects of major storm events on three critical coastal resources: beaches, offshore sand deposits, and coral reefs. The four studies (Fig. 1) were:

1. Shoreline erosion/beach recovery — The scope of this investigation was to quantify the changes in shoreline location along selected portions of the north and east coast of Puerto Rico using aerial photographs taken before and after Hugo. In addition, this study was designed to quantitatively document the impact of Hugo on recreational beaches, particularly in the San Juan area, where baseline data was available from years of beach-profile measurements made prior to the storm.

2. Offshore Sand Deposits — The scope of this study was to document the impact of Hugo on the Escollo de Arenas, a 90 million m^3 sand and gravel deposit, that was observed during a post-storm aerial reconnaissance survey to have been modified and eroded.

3. Insular Shelf Mapping — This investigation was designed to document the effect of major storm events on the shallow insular shelf off the town of Luquillo in order to assess the nearshore sand supply and the fate of the sand eroded from the shoreline.

4. Coral Reefs — This study was designed to document the effects of Hugo on coral reefs using the island of Culebra as the study area.

This report provides a brief summary of the objectives, rationale, fieldwork, results to date, and future plans for each study component.

Fig. 1 Map of Puerto Rico showing the location of the study areas used to assess the impact of Hurricane Hugo on coastal resources.

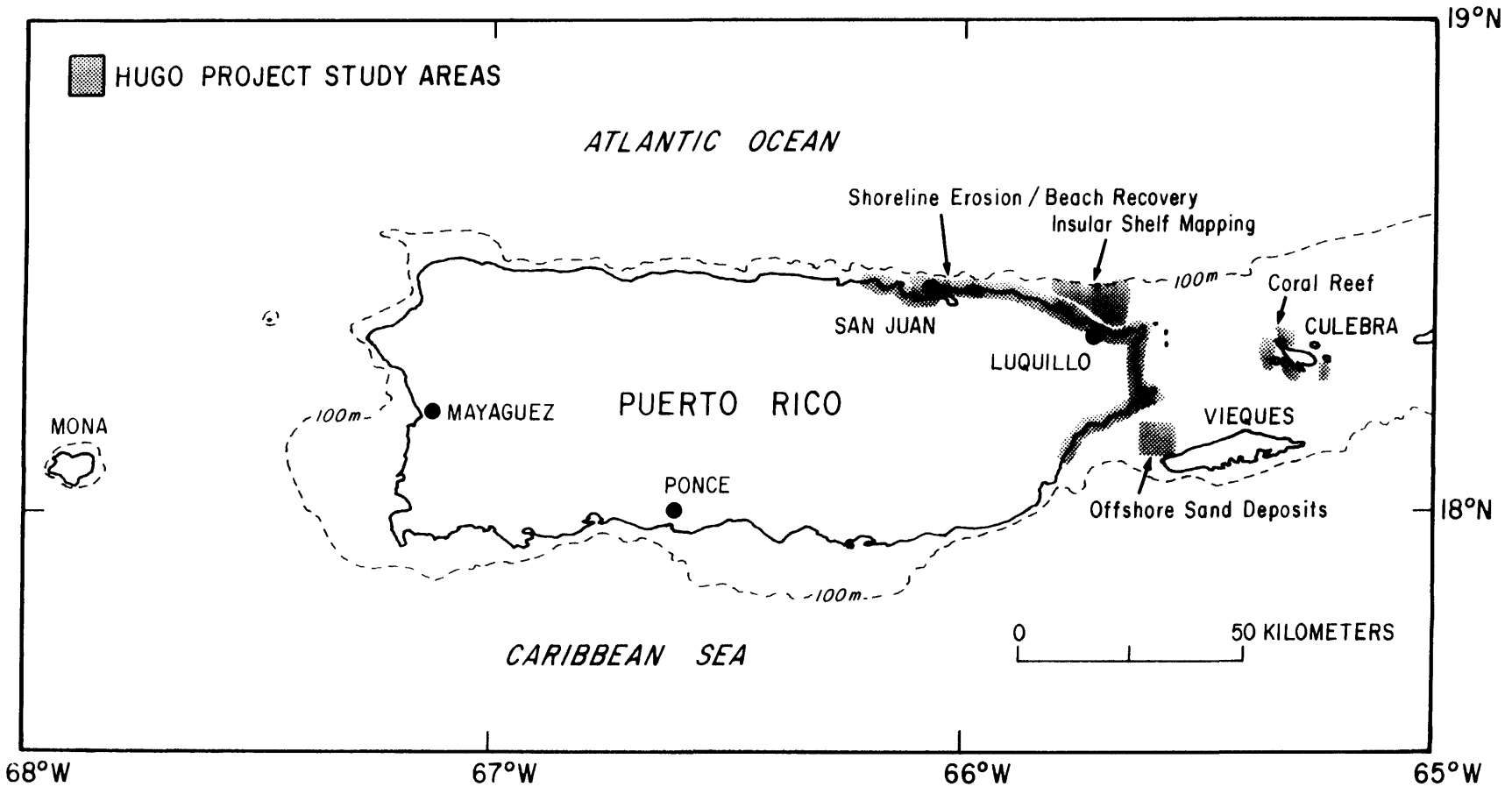
HUGO PROJECT STUDY AREAS
ATLANTIC OCEAN
Shoreline Erosion / Beach Recovery
Insular Shelf Mapping
100m
Coral Reef
CULEBRA
SAN JUAN
LUQUILLO
MAYAGUEZ
PUERTO RICO
VIEQUES
MONA
PONCE
Offshore Sand Deposits
100m
CARIBBEAN SEA
0
50 KILOMETERS
19°N
18°N
68°W
67°W
66°W
65°W

STUDY COMPONENTS

HURRICANE HUGO: A DESCRIPTION OF THE STORM

Rafael W. Rodriguez, Richard M.T. Webb
(U.S. Geological Survey, San Juan, Puerto Rico)
David M. Bush
(Duke University, Durham, North Carolina)

Hurricane Hugo approached the U.S. Virgin Islands on 17 September 1989 as a category-four hurricane with maximum sustained winds of 225 km/hr (140 mph) and a minimum sea-level pressure of 934 mb (NOAA, 1990). The eye of Hurricane Hugo passed directly over St. Croix in the U.S. Virgin Islands and continued travelling in a WNW direction. During the morning of September 18th, Hugo passed over the islands of Vieques and Culebra, and over the eastern and northeastern tip of Puerto Rico (Fig. 1). Radar observations and satellite images revealed that the west side of the eyewall moved over land while the eastern side of the eye remained over water. Maximum intensity in the San Juan metropolitan area was felt at approximately 10:30 a.m (Fig. 2). By noon, barely six hours after hitting Vieques, Hugo was approximately 30 km north of San Juan, with maximum sustained surface winds reduced to 123 km/hr (77 mph) with gusts to 147 km/hr (92 mph) and minimum sea level pressure of 957 mb (NOAA, 1990). The lowest surface pressure recorded in Puerto Rico during Hugo was 946 mb at Ceiba (NOAA, 1990).

Hurricane Hugo caused tremendous damage to development and infrastructure of eastern Puerto Rico. Over 80 percent of wooden structures were destroyed in Culebra and Vieques (FEMA, 1989). Thirty-thousand people were left homeless and property damage exceeded $1 billion. Thousands of boats were destroyed. Boat owners as far away as San Juan and St Thomas took their vessels to Ensenada Honda, a legendary "hurricane-proof" bay in Culebra (Fig. 1). Sustained southerly winds of 193 km/hr (121 mph) with gusts to 240 km/hr (150 mph) created a wave setup in Ensenada Honda estimated at greater than 4 m (Golden, 1990). Vessels, some in excess of 20 m in length, were carried up and over the coastal road with several sailboats wedged under a bridge (Fig. 3).

At approximately 10:30 a.m local time, the hurricane was reaching its maximum intensity in San Juan. In San Juan Bay (Fig. 1), a 0.73-m-high storm surge developed coincident with the predicted astronomical high tide of 0.61 m (Fig. 4) resulting in a water level of 1.34 m above Mean Low Water (MLW); the previous historical high of 0.73 m above MLW occurred in November of 1982 (NOAA, 1989). The SLOSH models hindcast a water level between 1.0 and 1.4 m above MLW for northern San Juan Bay.

Heavy rainfall fell in limited areas over the northeast part of the island, and Hugo passed over the island very quickly; Hugo was considered a "dry hurricane" (Fig. 5). Therefore, minimal flooding occurred away from the coastal zone. Rain gauges in Puerto Rico and the U.S. Virgin Islands averaged between 12 and 23 cm (5-9 in) of rainfall with a maximum of 34.41 cm (13.55 in) in the mountains of northeastern Puerto Rico (NOAA, 1990).

The combination of storm-induced waves and a record-level sea level surge caused severe to moderate erosion of the beaches in the San Juan area (Richmond and others, this report), modification of a large offshore sand and gravel deposit off Vieques Island

(DeLorey and others, this report), and devastated coral communities in Culebra Island (Shinn and others, this report) while inflicting minor damage to the corals of Vieques Passage (Rodriguez and others, 1993). Most of the beaches have now returned to their normal seasonally fluctuating behavior. New berms have formed with dimensions similar to those observed before the storm; the degree of protection to backbeach areas from moderate-energy (1 to 3 m swell) events is much the same as it was before Hugo. Considering the intensity of Hurricane Hugo, the impact on the coastal resources of the island was surprisingly limited.

Fig. 1. Index map of Puerto Rico showing the path of the eye of Hurricane Hugo on 17 September 1989.

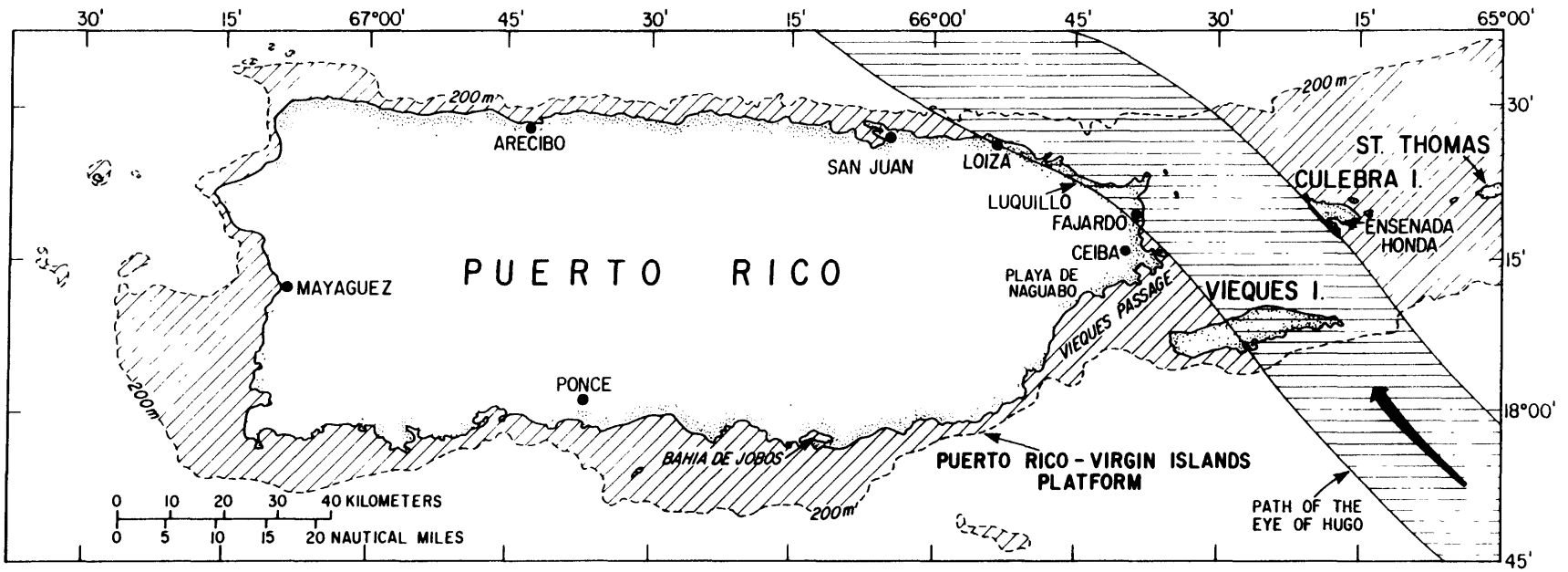
30'
15'
67°00'
45'
30'
15'
66°00'
45'
30'
15'
65°00'
30'
15'
18°00'
45'
200m
ARECIBO
SAN JUAN
LOIZA
LUQUILLO
FAJARDO
CEIBA
PLAYA DE NAGUABO
ST. THOMAS
CULEBRA I.
ENSENADA HONDA
VIEQUES I.
VIEQUES PASSAGE
PUERTO RICO
MAYAGUEZ
PONCE
BAHIA DE JOBOS
PUERTO RICO - VIRGIN ISLANDS PLATFORM
PATH OF THE EYE OF HUGO
0 10 20 30 40 KILOMETERS
0 5 10 15 20 NAUTICAL MILES

Fig. 2. Wind flow patterns for eastern Puerto Rico during (A) approach, (B) landfall, and (C) exit of Hurricane Hugo (modified from Bush, 1991). Short arrows with numbers are wind direction and speed (mph) measured on 18 September 1989 at the National Weather Service Forecast Office at the San Juan International Airport (denoted by the letter "S") and at the city of Ceiba on the Roosevelt Roads Naval Station (denoted by the letter "C") (data from Golden, 1990). Long arrows are generalized wind flow patterns for northern hemisphere cyclones. Times are Atlantic Standard Time, equals Eastern Daylight Time, add four hours for Universal Coordinated Time (UTC, GMT).

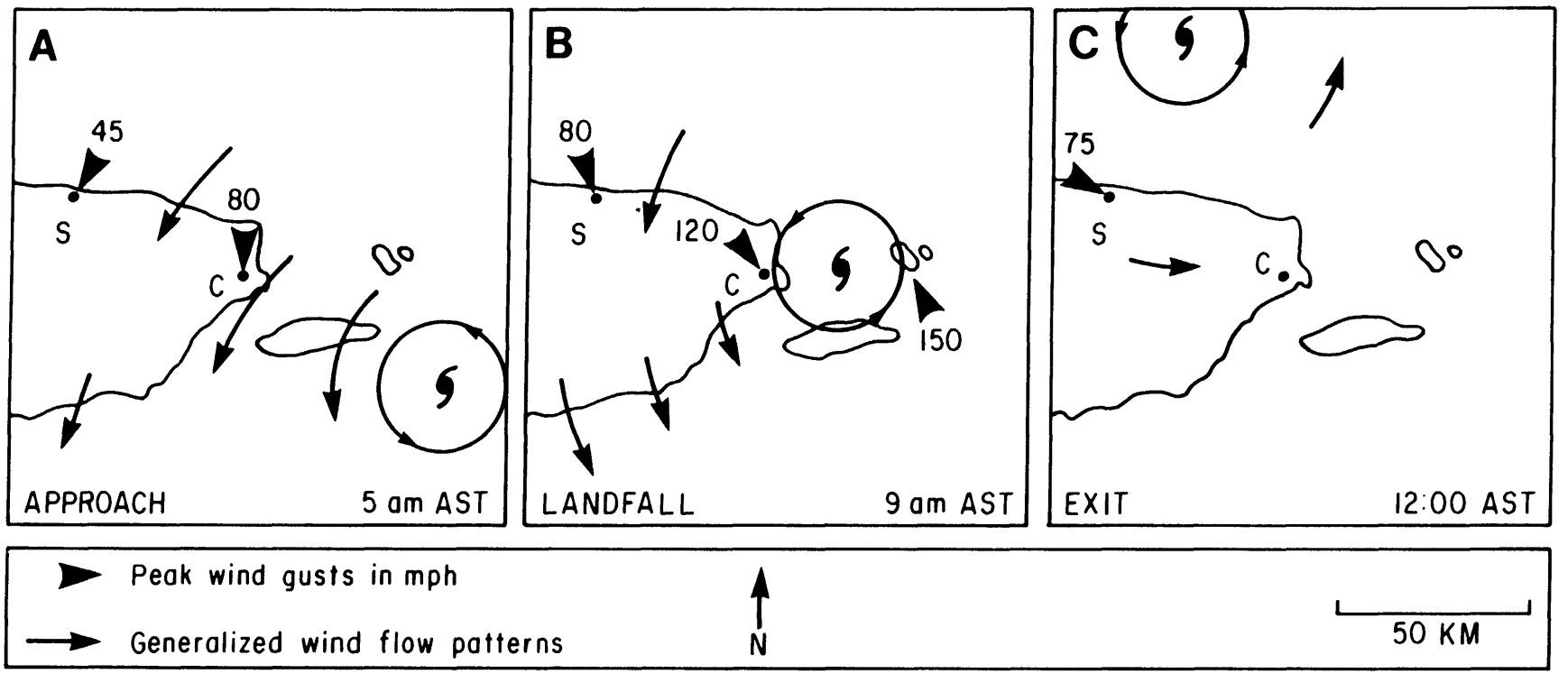
A
45
80
S
C
APPROACH
5 am AST
B
80
S
120
C
150
LANDFALL
9 am AST
C
75
S
C
EXIT
12:00 AST
Peak wind gusts in mph
Generalized wind flow patterns
N
50 KM

Fig. 3. Aerial photograph of Ensenada Honda, Culebra, Puerto Rico taken on October 1989. Strong winds combined with the storm surge jammed four sailboats under the bridge. Approximately 100 vessels out of 300 that took shelter in the "hurricane proof" harbor sank. The distance across the bottom of this photograph is approximately 340 m. North is toward the top of the photograph.


ENSENADA HONDA,
CULEBRA

Fig. 4. Hourly water levels at La Puntilla in San Juan Bay over three days (NOAA, 1989). The three curves shown are : observed water level (dashed line); predicted astronomical tide (dotted line); and the difference between the observed water level and the predicted astronomical tide, which is the storm surge (solid line).

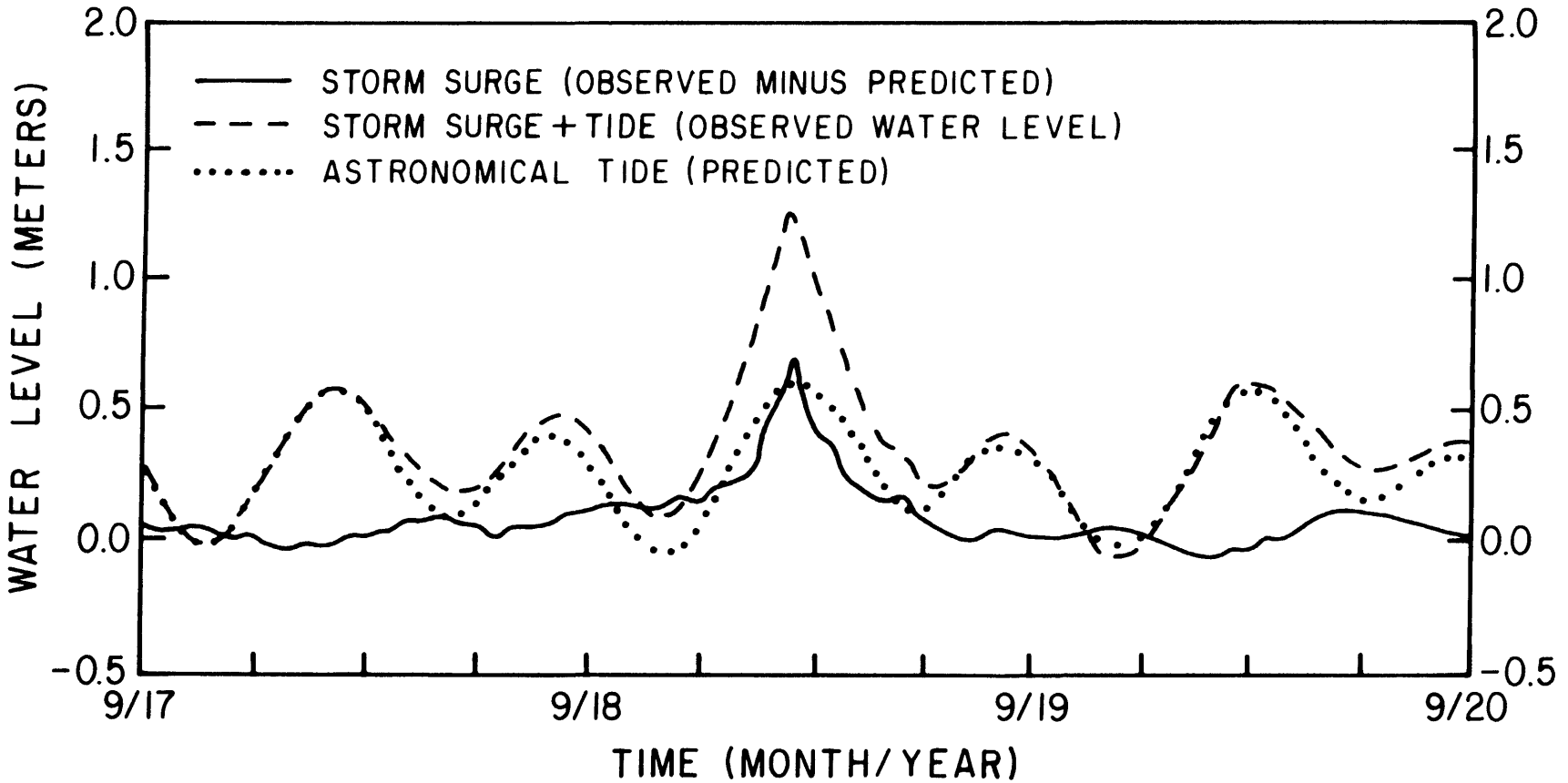
STORM SURGE (OBSERVED MINUS PREDICTED)
STORM SURGE + TIDE (OBSERVED WATER LEVEL)
ASTRONOMICAL TIDE (PREDICTED)
WATER LEVEL (METERS)
2.0
1.5
1.0
0.5
0.0
-0.5
9/17
9/18
9/19
9/20
TIME (MONTH/YEAR)

Fig. 5. Rainfall levels in centimeters associated with Hurricane Hugo (NOAA, 1990).

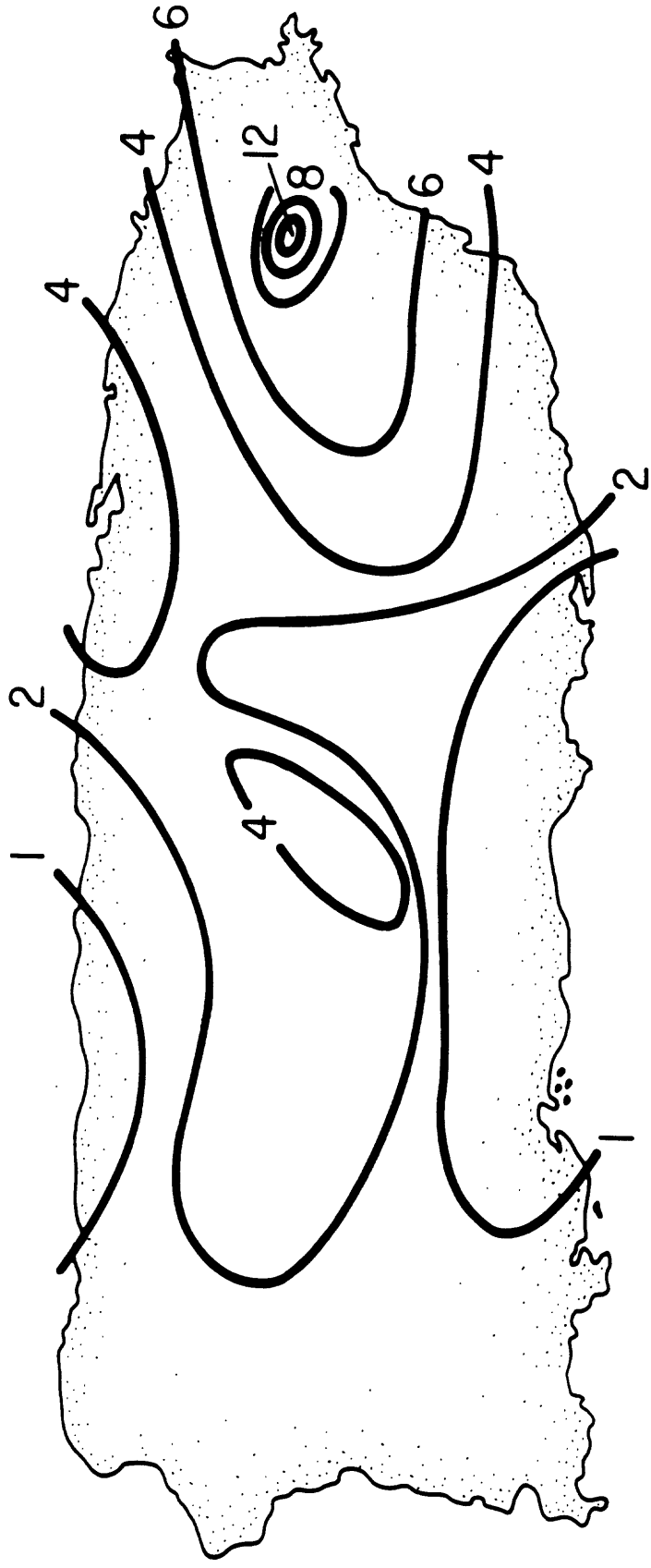
6
4
12
8
6
4
4
2
2
4
1
1

EFFECTS OF HURRICANE HUGO ON THE GREATER SAN JUAN SHORELINE

HISTORICAL SHORELINE ANALYSIS

Bruce R. Richmond
(U.S. Geological Survey, Menlo Park, California)
E. Robert Thieler
(Duke University, Durham, North Carolina)
William W. Danforth
(U.S. Geological Survey, Woods Hole, Massachusetts)

OBJECTIVE

Historical vertical aerial photographs of the Puerto Rico shoreline were examined for the purpose of delineating shoreline change over approximately the last 50 years.

RATIONALE

In order to fully appreciate the effects of a major storm on a shoreline, it is desirable to have historical information on the direction and rate of shoreline change (or stability). This background information provides valuable insights into the longer term stability of a section of coast. This information is invaluable in linking recent monitoring efforts with shoreline history.

FIELDWORK

Digital shoreline position data were produced from historical maps and charts, and available aerial photographs from the period of 1936-1987. Shoreline positions were digitized, corrected for distortions, and transformed into X-Y output for reproduction in a variety of cartographic projections. The methodology describing the production of digital shoreline maps is discussed by Danforth and Thieler (this report).

RESULTS

Several important trends are present in the greater San Juan area (Figs. 1, 2, and 3). These include:

1) Long-term accretionary trends occur within the embayments between headlands such as Balneario Isla Verde, Alambique, and Ocean Park. In general, these are areas where there is little or no man-made structures impinging on the littoral zone.

2) Quasi-stable to slightly erosional trends occur at headlands such as Punta El Medio, Punta Las Marias, and Punta Piedrita.

3) Erosion and/or disappearance of recreational beaches in areas where armoring is extensive, for example, near Condado beach, east of the Cementerio Puerto Rico Memorial, and the east end of Balneario Isla Verde.

4) An apparent possible long-term trend of shoreline straightening through headland erosion and embayment infilling.

Rates of shoreline change for the San Juan study area varied from an erosional high of about -1 m/yr immediately west of Punta Piedrita and -0.7 m/yr east of Punta El Medio to a depositional maximum of nearly +1.9 m/yr west of Alambique. In Alambique (station 15), the 1980 and 1987 shorelines are nearly identical implying most of the accretion occurred between 1964 and 1980. Overall the rates of shoreline position change in the San Juan area are not particularly large and are close to the minimum resolution of the method used to identify the change (minimum resolution is ± 0.5 m/yr).

At some stations, the rate of shoreline retreat experienced during the passage of Hurricane Hugo far exceed the average annual rate of change. For example, shoreline retreat of approximately 10 m (Rodriguez and others, 1993) occurred at station 6 (transect 71), where the average annual rate of accretion is about 0.5 m. However, post-Hugo accretion greatly minimize the apparent long term effects. Rapid shoreline modification that took place during the passage of Hugo appears to have had only a limited effect on the long-term shoreline stability in the area

FUTURE PLANS

Examination of the historical shoreline database will be completed and results be published as a USGS Miscellaneous Field Studies Map series around the entire island in 1993. These data and derivative mapping products will be released on CD ROM in 1994.

Fig. 1. Location of the greater San Juan study area on the north coast of Puerto Rico.

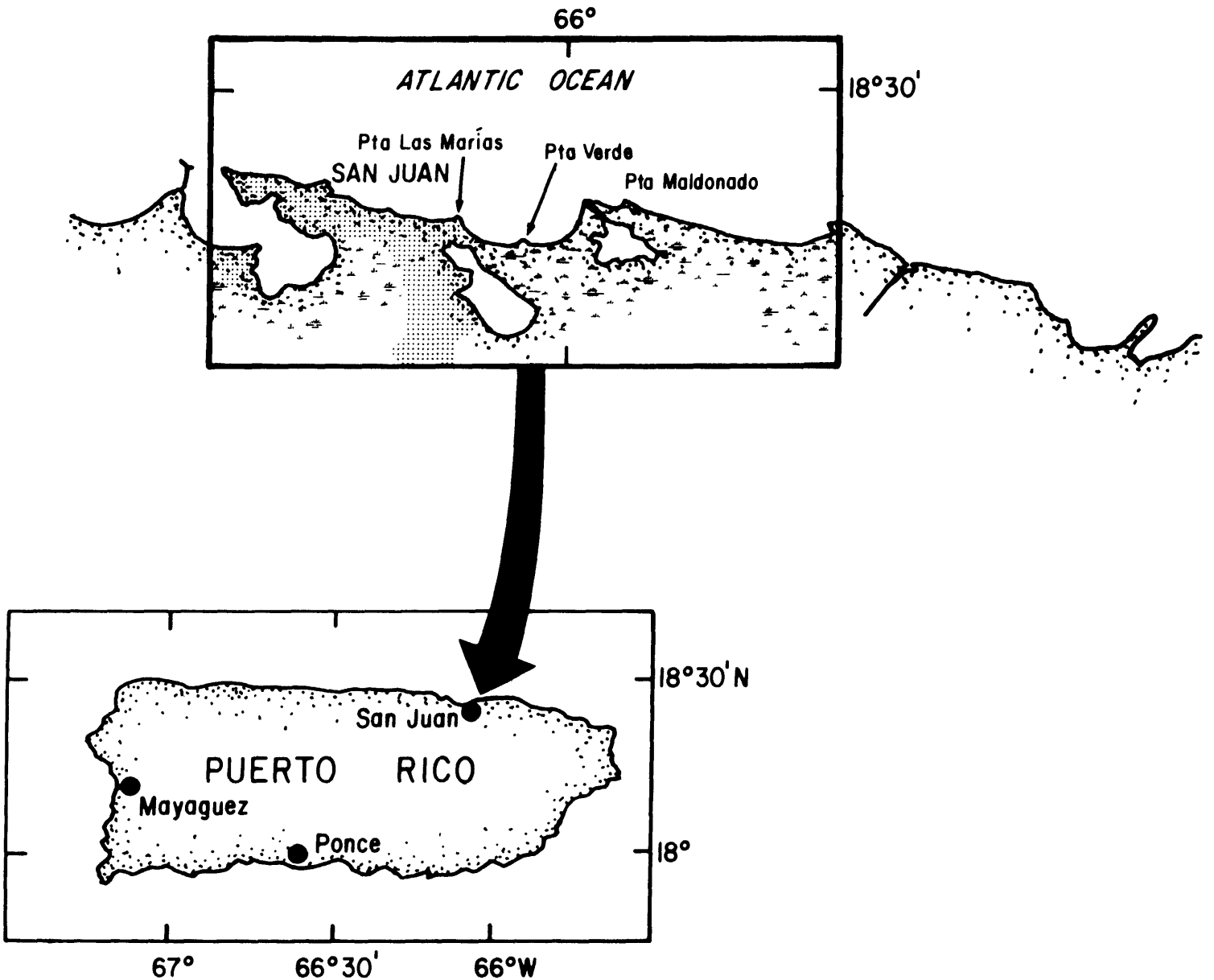
66°
ATLANTIC OCEAN
18°30'
Pta Las Marías
SAN JUAN
Pta Verde
Pta Maldonado
18°30'N
San Juan
PUERTO RICO
Mayaguez
Ponce
18°
67°
66°30'
66°W

Fig. 2. Reductions of the historical shoreline change maps for the San Juan area from Condado (A), Ocean Park (B), Punta Las Marias - Alambique (C), to Punta El Medio - Balneario Isla Verde (D). The numbers seaward of the shoreline (station locations) refer to the beach profile monitoring sites discussed in the chapter on coastal monitoring. Transect locations are the measurement points for the historical shoreline change analyses.

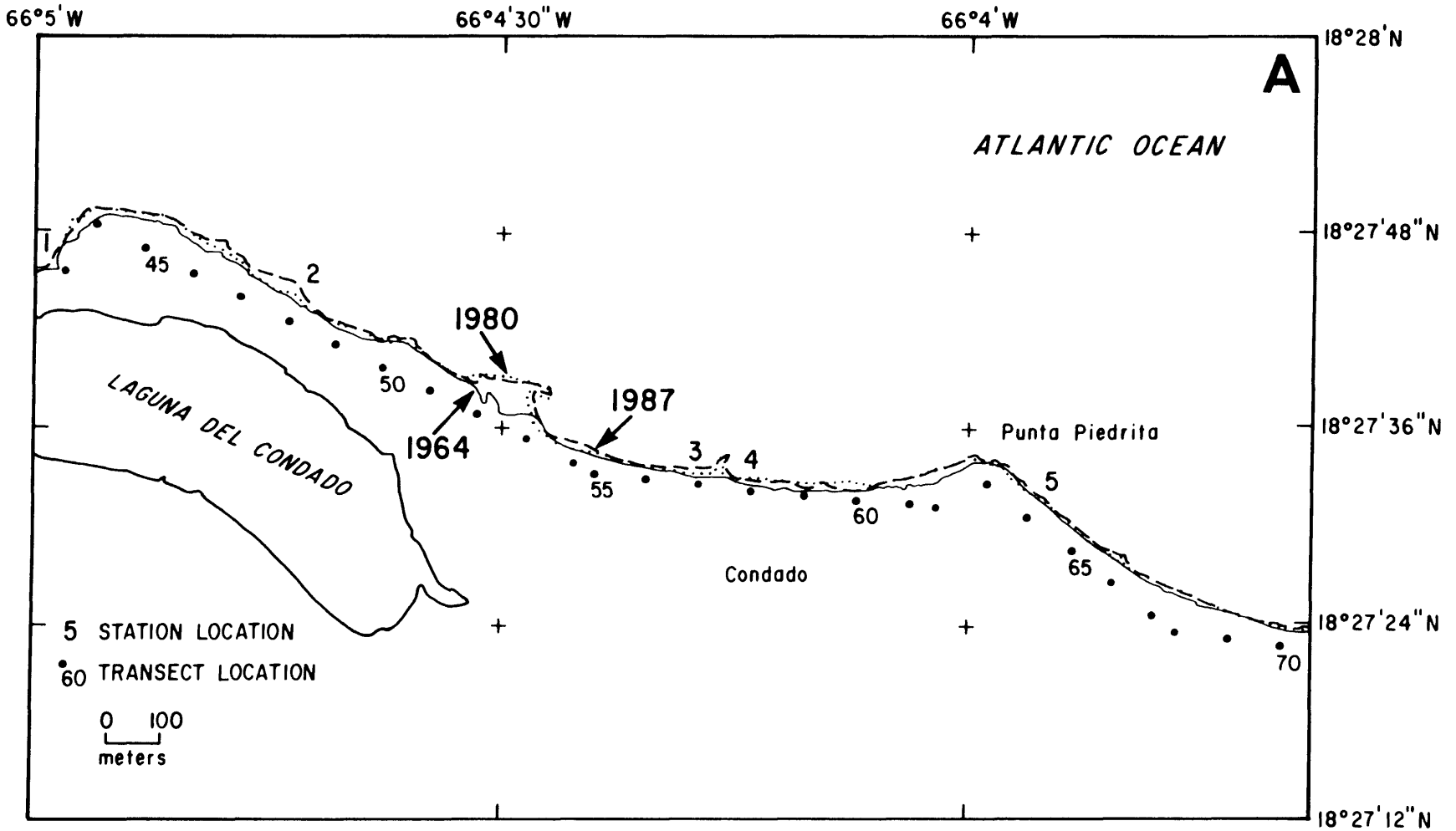
66°5'W
66°4'30"W
66°4'W
18°28'N
18°27'48"N
18°27'36"N
18°27'24"N
18°27'12"N
A
ATLANTIC OCEAN
LAGUNA DEL CONDADO
1980
1964
1987
1
2
3
4
5
45
50
55
60
65
70
Punta Piedrita
Condado
5 STATION LOCATION
60 TRANSECT LOCATION
0 100
meters

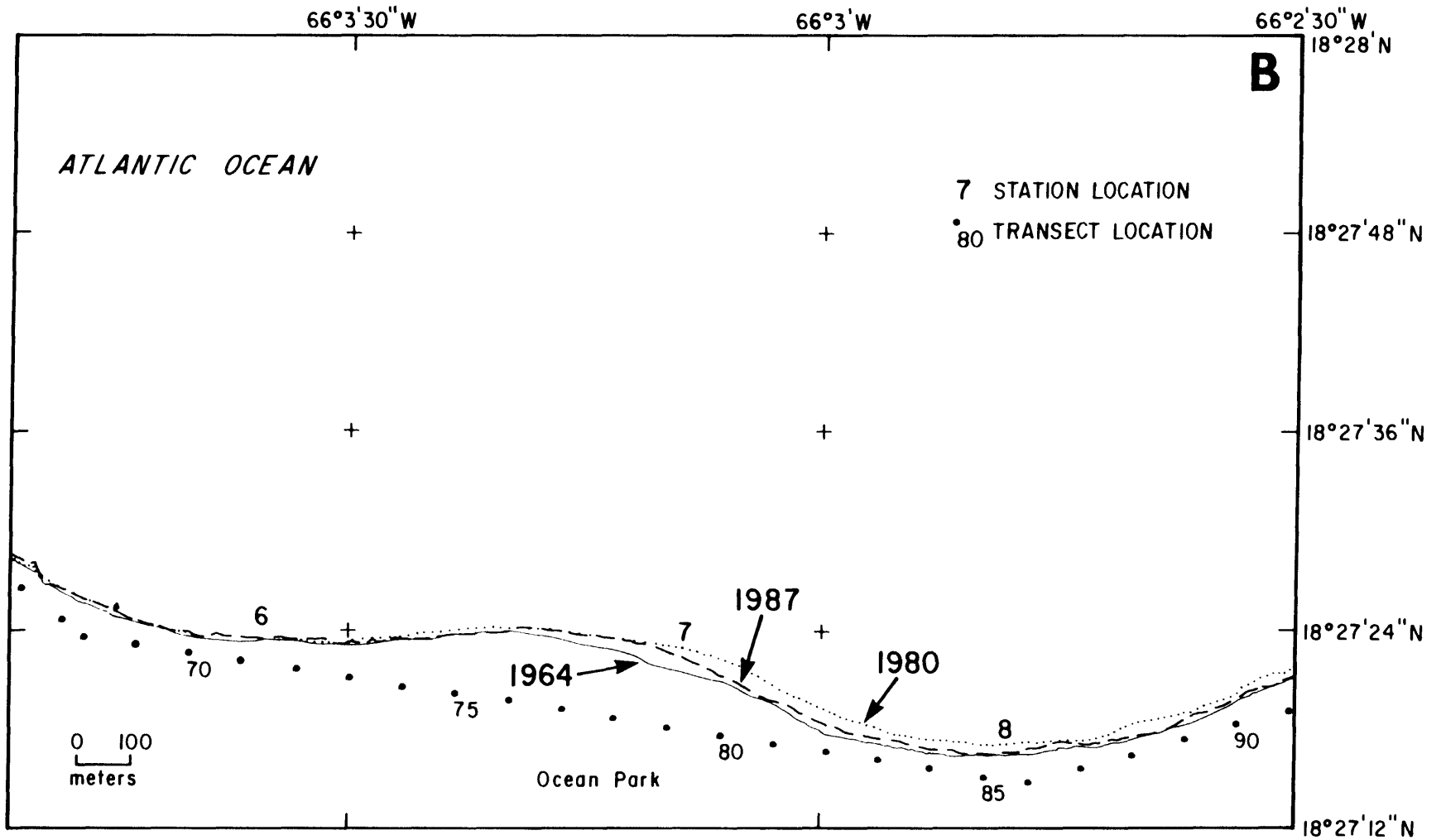
66°3'30"W
66°3'W
66°2'30"W
18°28'N
18°27'48"N
18°27'36"N
18°27'24"N
18°27'12"N
B
ATLANTIC OCEAN
7 STATION LOCATION
80 TRANSECT LOCATION
6
7
8
70
75
80
85
90
1964
1980
1987
0 100
meters
Ocean Park

981

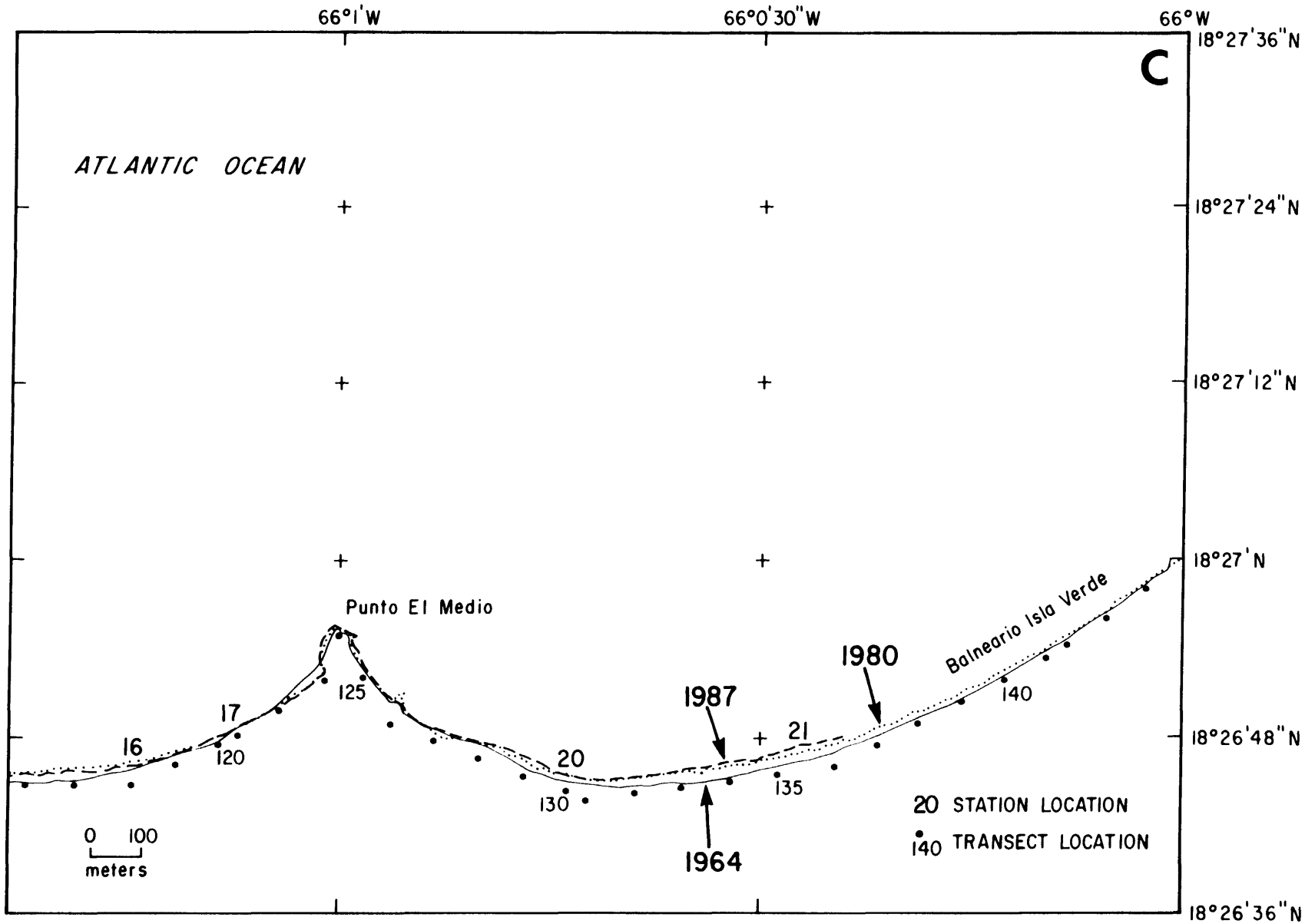
66°1'W
66°0'30"W
66°W
18°27'36"N
18°27'24"N
18°27'12"N
18°27'N
18°26'48"N
18°26'36"N
C
ATLANTIC OCEAN
Punto El Medio
Balneario Isla Verde
1980
1987
1964
16
17
120
125
20
130
21
135
140
0 100
meters
20 STATION LOCATION
140 TRANSECT LOCATION

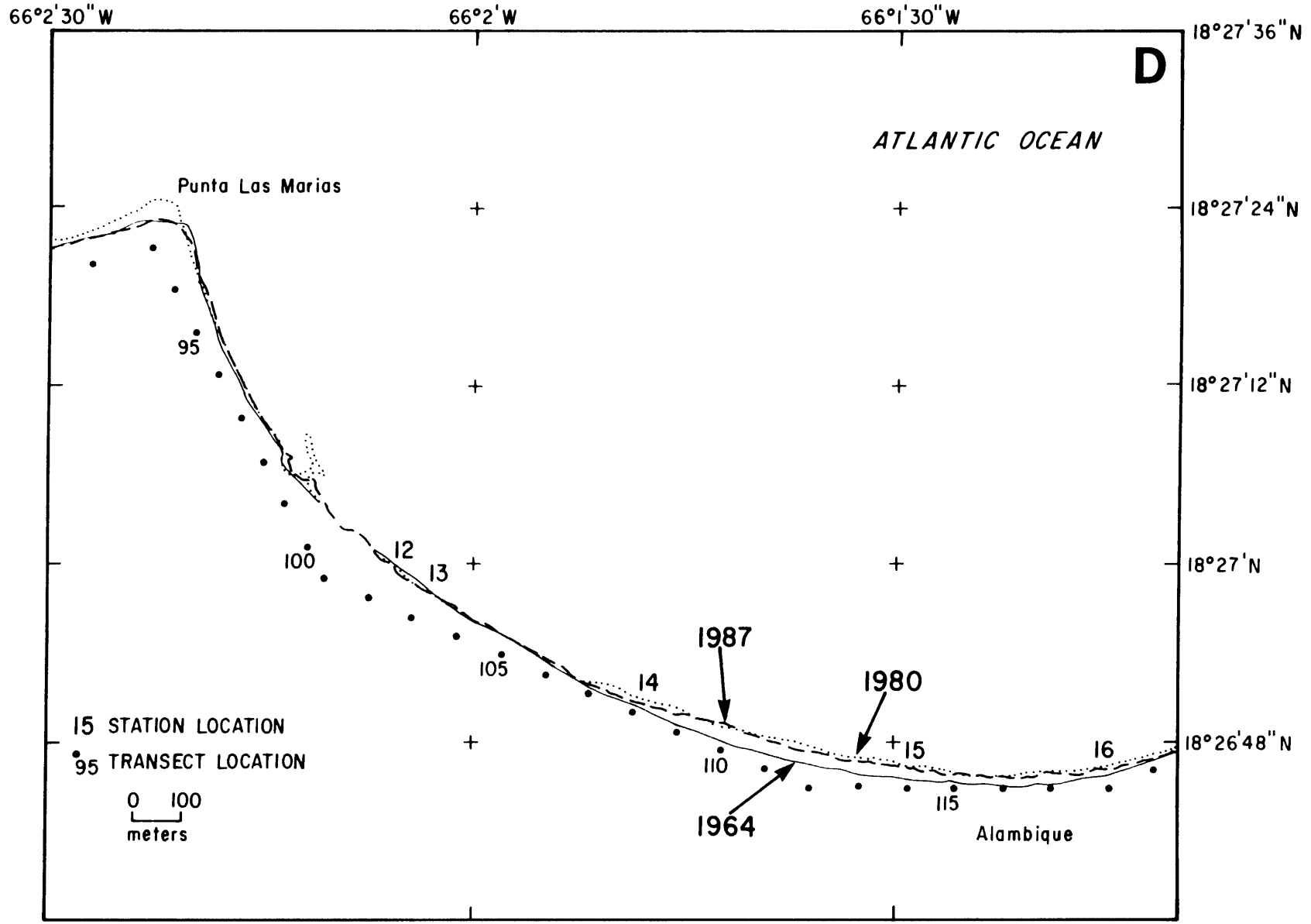
66°2'30"W
66°2'W
66°1'30"W
18°27'36"N
18°27'24"N
18°27'12"N
18°27'N
18°26'48"N
D
ATLANTIC OCEAN
Punta Las Marias
95
100
12
13
105
14
1987
1980
15
16
110
115
1964
Alambique
15 STATION LOCATION
95 TRANSECT LOCATION
0 100
meters

Fig. 3. Chart showing the average yearly rate of shoreline change between the period 1964 to 1987 (+ = accretion; - = erosion) using the *linear regression* method described in Danforth and Thieler (this report) Transect locations are shown in Figure 2. The lower diagram illustrates two broad accretionary embayments (Alambique and Balneario Isla Verde) which are separated by an erosional headland (Punta El Medio).

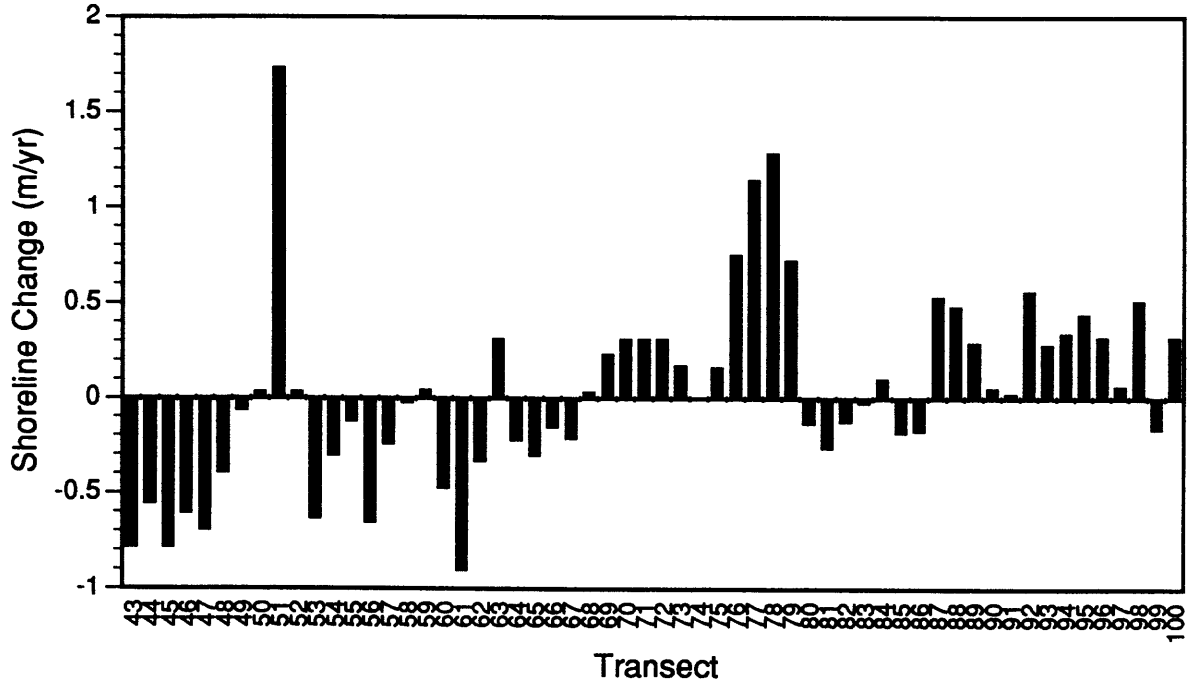
Shoreline Change (m/yr)
2
1.5
1
0.5
0
-0.5
-1
Transect

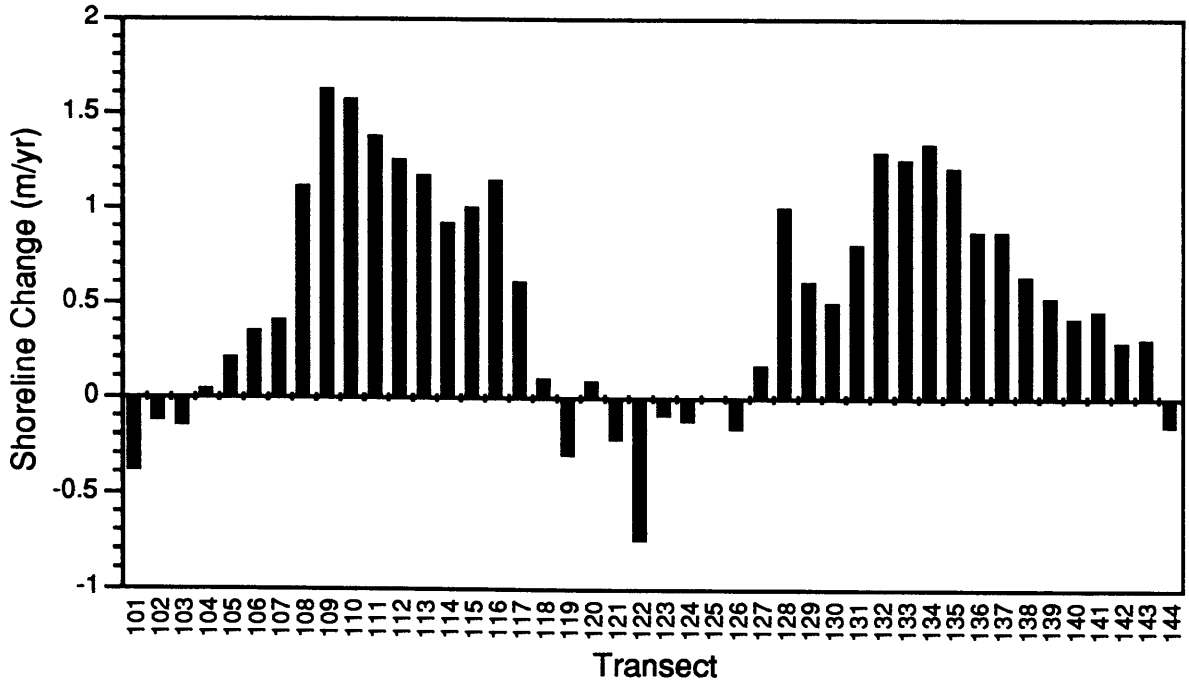
Shoreline Change (m/yr)
2
1.5
1
0.5
0
-0.5
-1
101 102 103 104 105 106 107 108 109 110 111 112 113 114 115 116 117 118 119 120 121 122 123 124 125 126 127 128 129 130 131 132 133 134 135 136 137 138 139 140 141 142 143 144
Transect

COASTAL MONITORING

Bruce. M. Richmond
(U.S. Geological Survey, Menlo Park, California)
Milton Carlo, Juan L. Trias, Rafael W. Rodriguez
(U.S. Geological Survey, San Juan, Puerto Rico)

OBJECTIVE

Beach profile response was measured prior to, and after the passage of Hurricane Hugo to quantitatively determine beach profile changes. In addition, a major component of the Hugo studies were technology transfer in the form of training activities for geologists and technicians of the USGS office in Puerto Rico. The beach profile monitoring program, which included data collection, reduction, and analysis, and maintenance of a digital database, served as the focal point for training activities.

RATIONALE

The beaches of the greater San Juan metropolitan area were chosen as the study area for several reasons. Beach profile data extending back to 1985 were available for a number of sites thus allowing a comparison of profile changes as a direct result of the passage of Hurricane Hugo. San Juan is the largest metropolitan area of Puerto Rico and an important tourist destination. Therefore, the beaches of San Juan are important both as a tourist resource and as a natural protective buffer for the coast. A variety of beach morphologies and orientations are present within a relatively short distance allowing for comparative analysis.

FIELDWORK

The area of intensive beach profile monitoring is between Playita del Condado, near the mouth of Laguna del Condado, and Playa de las Tres Palmitas, east of Piñones (Fig. 1). Twenty-four profile stations were established by R. Webb in 1985, although some are no longer in use (primarily due to erosion of the benchmarks). Two new stations were added on the open-coast beaches east of Punta Congrejos after the passage of Hugo.

Prior to 1990, beach profile data were collected by standard surveying techniques using stadia rod and level from known reference positions. The profiles extended from the backbeach and foredune to the toe of the beach along a single profile line normal to the shore. An example of several profiles from one location are shown on Figure 2. Post-1990 data were digitally collected and recorded with an infrared range-finder sighting off a reflective prism. In addition to a single profile line, several shore-normal and shore-parallel lines were surveyed at each station to water depths of 4 m. Shore-normal lines were continued up to a kilometer offshore by merging onshore profile data with high-resolution echosounder profiles. Single profile lines were collected at approximately monthly intervals (for example see Fig. 3). "Swath" profiling was completed during the winter and summer of 1991 resulting in the production of beach contour maps (Fig. 4). Offshore echosounding was completed during the summer of 1991 (Fig. 5). Centerline profiles have continued to be collected at monthly intervals.

RESULTS

The geology of the coast consists of Holocene beach deposits fronting Holocene

alluvial, swamp, and aeolian deposits which are separated by headlands of Quaternary eolianite (Monroe, 1977; Pease and Monroe, 1977). The coast forms several concave-seaward arcuate embayments (Fig. 1) separated by cuspate headlands developed in the lee of eolianite outcrops or submerged reefs. East of Punta Congrejos, the shoreline is very exposed with little or no offshore reef development, whereas to the west, a linear tract of eolianite ridges protect the coast from extreme open-coast wave conditions.

The complex offshore bathymetry results in variable beach morphology which is dependent upon local exposure. Where wave energy is higher due to exposure through gaps in the offshore eolianite ridges, the beaches tend to be somewhat steeper and higher such as near Piñones and some Condado beaches; conversely, in more protected areas like Balneario Isla Verde and Alambique the beaches are flatter and lower.

During the passage of Hurricane Hugo, damage to beaches occurred as a result of elevated water levels through a combination of storm surge (increase of mean water level in response to high winds and lower atmospheric pressure), wave set-up (the superelevation of mean water level due to the presence of breaking waves), and wave swash (the runup of waves at the shoreline). Estimated storm surge in the greater San Juan area varied between 0.73 and 1.34 m with wave runup reaching a maximum of just over 4 m above mean sea level (Rodriguez and others, 1992). The typical beach profile change resulting from Hugo was one of a general flattening coincident with erosion of the upper beach combined with deposition on the lower beach (for example see Fig. 2). In some areas, a pronounced backbeach scarp was produced. These profile changes are typical of beach response to large events and similar changes have been described in other areas (e.g., Dean, 1991). Sand was deposited inland as thin sheets where waves overtopped the foredune ridge (or in some cases man-made revetments and seawalls). The net effect of Hugo on the sandy beaches appeared to be one of beach-face flattening and erosion with eroded sediment transported both seaward and landward away from the beach face.

Post-Hugo changes to the beach profile have included a return to approximate pre-Hugo conditions in many localities. In general, the effects of Hugo on sandy beaches in the San Juan area has been an erosional perturbation in the seasonal cycle (Rodriguez and others, 1993). Typically, September is a month characterized by low wave energy along the north coast (Corson and others, 1981) which should result in accretionary beach profiles and seaward buildup of the beach. Hugo modified the beaches to a storm- or winter-like profile. Where engineering structures were extensively damaged because they extended too far seaward, beach recovery has been hindered. Vertical seawalls and groins can interfere with normal beach processes resulting in reduced deposition through scouring and increased backwash. Regular profiling at each station provides information regarding the "envelope" of active beachface change (Fig. 6) and when analyzed in time sequence can be used to quantify seasonal and longer trends in shoreline position. For example, Figure 6 shows nearly 50 m of lateral variation of beach width at the mean sea-level elevation for station 6. Most of the change in beach position can be attributed to seasonal variations in local wave climate.

In addition to seasonal changes, low-frequency/high-magnitude events also affect the beach profile. A large wave event, the "Halloween" storm of 1991, caused by North-Atlantic generated storm waves with heights exceeding 3 m, resulted in severe beach erosion and berm overwash (for example see Fig. 3) of a magnitude similar to, and in some areas greater than, the effects of Hurricane Hugo. Extensive damage to roads and other man-made structures occurred on the north coast. Over decadal time scales, events of this

magnitude probably occur regularly.

FUTURE PLANS

Complete descriptions of all the San Juan beach profile sites were published as a USGS Open-File Report (Trias and Carlo, 1992). All beach profile data are digitally stored and periodically updated in a coastal database at the USGS San Juan office. Examination of the beach profile database will be completed and results published as a USGS Miscellaneous Field Studies Map in 1993. These data and derivative mapping products will also be released on CD ROM in 1994.

Fig. 1. Location of the beach profile stations (solid lines), offshore surface sediment sample sites (heavy dots), and shoals (dashed lines) in the greater San Juan metropolitan area.

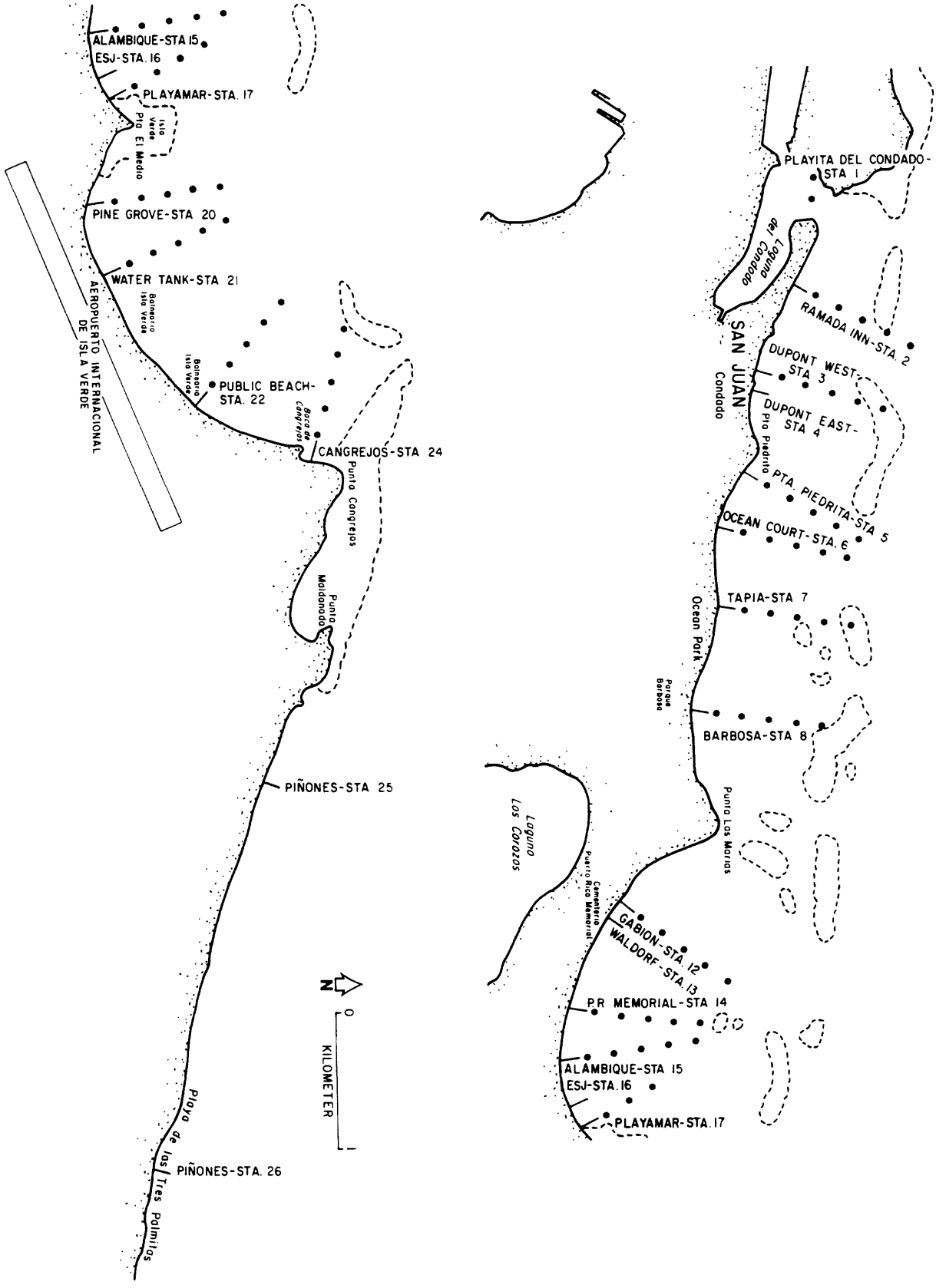
ALAMBIQUE-STA 15
ESJ-STA. 16
PLAYAMAR-STA. 17
Pta. El Medio
Isla Verde
PINE GROVE-STA 20
WATER TANK-STA 21
Balneario Isla Verde
AEROPUERTO INTERNACIONAL DE ISLA VERDE
Balneario Isla Verde
PUBLIC BEACH-STA. 22
Boca de Cangrejos
CANGREJOS-STA 24
Punta Cangrejos
Punta Maldonado
PIÑONES-STA 25
Playa de las Tres Palmas
PIÑONES-STA. 26
N
0
KILOMETER
PLAYITA DEL CONDADO-STA 1
Laguna del Condado
RAMADA INN-STA. 2
SAN JUAN
Condado
DUPONT WEST-STA 3
DUPONT EAST-STA 4
Pta. Piedrita
PTA. PIEDRITA-STA 5
OCEAN COURT-STA. 6
TAPIA-STA 7
Ocean Park
Parque Barbosa
BARBOSA-STA 8
Punta Las Marías
Laguna Los Corozos
Puerto Rico Memorial
Cementerio
GABION-STA. 12
WALDORF-STA. 13
P.R. MEMORIAL-STA 14
ALAMBIQUE-STA 15
ESJ-STA. 16
PLAYAMAR-STA. 17

Fig. 2. Beach profiles prior to (7/20/89) and after (9/28/89) the passage of Hurricane Hugo at station 6 (Ocean Court condominiums) in the Condado beach area. Data from R. Webb (written communication). Note that beach erosion was more extensive between 9/28/89 and 11/15/89 than before and after Hurricane Hugo.

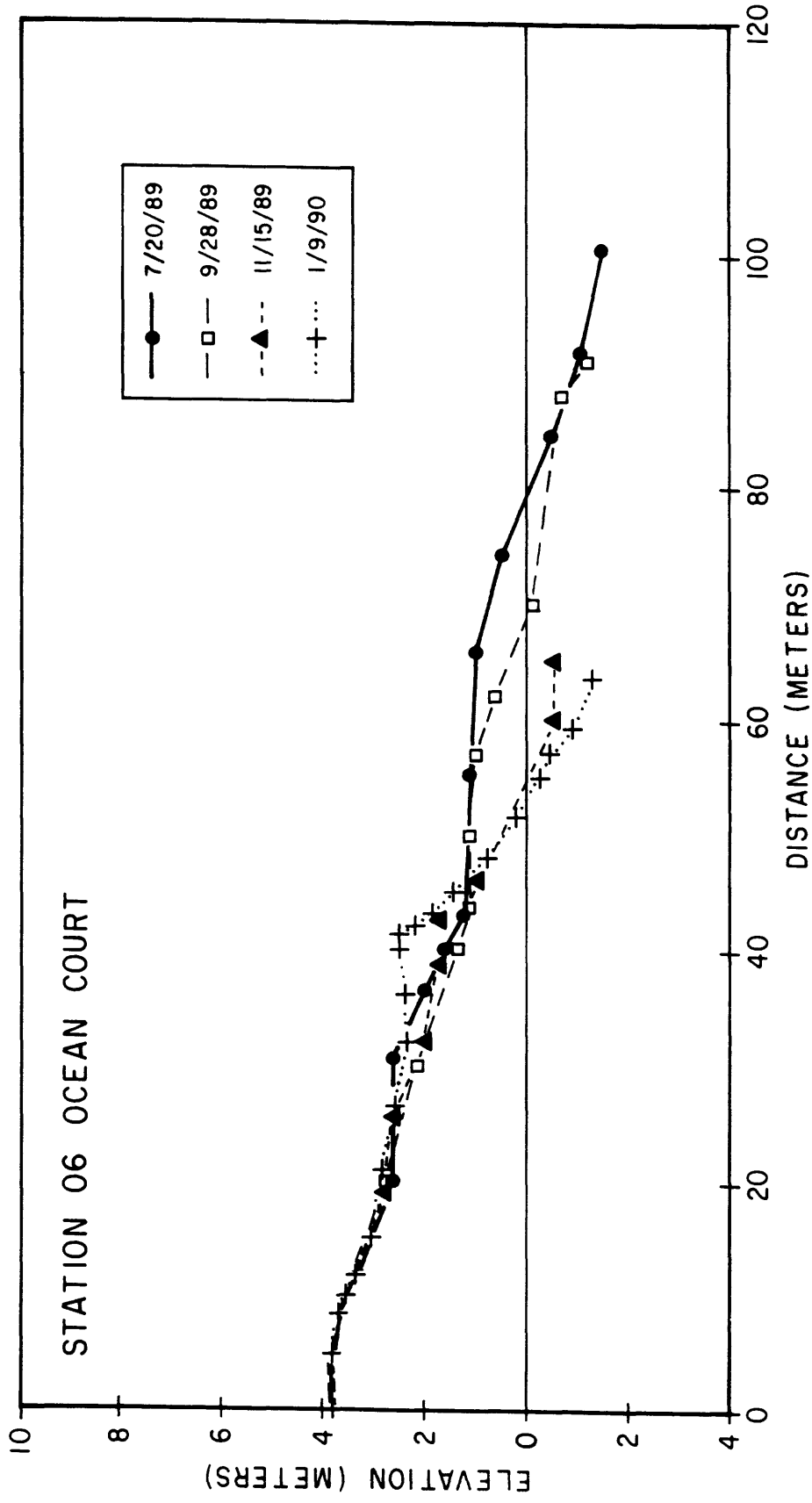
STATION 06 OCEAN COURT
7/20/89
9/28/89
11/15/89
1/9/90
ELEVATION (METERS)
DISTANCE (METERS)
10
8
6
4
2
0
2
4
0
20
40
60
80
100
120

Fig. 3. Centerline profiles before and after the "Halloween" storm (10/31/91) for station 6. The storm occurred a few days prior to the 11/02/91 profile. Because of hazardous wave conditions, the 12/10/91 profile extends only to the approximate mean sea-level position.

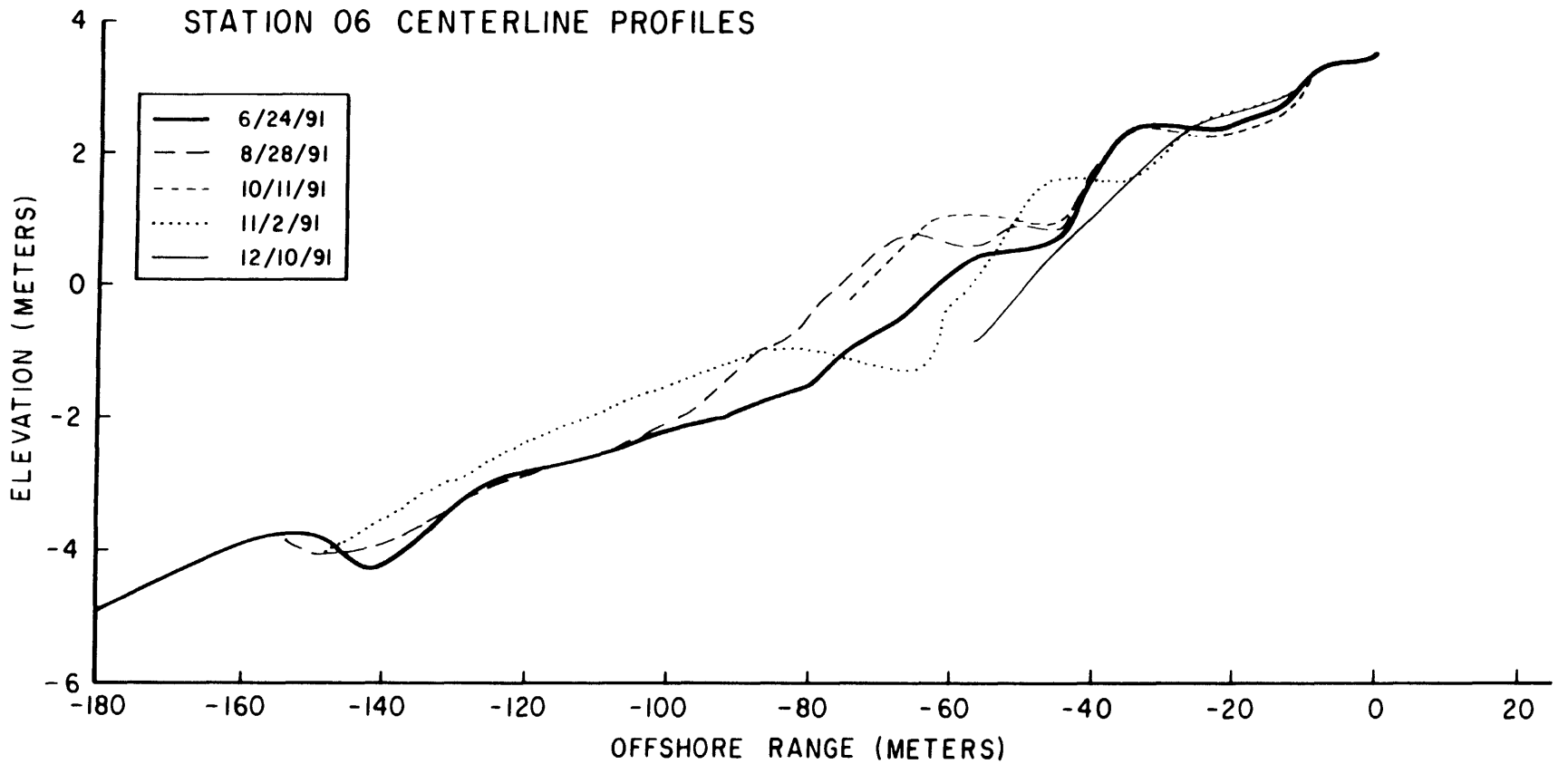
STATION 06 CENTERLINE PROFILES
6/24/91
8/28/91
10/11/91
11/2/91
12/10/91
ELEVATION (METERS)
4
2
0
-2
-4
-6
-180
-160
-140
-120
-100
-80
-60
-40
-20
0
20
OFFSHORE RANGE (METERS)

Fig. 4. Computer generated contour maps from 3-dimensional beach grids for: A) winter (3/05/91) and B) summer (6/24/91) at station 06. The dots represent data point collection sites. The zero contour is the approximate mean sea-level (msl) position; negative numbers are below msl and positive numbers are above msl. Contours in meters. C) Contour grid of the elevation differences between winter and summer. Negative numbers indicate erosion while positive values denote accretion between the two surveys. In the winter example (A), the beach is reasonably regular with near-parallel contours in the nearshore, however, in the summer (B) much more irregularity exists in the nearshore perhaps in response to seasonal wind/wave variations. Erosion in the nearshore trough appears to be offset by deposition further offshore (C).

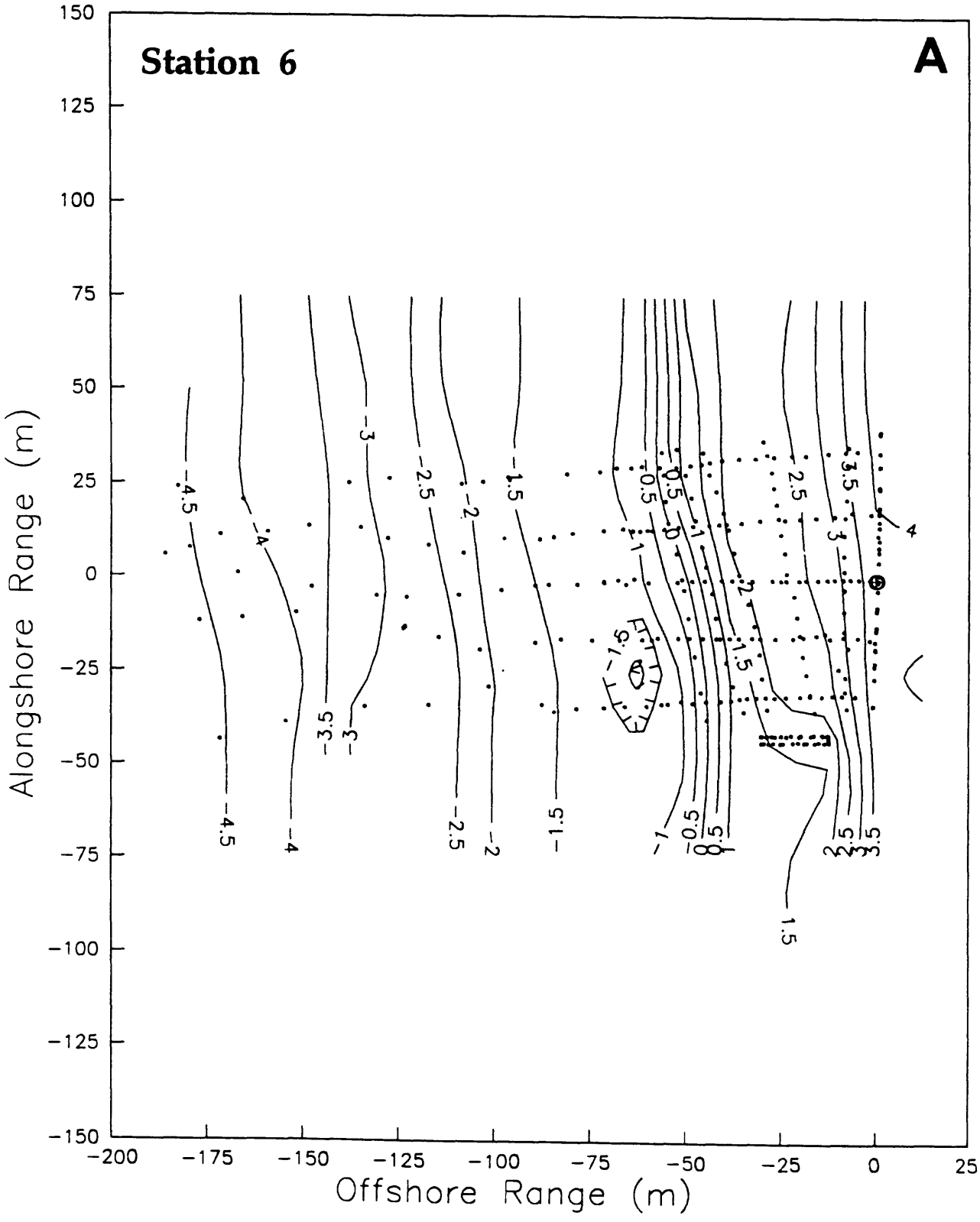
Station 6
A
Alongshore Range (m)
Offshore Range (m)
150
125
100
75
50
25
0
−25
−50
−75
−100
−125
−150
−200
−175
−150
−125
−100
−75
−50
−25
0
25
−4.5
−4
−3.5
−3
−2.5
−2
−1.5
−1
−0.5
0.5
1
1.5
2
2.5
3
3.5
4

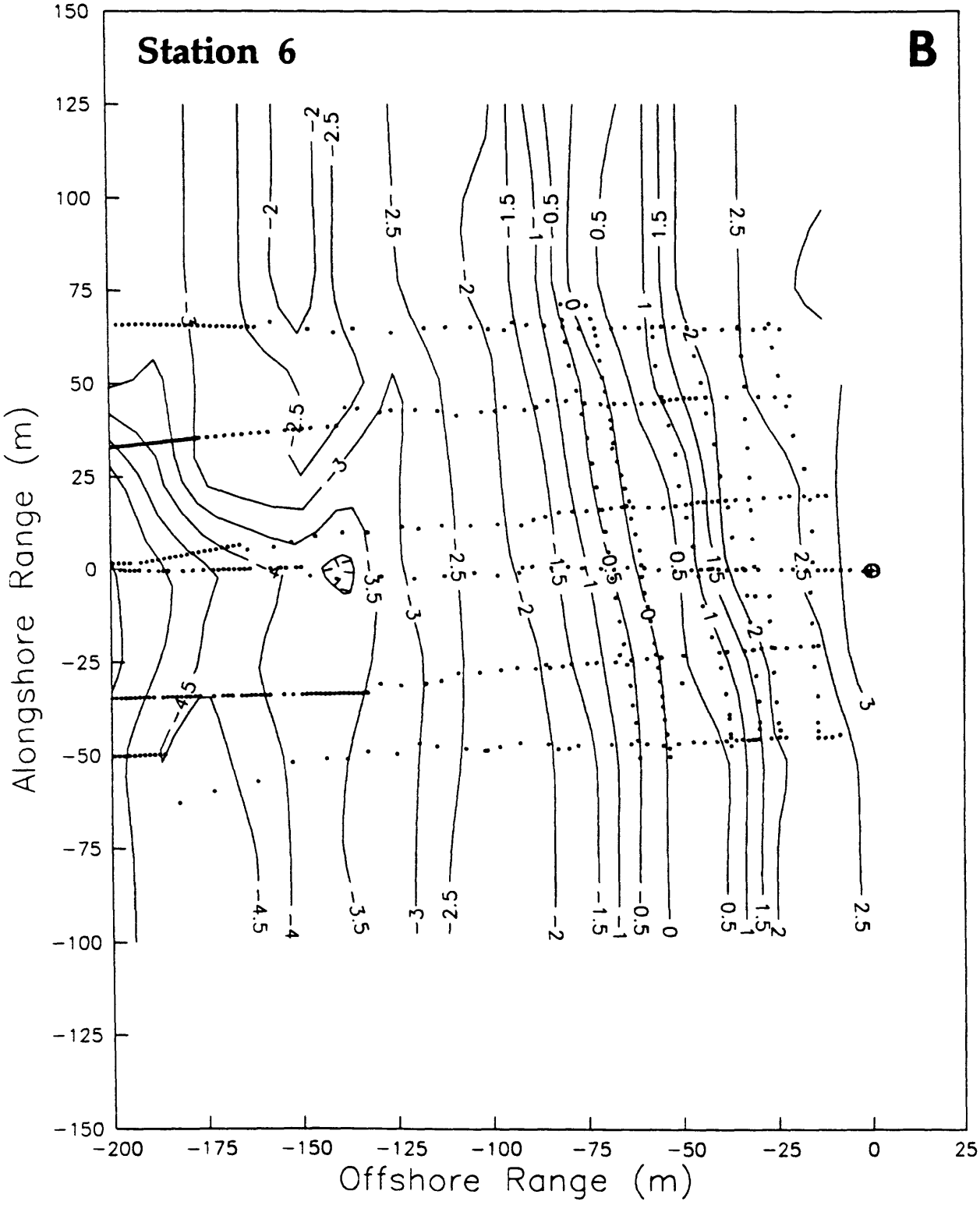
Station 6
B
Alongshore Range (m)
Offshore Range (m)
150
125
100
75
50
25
0
-25
-50
-75
-100
-125
-150
-200
-175
-150
-125
-100
-75
-50
-25
0
25

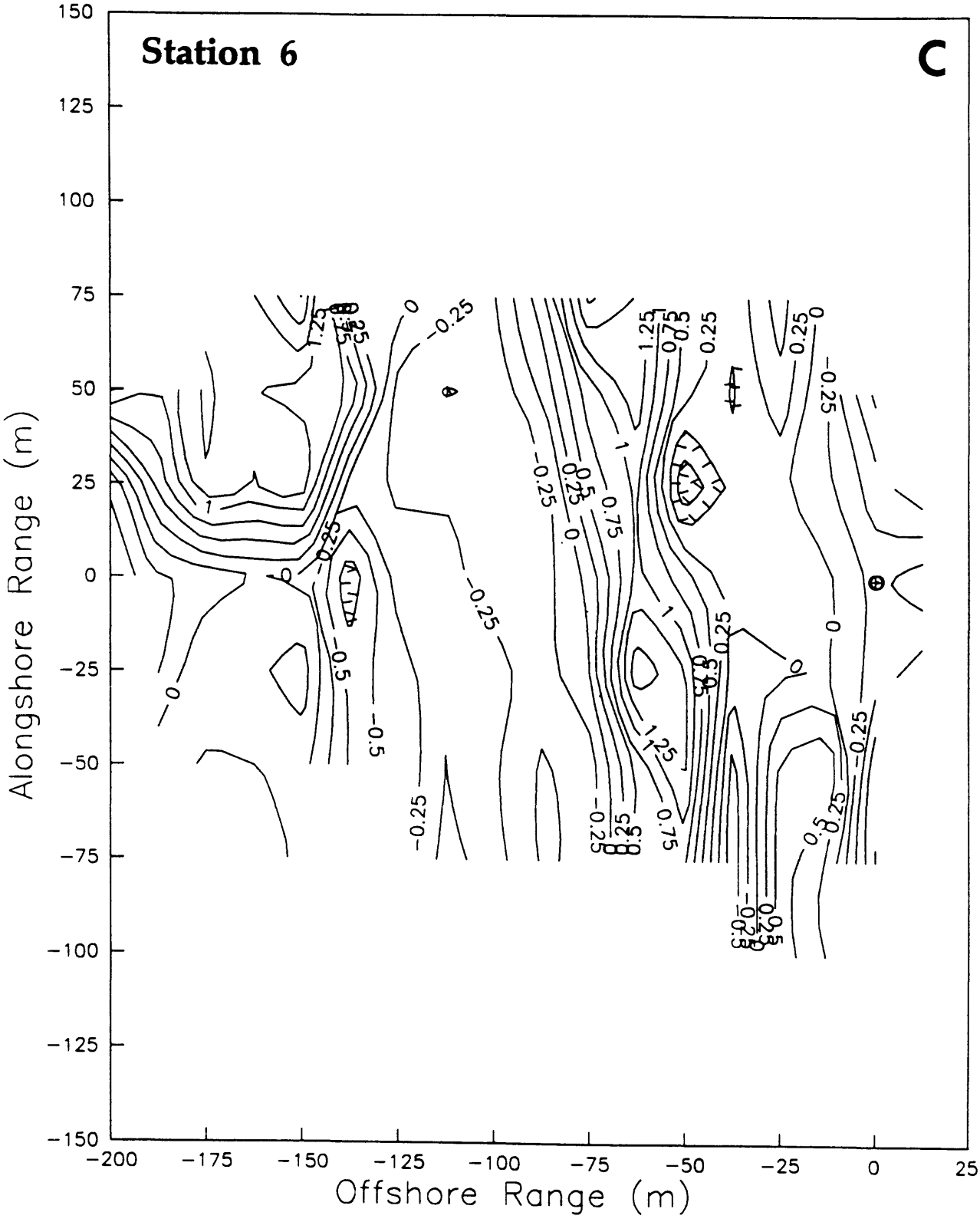
Station 6
C
Alongshore Range (m)
Offshore Range (m)
150
125
100
75
50
25
0
−25
−50
−75
−100
−125
−150
−200
−175
−150
−125
−100
−75
−50
−25
0
25

Fig. 5. Offshore centerline profile (top) and contour map (bottom) generated by merging onshore profiles and offshore echosounder records for station 6. FFT bathymetry is derived from fast fourier transform analysis of digitized data. The regularity of the nearshore contours is due to the deposition and reworking of sandy sediment. Farther offshore the seabed becomes more irregular due to the presence of reefs. These reefs probably have a dramatic effect on local wave refraction and diffraction patterns, thereby influencing sediment transport at the shoreline.

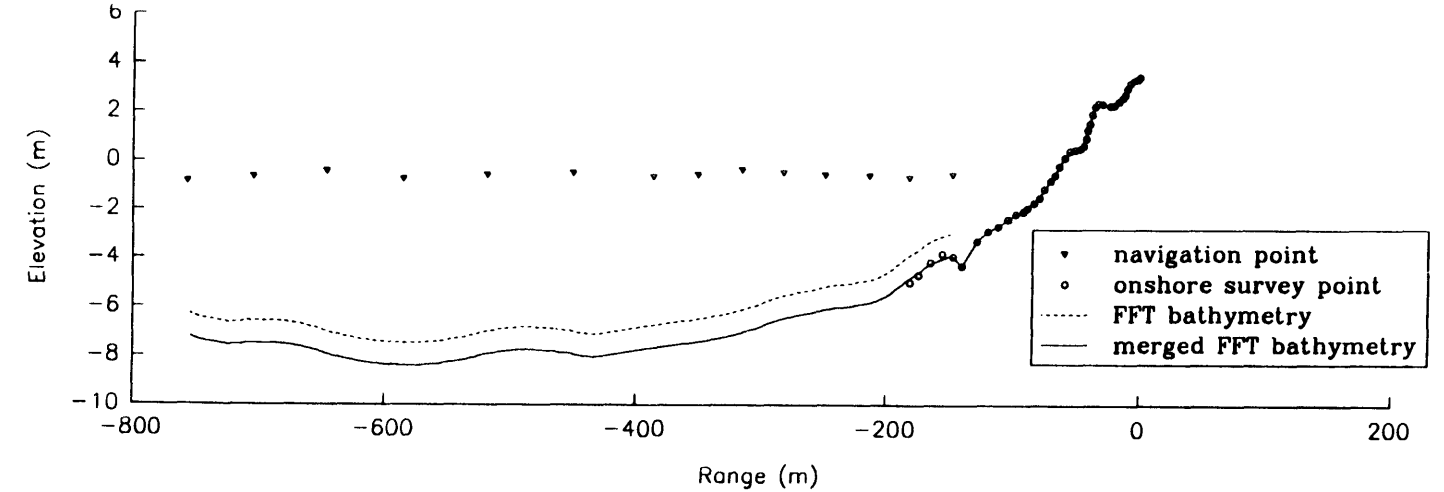
Elevation (m)
6
4
2
0
-2
-4
-6
-8
-10
-800
-600
-400
-200
0
200
Range (m)
navigation point
onshore survey point
FFT bathymetry
merged FFT bathymetry

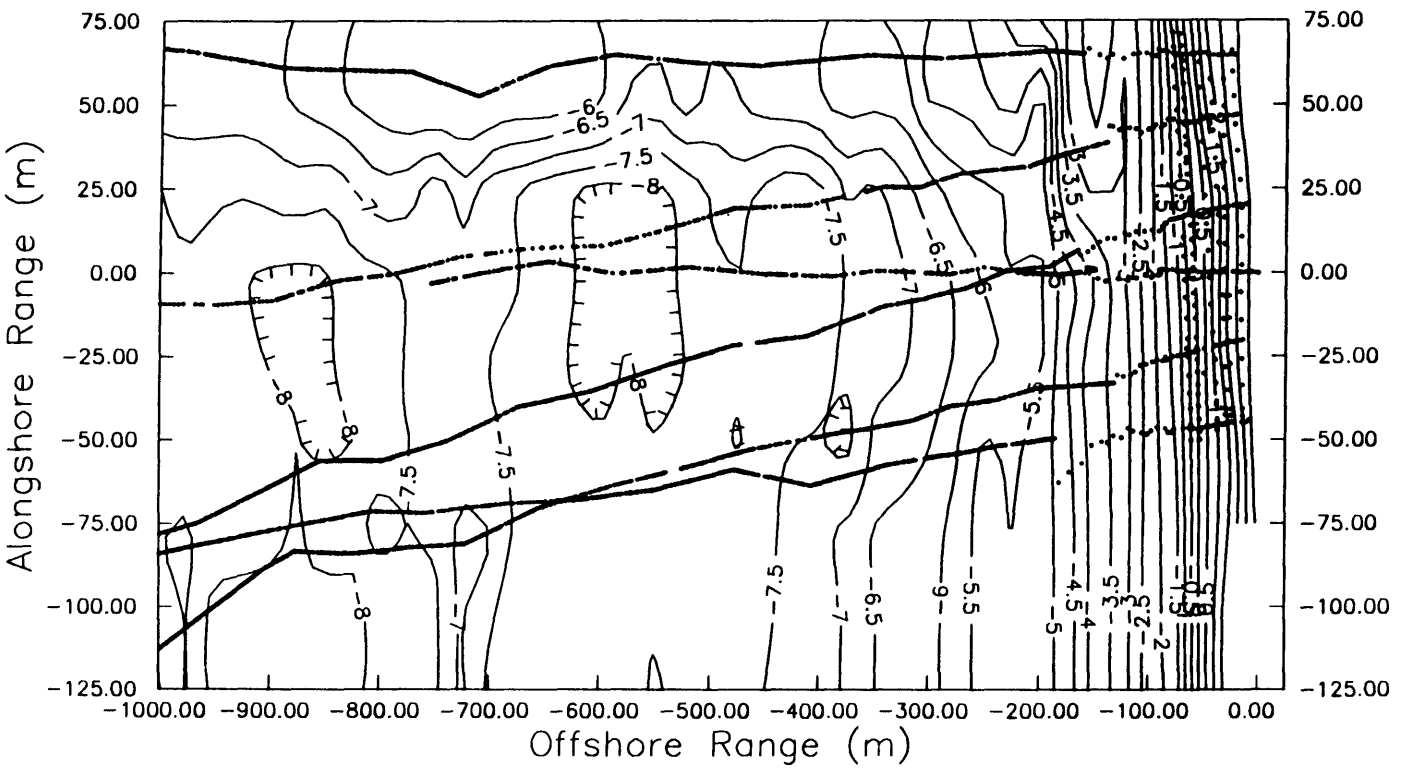
Alongshore Range (m)
75.00
50.00
25.00
0.00
-25.00
-50.00
-75.00
-100.00
-125.00
-1000.00 -900.00 -800.00 -700.00 -600.00 -500.00 -400.00 -300.00 -200.00 -100.00 0.00
Offshore Range (m)

Fig. 6. Plots of all available beach profiles for station 6 showing the "envelope" of profile change. Geodimeter data refers to post-1990 digitally collected data (this study). Webb's data is from R. Webb (written communication).

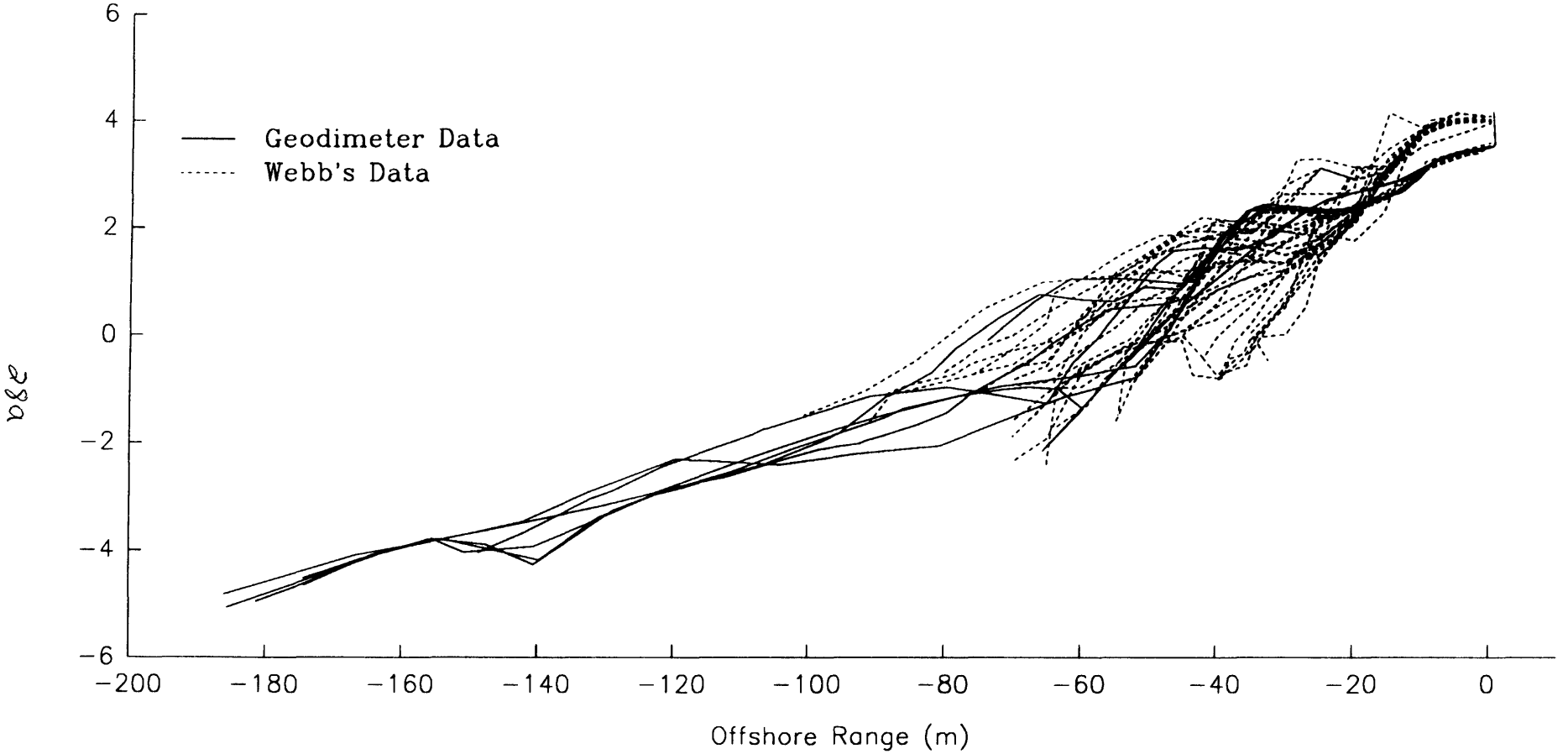
Geodimeter Data
Webb's Data
6
4
2
0
−2
−4
−6
−200
−180
−160
−140
−120
−100
−80
−60
−40
−20
0
Offshore Range (m)

COASTAL HAZARD MAPPING

David M. Bush
(Duke University, Durham, North Carolina)
Bruce M. Richmond
(U.S. Geological Survey, Menlo Park, California)

OBJECTIVE

This study focuses on the multiplicity of coastal geologic hazards and their identification. Coastal Hazard Maps were prepared for Puerto Rico depicting coastal geology and geomorphology, beach characteristics, offshore (inner shelf) characteristics, and hazard potential from such events as flooding, overwash, erosion, earthquake damage and landslides.

RATIONALE

Shoreline erosion, both long-term due to sea-level rise and short term due to storms, is only one of many hazards affecting coastal areas. Other hazards include tsunamis, earthquake-induced slope failure, river flooding, and landslides. The assessment of all potential coastal hazards, both natural and man-made, is necessary for a complete understanding of shoreline response to geologic events. The heavy industrialization and the corresponding intense coastal zone development of Puerto Rico in the past 40 years has placed an enormous number of people and amount of property at risk. Most development took place without knowledge or regard for geologic hazards which affect the coastal zone.

FIELDWORK

Using USGS topographic maps as a base, Coastal Hazard Maps were prepared for the 15 quadrangles representing the portión of the Puerto Rico shoreline impacted by Hurricane Hugo (Fig. 1). Within each quadrangle, the shoreline is divided into natural geomorphic units which are numbered sequentially for referencing to a database containing detailed geologic information. Each Coastal Hazard Map contains detailed information regarding individual shoreline segments including schematic representation of the shoreline type. In addition, dominant hazards for each segment are identified and an overall risk assessment for each segment is assigned. Coastal Hazard Maps 1 (San Juan quadrangle) and 2 (Carolina quadrangle) are presented here as examples (Figs. 2 and 3).

Risk is difficult to quantify, but, in general, the map terms imply the following: extreme, more than 4 identifiable hazards; high, 3 to 4 identifiable hazards; moderate, at least two hazards; and low, one hazard or less (these are displayed as E = extreme, H = high, M = moderate, and L = low on Figures 2 and 3). Low risk does not imply site safety because a single, potentially devastating hazardous event is always possible. For example, the Puerta de Tierra section of San Juan, built on rock and at high elevation, is relatively low risk from hurricane flooding and/or shoreline erosion and from landsliding, however, hurricane-related wind damage, and storm wave damage from exceptional storms or tsunami would be potentially devastating.

Few truly "safe" sites exist on shorelines, but likelihood of property loss is expected to be lower in low risk areas than in high risk areas. The maps are intended to be as close to site specific as possible, however, shoreline characteristics vary over such short distances that the generalized maps cannot always show site-specific risk. Individual sites

should always be evaluated in the field. Isolated dangerous sites can occur in low-risk zones, and visa versa.

The following hazard categories are presented on the Hazard Maps:

S — Shoreline-setting hazards. Long-term problems such as severe erosion history or low elevation. Differs from *Development hazards* because it coincides only with the natural setting, regardless of the type of coastal development.

M — Marine hazards. Short-term impacts of wave runup and overwash, storm surge and storm-surge ebb from hurricanes and other coastal storms, plus potential tsunami impact.

Q — Earthquake and slope hazards. Areas with steep slopes, active faults that are prone to slope failure and landslides during earthquakes and heavy rains, or areas of unconsolidated material or artificial fill prone to liquefaction during earthquakes.

R — Riverine hazards. Areas on floodplains, with historic severe floods or with dams upstream where flood potential is high.

D — Development hazards. Varies from high density development where a great deal of property is at risk to low density development in high risk areas because of siting at low elevation or extremely close to the ocean. Differs from *Shoreline-setting hazards* because it considers development (where the natural setting of the shoreline has been altered for development in such a way as to place people or property at risk).

E — Engineering hazards. Special cases where shoreline engineering projects have had significant detrimental effects to portions of the shoreline. Examples are the breakwater at Boca de Cangrejos or the causeway to Isla de Cabras. Also includes areas where natural protection has been removed through sand mining of the dunes and beaches.

NOTE: For shoreline segments where a given hazard applies to only a portion of the shoreline or for which there is some special consideration, the hazard is enclosed is parentheses and is counted as 1/2 a hazard for the Rick Classification on the Hazard Maps.

The database provides a more complete description of each shoreline segment including:

1) General shoreline description which includes shoreline orientation, shoreline type such as consolidated (eolianite, Tertiary limestone, metamorphic rocks, and igneous rocks), or unconsolidated (alluvial fans, eolian dunes, and beach). If the shoreline is armored, the type of

engineering structure is identified as either a revetment, seawall, groin, or breakwater. Artificial beach nourishment sites are also identified (where known). Wetlands are broken down into mangrove swamps, freshwater swamps, brackish lagoons, and freshwater lagoons. Rivers, streams, and other inlets are identified as well as discharge information if known, and the presence or absence of barrier spits.

2) Beach descriptions for shorelines that are predominantly beaches include beach type (sand, gravel, mud, pocket), composition, (mostly carbonate, siliciclastic, or mixed), the presence of beachrock or abundant heavy mineral concentrations, and beach slope, width, and thickness, and critical erosion areas.

3) Descriptions of the offshore areas focus on the sediment grain size, sediment composition, shelf slope, shelf width, and the presence of offshore barriers and reefs.

4) In areas prone to coastal flooding where previous information is available, the storm wave swash elevation and penetration and velocity zone elevation and penetration is presented. Potential storm surge elevation from model studies is also presented.

5) Shoreline erosion history based on data from the historical shoreline analysis incorporates the historical erosion rate and inclusive years of study.

6) General quadrangle descriptions are also given and include the coastal plain width, range of elevations, landslides that have been mapped on geologic maps or observed and areas of artificial fill.

RESULTS

Coastal erosion is a severe and persistent problem of the Puerto Rico shoreline. It is far more critical along unconsolidated shorelines than on rocky stretches. There are several probable causes for the erosion. Poorly designed engineering structures that interfere with the natural movement of beach sand are probably responsible for much of the sand loss. Other human-induced factors include mining of sand from beach and dune areas and the changes to the nearshore hydraulic regime through activities such as dredging, harbor construction, jetties, and breakwaters. Potential accelerated sea-level rise as a result of global warming would also contribute to coastal erosion.

Natural causes of shoreline erosion include the effects of large events such as hurricanes and large ocean swell from north Atlantic winter storms. Sandy shorelines respond to changes in the nearshore current and wave regime. Changes or variations in the supply of sediment to the beaches can also lead to local erosion.

Other natural hazards have the potential for severe impact on the coastline. Though remote, the probability exists for future losses of life and property in the event that seismic sea waves (tsunami) strike the coast of Puerto Rico (Schwab and others, 1991). The entire island of Puerto Rico is susceptible to damage from earthquakes. The island lies in a relatively active tectonic zone (Sykes and others, 1982) and is so small that essentially the

entire island has the same risk of suffering the impacts of a major seismic event. Differences in amounts of damage around the island will thus be a factor of development density, age, and type of structure. Structures built on landfill (the case of most of the development in the San Juan metropolitan area) susceptible to earthquake-induced liquefaction and/or slope failure may suffer extreme damage.

Flooding in low-lying coastal areas is a chronic and potentially severe hazard. The rainy season creates an annual threat of intense river flooding which is further increased during hurricanes that can release large volumes of water in a relatively short time span. Fortunately, Hugo was a relatively "dry" hurricane and coastal flooding was less than expected for a storm of this size. With industrialization and increase in island population, more and more development has, by necessity, taken place in coastal flood-plain zones. As a result, the potential and occurrence of damage on the island resulting from flooding has increased.

FUTURE PLANS

All Hazard Maps in the coastal areas impacted by Hugo will be completed and published as a USGS Miscellaneous Field Studies Map series in 1993. These products will also be released on CD ROM in 1994.

RECOMMENDATIONS

The beaches of Puerto Rico are very dynamic features that respond to both seasonal variations in wave climate as well as large storm events. The present study provides a means of assessing beach response. Two major causes of erosion along the Puerto Rico shoreline are shoreline engineering structures and mining of sand on beaches (including rivers where they are sources of beach sand). Both cause a loss of sand from the beaches. Shoreline stabilization in Puerto Rico is largely uncontrolled. Most states in the U.S. have begun to control hard stabilization (construction of seawall, revetments, and other types of shoreline armoring) and two states prohibit it all together (NRC, 1990). Often in Puerto Rico the cost of saving erosion-threatened buildings is much more than the buildings are worth. Inconsistencies in the type and degree of hard stabilization can lead to differential erosion and accelerated erosion.

Recently, shoreline management policies are more commonly considering controlling hard stabilization. Closer monitoring of beach dynamics, including beach profiling and beach volume-change studies, are imperative and have begun in Puerto Rico (Richmond and others, this report). Alternatives to hard stabilization that are being considered in other areas include development set-backs, relocation or demolition of low-cost shorefront buildings and beach replenishment. The problem is that building of walls and revetments is usually done on a crisis basis allowing no time for deliberation concerning other alternatives. Many miles of the world's recreational beaches have been seriously degraded and even destroyed through attempts to halt shoreline erosion to protect buildings. Preservation of recreational beaches are now more frequently given high priority, in many cases higher priority than preservation of shorefront buildings. Mining sand from beaches is no longer legal in most places. This includes the removal of sand from rivers which would ultimately be deposited on the beach.

Fig. 1. Map of Puerto Rico. Numbers refer to USGS Topographic Quadrangles along the portion of the Puerto Rico coast impacted by Hurricane Hugo and included in the Coastal Hazard Map series. There are 36 separate USGS Topographic Quadrangles around the Puerto Rico coast (including the islands of Culebra and Vieques). The San Juan Quadrangle was titled Coastal Hazard Map 1, and numbering continued sequentially clockwise around the island. Maps 1 and 2 (highlighted) are included as examples in this report.

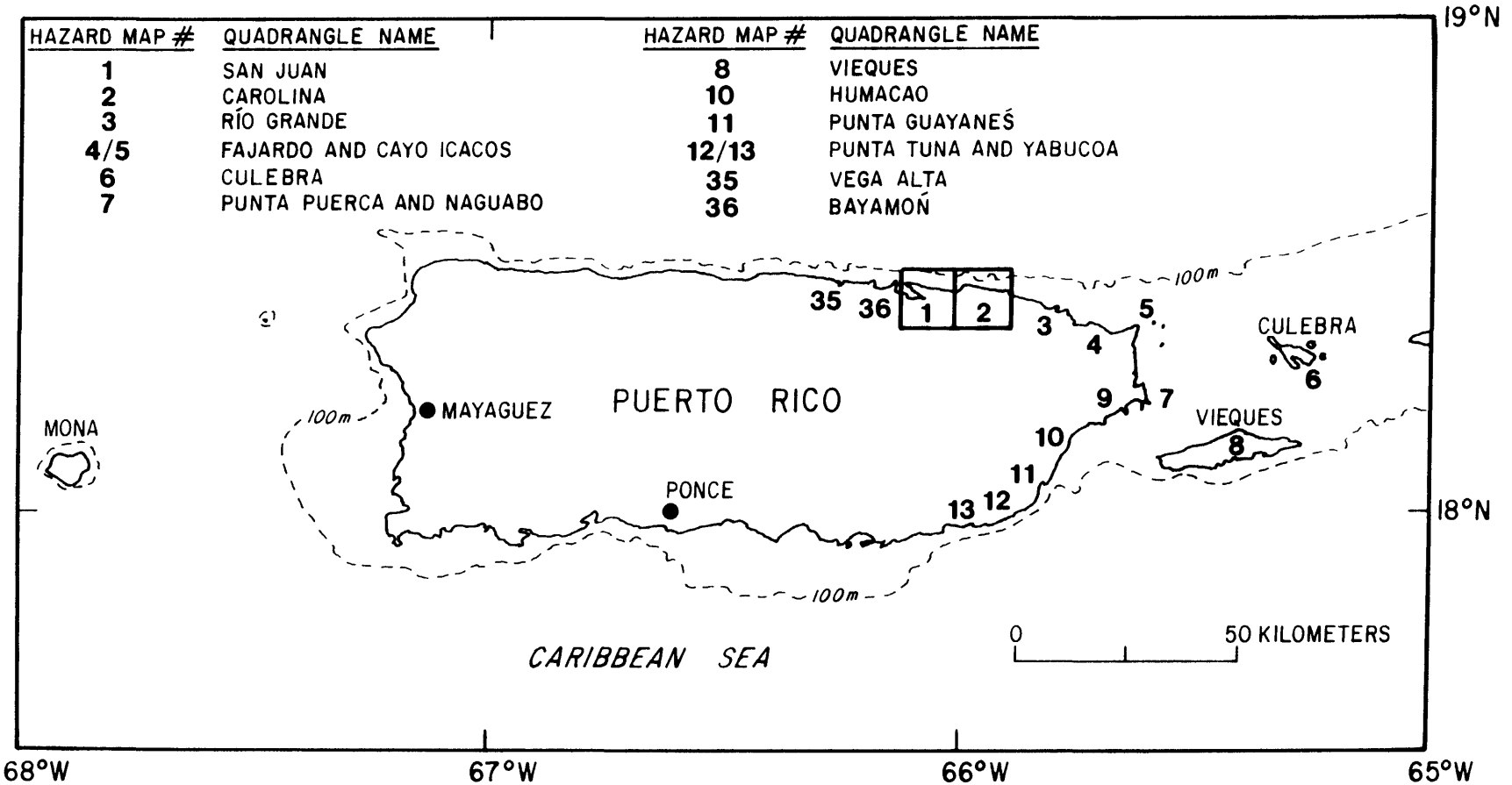
HAZARD MAP #
QUADRANGLE NAME
1 SAN JUAN
2 CAROLINA
3 RÍO GRANDE
4/5 FAJARDO AND CAYO ICACOS
6 CULEBRA
7 PUNTA PUERCA AND NAGUABO
8 VIEQUES
10 HUMACAO
11 PUNTA GUAYANEŚ
12/13 PUNTA TUNA AND YABUCOA
35 VEGA ALTA
36 BAYAMOŃ
19°N
18°N
68°W
67°W
66°W
65°W
100m
MAYAGUEZ
PUERTO RICO
PONCE
MONA
CULEBRA
VIEQUES
CARIBBEAN SEA
0
50 KILOMETERS

Fig. 2. Coastal Hazard Map 1 (San Juan Quadrangle). For location see Figure 1. This map contains the densest population and development on Puerto Rico. The several headlands (puntos) attest to the rocky nature of the shoreline, offering some protection from storms (note low to moderate risk rating for segments 1.1 to 1.6). Most sandy stretches, however, are heavily developed with hotels, condominiums, or houses (segments 1.8 tp 1.15). Also included in this section is the important recreational beach Balneario Isla Verde (segment 1.16) with the main airport located just inland. This segment was heavily impacted by major beach and dune-sand mining, causing high present day erosion rates.

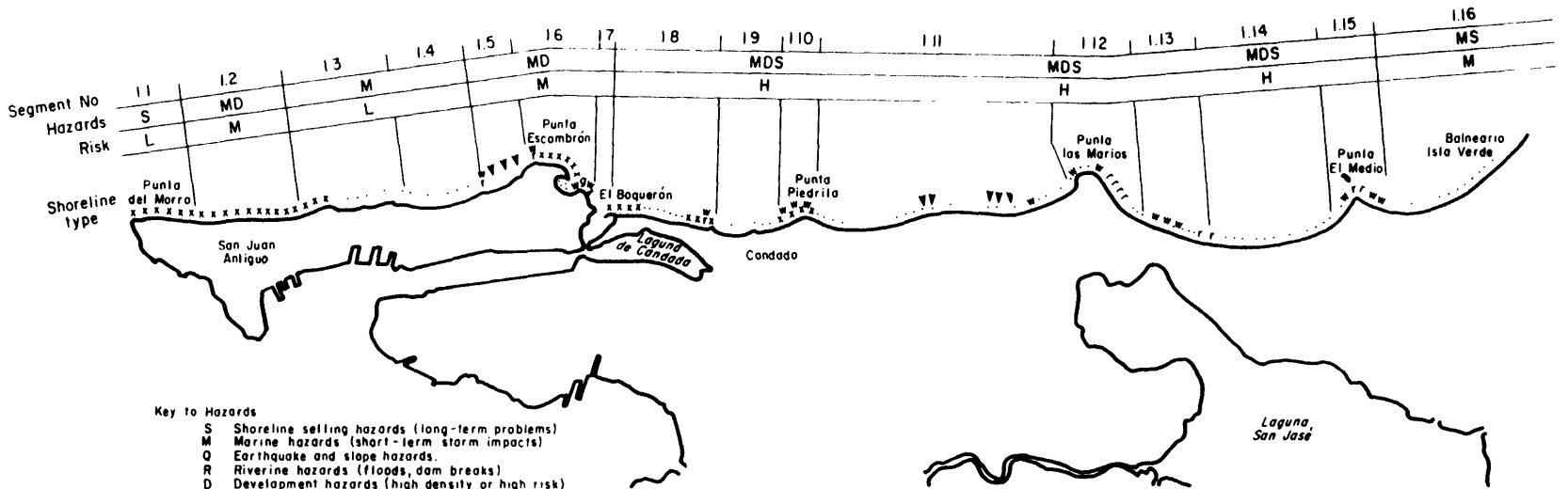

Key to Hazards

- S Shoreline setting hazards (long-term problems)
- M Marine hazards (short-term storm impacts)
- Q Earthquake and slope hazards.
- R Riverine hazards (floods, dam breaks)
- D Development hazards (high density or high risk)
- E Engineering hazards (construction or sand mining)

Key to Risk

- ≤ 1 Hazard = Low Risk
- 2 Hazard = Moderate Risk
- 3-4 Hazard = High Risk
- > 4 Hazard = Extreme Risk

Shoreline information (symbols placed offshore along coast):

Shoreline Type

- ..... sandy beach
- x x x natural rocky beach
- mmm mangroves
- b---b beachrock
- ---- submerged offshore rock or reef

Coastal Engineering Structures

- b breakwater
- w seawall
- g groin
- r riprap
- o outfall on the beach
- + extensive beach or dune sand mining

▼ overwash sand from Hurricane Hugo

N

0 1 mile

0 1 km

Fig. 3. Coastal Hazard Map 2 (Carolina Quadrangle). For location see Figure 1. While not as densely populated or developed as San Juan, this stretch of the shoreline contains an important recreational beach (Balneario Isla Verde segments 2.1 and 2.2), the international airport, and a beautiful stretch of beach with a single ocean-front road for access and evacuation (the Piñones road, Rt 187, running along the shore of shore of segments 2.6 to 2.13.

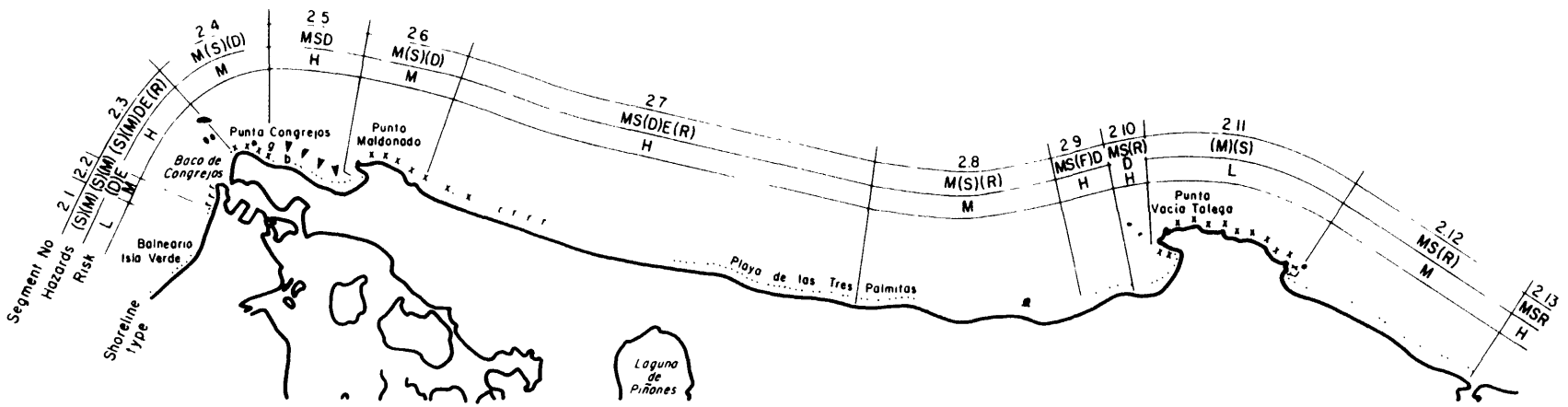

Shoreline information (symbols placed offshore along coast)

Shoreline Type
- sandy beach
- xxx natural rocky beach
- mmm mangroves
- b---b beachrock
- ---- submerged offshore rock or reef

Coastal Engineering Structures
- b breakwater
- w seawall
- g groin
- r riprap
- o outfall on the beach
- + extensive beach or dune sand mining

▼ overwash sand from Hurricane Hugo

Key to Hazards
- S Shoreline setting hazards (long-term problems)
- M Marine hazards (short-term storm impacts)
- Q Earthquake and slope hazards
- R Riverine hazards (floods, dam breaks)
- D Development hazards (high density or high risk)
- E Engineering hazards (construction or sand mining)

Key to Risk.
- ≤ 1 Hazard = Low Risk
- 2 Hazard = Moderate Risk
- 3-4 Hazard = High Risk
- > 4 Hazard = Extreme Risk

HISTORICAL SHORELINE ANALYSIS USING DIGITAL TECHNIQUES

William W. Danforth
(U.S. Geological Survey, Woods Hole, Massachusetts)
E. Robert Thieler
(Duke University, Durham, North Carolina)

OBJECTIVE

In order to accurately measure changes in shoreline location a methodology was developed in order to produce accurate digital shoreline position data using historical charts, maps, and aerial photographs and quantitatively measure the changes in shoreline position over time using these data.

RATIONALE

Accurate measurements of historical shoreline changes have become a prerequisite for coastal management as development in coastal areas has increased. Historical erosion rates, for example, are presently used in several states to locate oceanfront setback lines. Therefore, a critical need has developed among coastal researchers and policy-makers for a standardized method to obtain accurate shoreline position data, as well as a means to quantify changes in shoreline position over time. A number of methods exist to produce these data, however the approach and application vary considerably from method to method (e.g., Dolan and others, 1978; McBride, 1989; Letherman, 1984; Leatherman and Clow, 1983; Stafford and Langfelder, 1971). A standard quantitative (digital) method for generating shoreline position data not only facilitates the process of rectifying shoreline positions as seen on aerial photographs, but also allows data sets from different areas to be compared in a confident manner.

FIELDWORK

Shoreline positions in a suite of historical aerial photographs, taken between 1936 to 1989 of the northeastern coastline of Puerto Rico (San Juan to Humacao), were digitized and stored on a UNIX RISC-based computer. In addition, ground control points and shorelines from National Ocean Service T-sheets covering the study area were digitized to provide basemap control data. These data formed the basic "raw" data set necessary for designing a system that would produce digital shoreline position data.

Two software routines, the General Integrated Analytical Triangulation (GIANT) program (Elassal and Malhotra, 1987) and a program designed to yield a first estimate of camera parameters (position, pitch, roll, and yaw), were modified to form the core of the shoreline mapping system. A set of processing and support software were written to facilitate processing and reformatting of the digitized data, as well as providing a suitable interface that make the data entry and processing procedure more intuitive and easier for a novice computer user. The resulting software development constitutes the Digital Shoreline Mapping System (DSMS) (Danforth and Thieler, 1992a). All of this software with the exception of GIANT run on UNIX based computer systems. GIANT was written in Fortran and tailored to run on the VMS operating system. Output from DSMS is shoreline position data stored in two different ASCII data files. One file is a format that MapGrafix™, an Apple Macintosh®-based Geographic Information System (GIS), will recognize and the other is simply latitude and longitude information for each shoreline digitized.

A second set of software, named the Digital Shoreline Analysis System (DSAS) (Danforth and Thieler, 1992b), was written to quantify changes in shoreline positions over time. Output from DSAS calculates shoreline rates-of-change at user specified intervals along the digitized shoreline. DSAS runs on Unix-based systems, and utilizes standard ASCII files for input and output. The input format required by DSAS was designed to be entirely consistent with the ASCII output format from DSMS.

RESULTS

Most GIS computer software presently in use supports the digitization of maps and charts, and analyses of errors resulting from the transformation of digitizer coordinates to geographic coordinates. The transformation (scaling and rotation) of two-dimensional data required for maps is fairly straightforward (Evenden, 1991). In the case of analyses of aerial photographs, however, a more complex three-dimensional transformation is required to correct distortions within a photograph that are caused by scale changes, relief, and tilt displacement. Other sources of error inherent in aerial photography, such as atmospheric refraction, lens distortion, and media distortion, must also be removed. DSMS provides support for digitizing and transforming maps, but its primary emphasis is on the processing of digitized aerial photographs to remove most of these errors.

DSMS has several advantages over other shoreline mapping systems (Leatherman, 1983), including:

1. DSMS supports a wide variety of map projections and reference spheroids (see Evenden, 1990) for both map and photographic data.

2. DSMS offers distortion correction and user control of various parameters that affect the space resection solution for aerial photographs including:
   a) correction for atmospheric refraction;
   b) weighing of ground control and camera parameters to reflect *a priori* knowledge of their position;
   c) providing an initial estimate of camera position, altitude, and residual errors early in the mapping process to allow the user to check for bad data, and either redigitize or discard a given photograph;
   d) simultaneous triangulation of large groups of photographs, including photos of differing years, camera focal lengths, etc., using the same set of ground control points;
   e) adjustment to reflect the accuracy of the digitizing table and the digitizer operator and to reflect the elevation of the feature being mapped.

3. DSMS contains extensive facilities for examining error propagation and assessing the accuracy of photographic transformations.

4. DSMS is flexible in that standard ASCII files are used throughout the system, and output can be easily modified to conform to common GIS input file formats (e.g., Arc/Info, Atlas GIS, AutoCAD, Intergraph WMS, etc.).

5. DSMS can be used for mapping any feature that has a known, uniform elevation, such as wetland boundaries or lake/reservoir shorelines.

Shoreline positions calculated by DSMS from digitized aerial photographs for the years 1936-1987 are presented in Figure 1. It can be seen from the map that the popular bathing spot at Boca de Cangrejos has lost more than 100 m of shoreface since 1951. In order to quantify parameters such as the above rate of erosion, the results from DSMS are used in DSAS.

DSAS employs a measurement baseline approach (e.g., Leatherman and Clow, 1983) to calculate shoreline rates-of-change at a user-specified interval along the shoreline (Danforth and Thieler, 1992b). Using the output from DSMS (or any ASCII data file of compatible format), DSAS calculates shoreline rate-of-change data by using two programs. The first, called Transect, is used to specify the longshore spacing of transects along the measurement baseline (Fig. 1), determine the X-Y coordinates of each shoreline that lies along each transect, and input the dates associated with each shoreline position. An additional option allows the specification of a "tolerance distance" to be used to exclude data that lie more than the tolerance distance away from the baseline. The algorithm also includes a solution whereby transects are always measured at changes in the angle of the baseline, as occurs around tidal inlets, headlands, etc. where data are desired.

The second program, called Rates, computes the rate-of-change for each transect using the shoreline points and dates output from Transect. DSAS performs the four rate-of-change calculations reviewed by Dolan and others (1991) (end-point rate, average of rates, linear regression, and jackknifing) (Figs. 2 and 3). The output from Rates consists of tab-delimited ASCII files that can be used in spreadsheet and statistical software (e.g., Excel, Lotus 1-2-3, MATLAB, SAS, Wingz) for presentation and further data analysis. In summary, these methods provide a measure of the change in shoreline position over time. The first, simplest, and most widely used method is the End Point Rate (epr) technique where the total shoreline movement for a shoreline position along a transect is divided by the elapsed time between measurement dates. Generally, the earliest and latest dates for a set of measurements are used. The second method, Average of Rates (aor), takes the epr method a step further by averaging all possible epr combinations from a shoreline transect data set (of more than two points) that meet a minimum time criterion (a summation of estimated or measured error in each two end points divided by the largest epr for the data set). Each epr that survives the criterion is used in the average. The third method, Linear Regression (lr), fits a line through the entire transect of shoreline positions using a least squares fit. The slope of this best fit line is the shoreline rate of change. Lastly, Jacknifing (jk) extends the concept of the lr method to try and minimize biasing of any one data point or points on the entire set, particularly if the data set is clustered. The jk method iterates through the data set, calculating the lr line for all data points minus one, then averages all the calculated regression line slopes.

Results of shoreline analysis using DSMS and DSAS for the area in Puerto Rico affected by Hurricane Hugo are presented in Richmond and others (this report), however a subset is presented in Figures 1-3. Shoreline positions calculated by DSMS for areas not adversely affected by Hurricane Hugo were verified by field checks, indicating the reliability of the system for shoreline mapping. Error estimates for each aerial photograph are ± 8 m for digitized shoreline positions. Careful digitizing techniques as well as a large-format digitizing table with good resolution will tend to bring these estimates down. The photo error estimate translates into an epr resolution of about 0.3 m/yr (18 m maximum error divided by the 51 yr time frame for two common shoreline dates, 1936 and 1987).

Thus, everything we see that exceeds 0.3 m is probably real (i.e., the rate exceeds the signal to noise ratio for that particular time span). We use 0.5 m/yr as an estimate error, given the fact that much of the data span only 30 or so years, but have a number of shorelines in that 30-yr timespan (e.g., '51, '63, '64, '80, '87). A visual inspection of a plot of shoreline position versus time for each of those years show that our error estimate is not unrealistic. In addition, areas that have rocky headlands plotted consistently within the digitized photo error estimate of ± 8 m for different years, showing that as long as the digitization procedure is carefully executed, DSMS will accurately calculate shoreline positions as seen on a suite of historical aerial photographs. For the aor calculations, we used 0.5 m/yr as the minimum criterion for inclusion in the aor calculations. Thus, the results from DSAS, shown in Figures 2-4, can be interpreted with a high degree of confidence, and provide a useful tool for documenting historical shoreline changes.

FUTURE PLANS

The DSMS and DSAS software is available in its present form (Danforth and others, 1992a, 1992b). Giant is being ported to the UNIX operating system and should be operational in 1993. In addition, ASCII output formats that other GIS systems recognize, such as Arc/INFO, are being added to the software package.

Fig. 1. Map showing shoreline positions digitized from a suite of historical aerial photographs using the Digital Shoreline Mapping System (DSMS). The shoreline positions were digitized from a series of historical aerial photographs taken of the San Juan metropolitan area, Puerto Rico, dating from 1951 to 1987 (see Richmond and others and Bush and others, this report). Note the severe erosion that has taken place along Balineario Isla Verde (see Figure 2 for rates of erosion). These data can be analyzed using the Digital Analysis System (DSAS) to produce useful shoreline rates-of-change calculations.

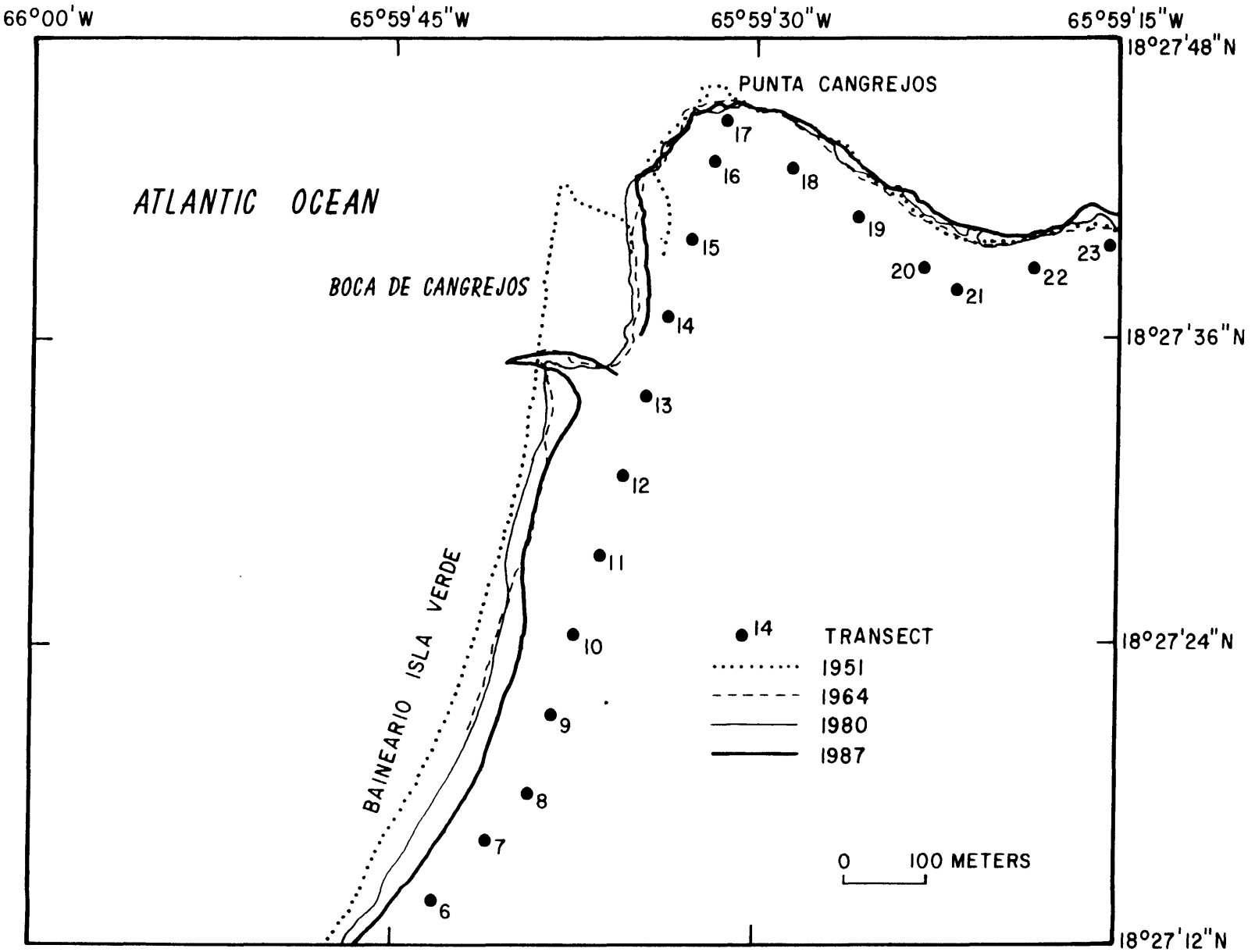
66°00'W
65°59'45"W
65°59'30"W
65°59'15"W
18°27'48"N
18°27'36"N
18°27'24"N
18°27'12"N
PUNTA CANGREJOS
ATLANTIC OCEAN
BOCA DE CANGREJOS
BAINEARIO ISLA VERDE
17
16
18
19
15
23
20
22
21
14
13
12
11
10
9
8
7
6
14 TRANSECT
1951
1964
1980
1987
0 100 METERS

Fig. 2. Rates of change data calculated from the shoreline position data shown in Figure 1 using DSAS. Transect numbers correspond to transect locations shown if Figure 1 and as tabulated in Table 1. The top half of the figure shows rates calculated using the End Point Rate method (epr), and the bottom shows calculations using the Average of Rates method (aor). Positive numbers reflect shoreline accretion and negative numbers reflect shoreline erosion.

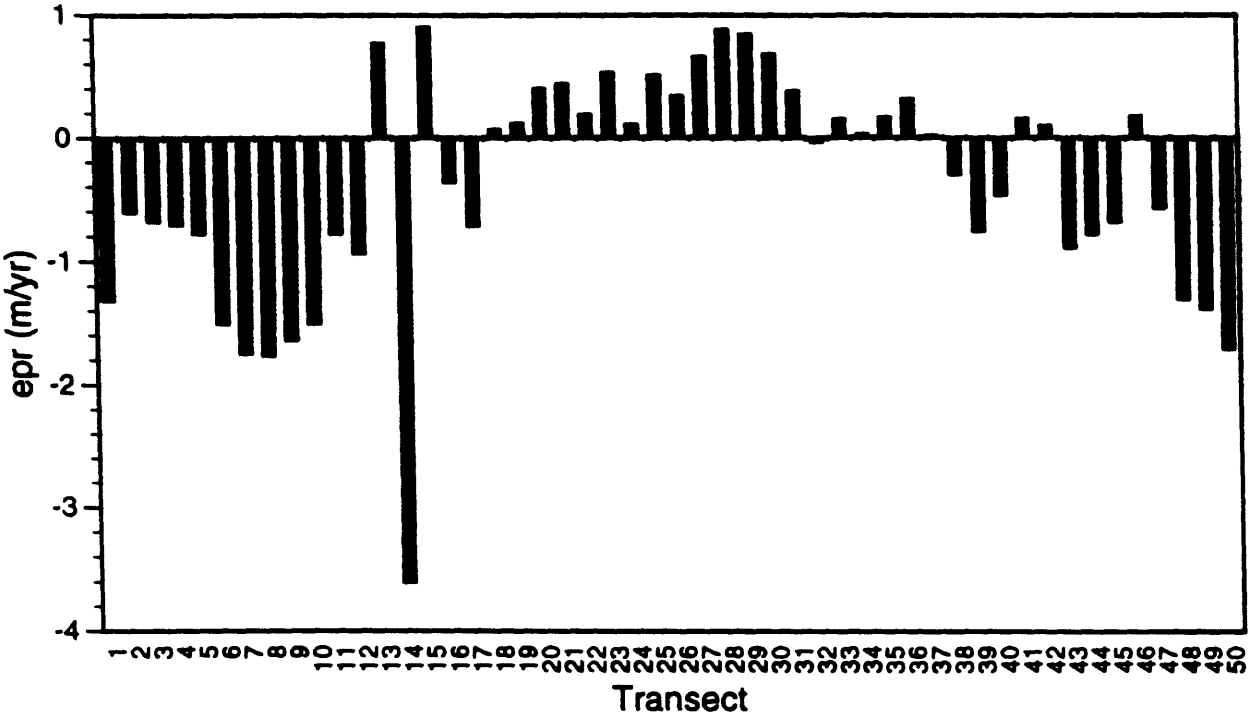
epr (m/yr)
1
0
-1
-2
-3
-4
1 2 3 4 5 6 7 8 9 10 11 12 13 14 15 16 17 18 19 20 21 22 23 24 25 26 27 28 29 30 31 32 33 34 35 36 37 38 39 40 41 42 43 44 45 46 47 48 49 50
Transect

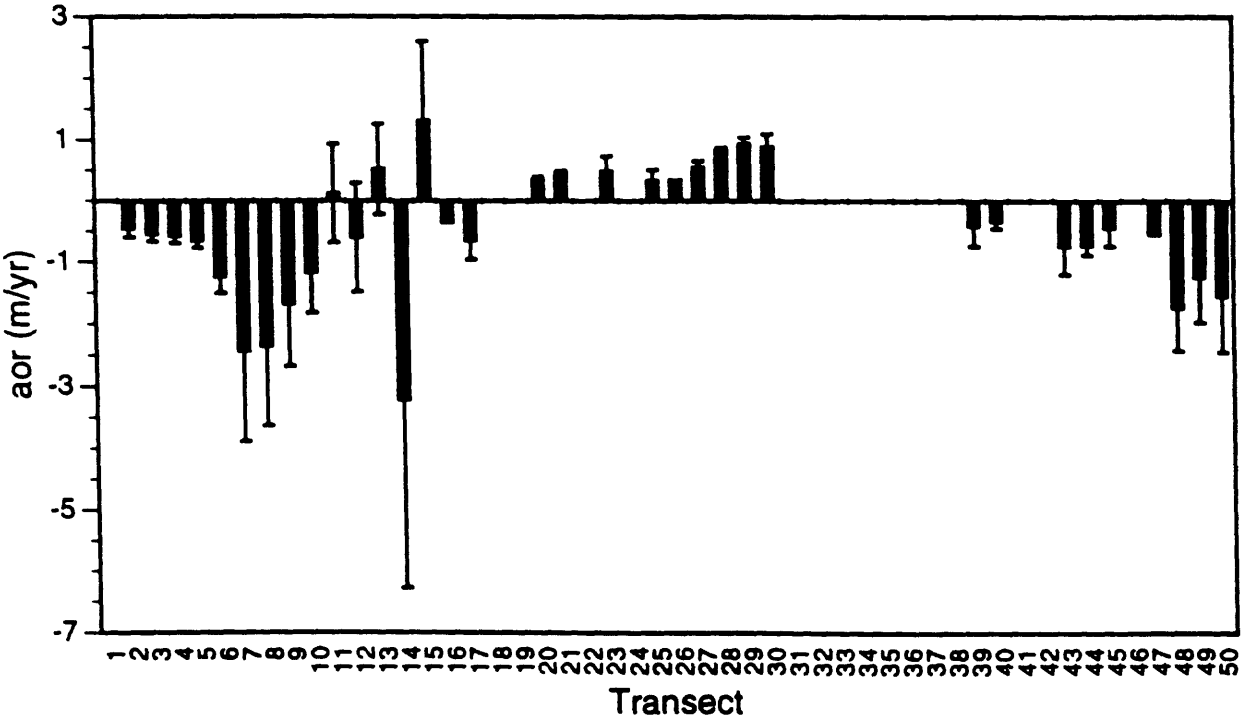
aor (m/yr)
3
1
-1
-3
-5
-7
1 2 3 4 5 6 7 8 9 10 11 12 13 14 15 16 17 18 19 20 21 22 23 24 25 26 27 28 29 30 31 32 33 34 35 36 37 38 39 40 41 42 43 44 45 46 47 48 49 50
Transect

Fig. 3. Graph showing rates of change data calculated using DSAS. This graph was created using the shoreline position data shown in Figure 1, and displays rates-of-change data from the years 1936 to 1987 as calculated by the linear regression method in DSAS. Transect numbers correspond to transect locations shown in Figure 1 and as tabulated in Table 1. Positive numbers reflect shoreline accretion and negative numbers reflect shoreline erosion.

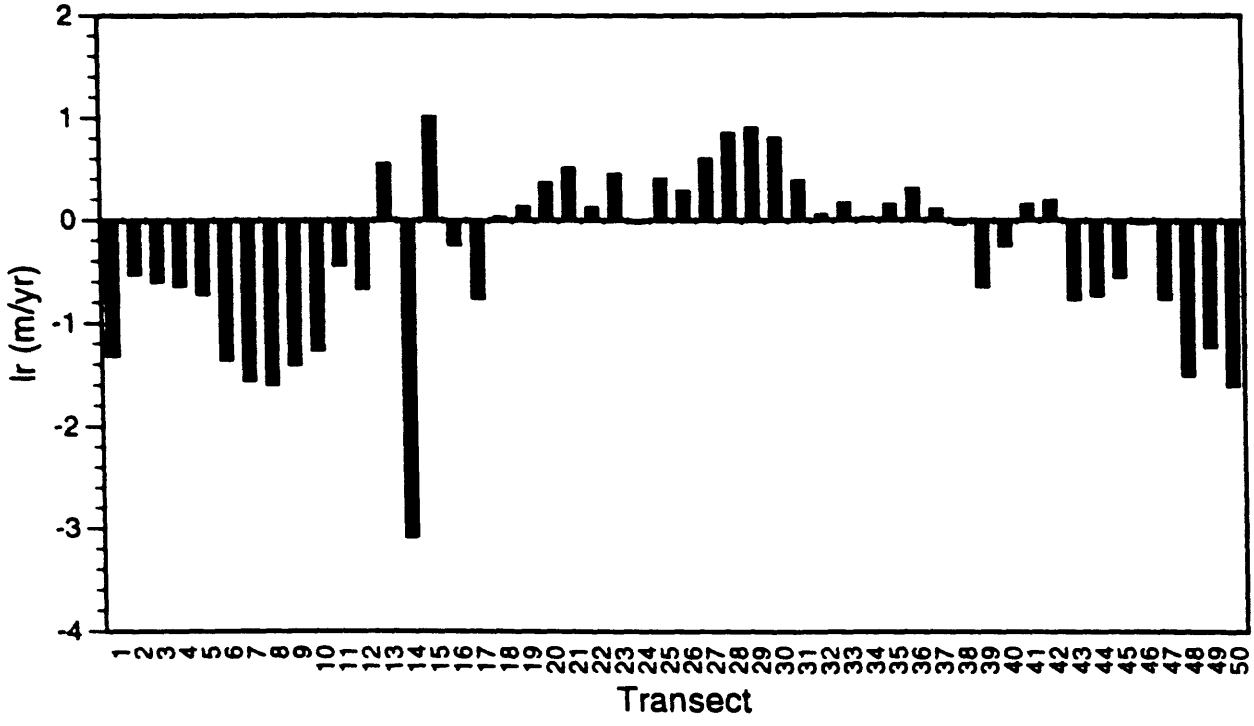
2
1
0
-1
-2
-3
-4
lr (m/yr)
1 2 3 4 5 6 7 8 9 10 11 12 13 14 15 16 17 18 19 20 21 22 23 24 25 26 27 28 29 30 31 32 33 34 35 36 37 38 39 40 41 42 43 44 45 46 47 48 49 50
Transect

EFFECTS OF HURRICANE HUGO ON OFFSHORE SAND DEPOSITS

Catherine M. DeLorey, Lawrence J. Poppe
(U.S. Geological Survey, Woods Hole, Massachusetts)
Rafael W. Rodriguez
(U.S. Geological Survey, Sand Juan, Puerto Rico)

OBJECTIVE

The Escollo de Arenas is one of three major offshore sand and gravel deposits situated on the insular shelf of Puerto Rico. This deposit was thought to have been negatively impacted by Hurricane Hugo (Rodriguez and others, 1992). This study describes the present condition of the Escollo de Arenas through the use of aerial photographs, bathymetric data, high-resolution seismic-reflection profiles and sediment samples collected after Hurricane Hugo. These data are used to determine how and to what extent this deposit was changed by the hurricane.

RATIONALE

The Escollo de Arenas is an elongate shoal that extends 6 km into Vieques Passage from the northwest corner of Vieques Island, Puerto Rico (Fig. 1). The shoal is composed of approximately 90 million m^3 of Holocene sand and gravel. With the depletion of suitable onshore sand and gravel deposits for the construction industry and beach replenishment projects, the Escollo de Arenas was studied in detail prior to Hurricane Hugo (Grove and Trumbull, 1978; Rodriguez, 1979; Rodriguez and Trias, 1989) to assess it as a potential resource. These previous studies described the location, areal extent and morphology as well as sediment thickness and volume, sediment-type distribution, and the effect of tidal currents on the deposit and serve as a benchmark for what the Escollo de Arenas looked like before the impact of Hurricane Hugo. This study describes the present condition of the Escollo de Arenas through the use of aerial photographs, bathymetry, high-resolution seismic-reflection profiles, and sediment samples collected after Hurricane Hugo. These data are used to determine how and to what extent this deposit was changed by the hurricane.

A post-Hugo aerial reconnaissance survey suggested that the Escollo de Arenas had been significantly altered as a result of Hurricane Hugo (Fig. 2). This suggestion was based on comparison of its appearance to a pre-Hugo photograph (Fig. 3). Because it was unclear how extensive the changes to the Escollo de Arenas had been as a result of Hurricane Hugo, seismic-reflection profiles were collected to assess changes in the internal structure of the deposit, bathymetric data were collected to define any large scale changes in its morphology, aerial photographs were taken to define finer scale morphologic changes, and sediment samples were collected on and around the shoal to define changes in the distribution of surficial sediments.

FIELDWORK

Fieldwork was conducted aboard the research vessel JEAN A in October - November, 1990. Navigation for all the data was by a shore-based Miniranger Falcon IV navigation system which has as accuracy of +/- 4m.

A total of 116 line km of high-resolution seismic-reflection and bathymetric data were collected using a Huntec Sea Otter system, a 3.5-kHz subbottom profiler, and a 24 kHz Odem echosounder. These data were digitally recorded and corrected for tidal variations following the cruise.

Surface sediment samples were collected at 28 locations using a Shipek grab sampler and 11 sediment cores up to 262 cm long (Fig. 4). Nine of the cores were obtained using a short diver-assisted hammer-coring device, and two were obtained using a hydraulically powered, diver-operated vibrating corer. Analyses of calcium carbonate content and grain size distribution were performed at Puerto Rico's Department of Natural Resources sedimentological laboratories using methods similar to those described by Rodriguez and Trias (1989).

RESULTS

An isopach map of the Escollo de Arenas study area showing the thickness of Holocene sediment above an underlying Pleistocene substrate was produced from analysis of the seismic-reflection profiles (Fig. 5). This map shows that the Escollo de Arenas pinches out along its western extent where an underlying Pleistocene surface crops out, but thickens to 45 feet (14 m) in the central and eastern portions of the deposit. The similarity of this isopach map to the pre- Hugo isopach map of Rodriguez and Trias (1989) indicates that large-scale changes affecting the internal structure (sediment volume) and overall shape of the Escollo de Arenas did not occur.

Changes of a smaller scale that affected only the surficial sediment of the deposit are readily apparent upon comparison of pre- and post-Hugo aerial photographs (Fig. 6). Numerous northwest-southeast trending sand waves are prominent in the pre-Hugo photograph, but these are not as numerous and their expression is suppressed in the post-Hugo photograph. In addition, changes in the areal extent of the deposit are also suggested by the disparity in the aerial photographs between the pre- versus post-Hugo Thalassia grass/sand body boundary. Thalassia is present over most of the shelf which surrounds the shoal, and the photographs suggest that there has been an increase in the areal extent of the sand deposit both along its southwestern and northeastern sides (Fig. 6).

Small-scale alterations affecting the surficial sediments of the Escollo de Arenas are also manifested as changes to the bathymetry. Although the overall shape and location of the Escollo de Arenas are the same before and after the hurricane, changes affecting the fine-scale relief of the deposit have occurred. In the pre-Hugo bathymetry (Fig. 7), 1,100 m separates the 30-foot (9 m) contour whereas this distance is increased to 1,550 m in the post- Hugo data (Fig. 4). The effects of storm waves on the Escollo de Arenas resulted in levelling of preexisting sand waves and a broadening of the deposit along its entire length. Sand waves that measured 2 m in height prior to Hugo evidently have been reduced in height with the effect of laterally redistributing the sediment of which they were composed, resulting in an overall broadening of the deposit.

Sediment samples collected at sites occupied during a study prior to Hurricane Hugo (Rodriguez and Trias, 1989) were analyzed to assess surficial storm-related compositional and textural changes to the surface sediments. Sediments of the Escollo de Arenas are still much coarser than the surrounding sediments, but carbonate gravel content does not exceed 20 percent after the storm while it exceeded 60 percent in places prior to the storm (Fig. 10). These gravel deposits presumably are now covered by sand-sized material from the sand waves that were "knocked-down" by the storm. Similarly, areas

that had contained greater percentages of the silt and clay fraction, such as the adjacent Thalassia meadows to the east, are now covered by coarser (sand- and gravel-sized) material removed from the crest of the shoal (Fig. 11). Some of the sediments from the Thalassia meadows contained over 4 percent silt and clay prior to the storm, but the surficial sediments in these areas now have generally less than 1 percent silt and clay (Fig. 12). The calcium carbonate content of the surficial sediments still increases with distance seaward along the Escollo de Arenas and into the Thalassia meadows southwest and northeast of the sand body (Rodriguez and Trias, 1989; Fig. 13). However, carbonate percentages are significantly lower in the Thalassia meadows than prior to HUGO. Inasmuch as the carbonate content of the surficial sediments of the Thalassia meadows was near 100 percent before HUGO, the present distribution of carbonate content values suggests that the siliclastic fraction can be used as a tracer to show the areal extent of the sediments lost from the deposit during the storm.

A coarse layer of carbonate fragments was observed in the upper portions of the hammer cores collected off the northeastern flank of the Escollo de Arenas (Fig. 14). This layer, which is distributed over an area of about 7.4 km^2, forms a wedge that is about 10 cm thick near the shoal, but thins toward the north and east. This wedge of coarse sediment pinches out about 1.2 km to the east of the shoal. Inasmuch as a surficial coarse layer covering the muddy Thalassia beds was not described during studies preceding Hugo (Rodriguez and Trias, 1989), these coarse sediments probably represent a deposit formed as a result of Hugo. The sediments in this layer consist of a mixture of ripped up organic-rich, poorly sorted, muddy calcareous sands typical of the Thalassia beds in this area and a component of gravelly sand presumably swept from the Escollo de Arenas. The fine-grained nature of the underlying strata suggests that the energy of the environment normally is much lower here and, therefore, any loss of the sand and gravel from the shoal into this area is permanent. Assuming that the average thickness of this wedge is 5 cm, the volume of sediment in this coarse layer is roughly 371,500 m^3 or slightly less than 4 percent of the volume of the sand and gravel originally estimated to be present in this deposit (Rodriguez and Trias, 1989). However, this estimated loss should be considered a maximum because at least some portion of this coarse bed was contributed as rip up clasts from the pre-existent Thalassia beds. Most of the hammer cores were collected to the east of the Escollo de Arenas because any sediment loss to the west is probably not permanent due to the thin sandy nature of the bottom sediment over the lithified Pleistocene substrate and the dominant northward (toward the Escollo de Arenas) movement of the bottom currents and sediment.

Interestingly, a vibra-core, which was collected just beyond the eastern edge of the Hugo-deposited coarse sediment wedge contained numerous other coarse-grained sediment layers deeper in the core intercalated with muddy carbonates (Core VC 1; Fig. 4). Many of these coarse layers contain gravel-sized faunal remains (such as coral fragments) that were not indigenous to the muddier sediments of the Thalassia meadows. These layers suggest that many earlier storms, perhaps much more devastating to the Escollo de Arenas than Hugo, have previously impacted the area.

FUTURE PLANS

Examination of existing data related to the Escollo de Arenas is complete and results will be published as a USGS Miscellaneous Field Studies Map in 1993. These data and derivative mapping products will also be released on CD ROM in 1994.

Fig. 1. Map showing the location of the Escollo de Arenas. North is towards the top of the photograph.

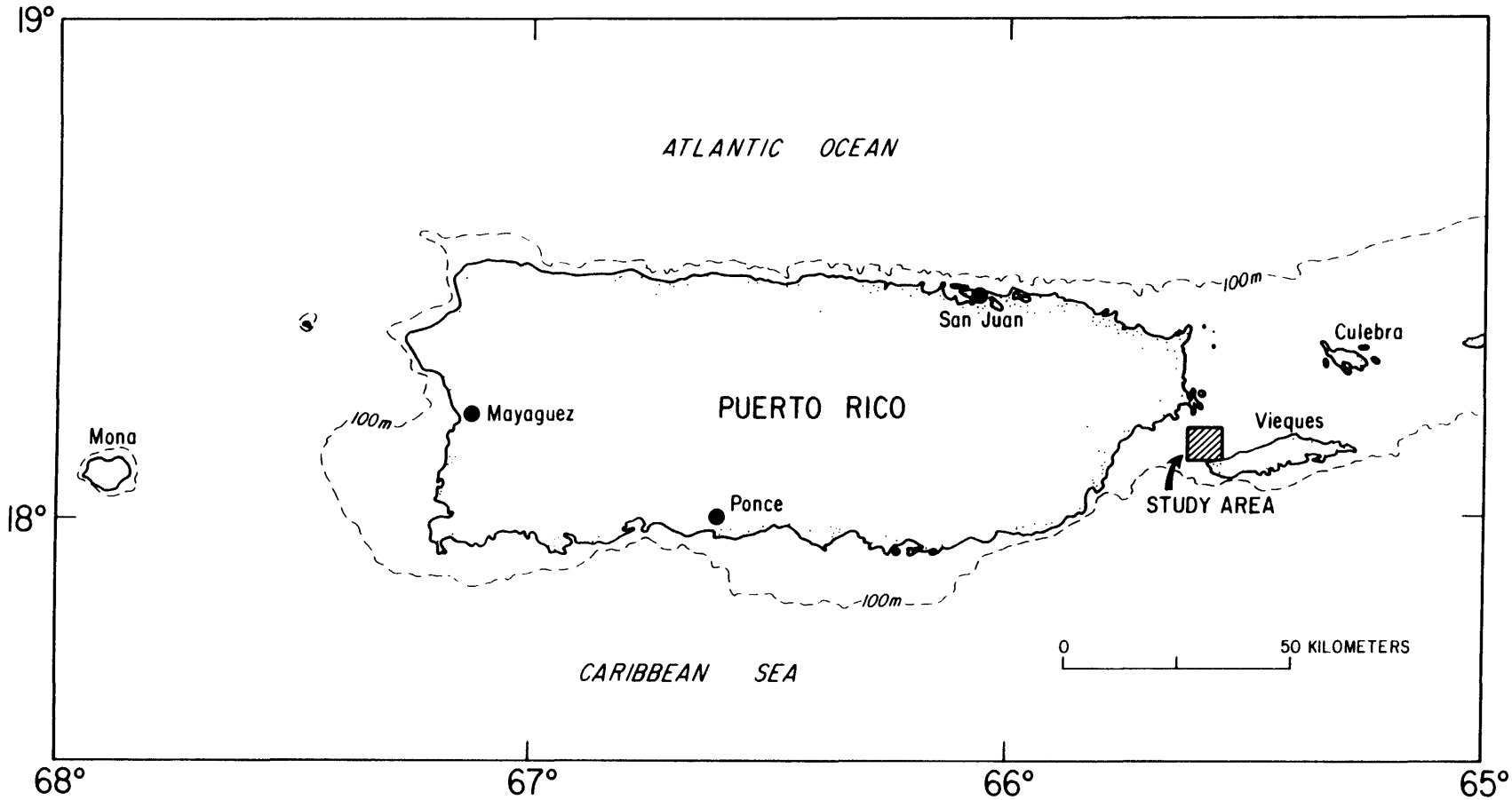
19°
18°
68°
67°
66°
65°
ATLANTIC OCEAN
CARIBBEAN SEA
PUERTO RICO
San Juan
Culebra
Mayaguez
Ponce
Mona
Vieques
STUDY AREA
100m
100m
100m
0
50 KILOMETERS

4/6 a

Fig. 2. Post-Hugo aerial photograph of Escollo de Arenas. North is towards the top of the photograph. Note that sand ridges on the Escollo de Arenas are suppressed in comparison to the pre-Hugo photograph. See Figure 6 for scale.


ESCOLLO DE ARENAS,
AFTER HUGO

Fig. 3. Pre-Hugo aerial photograph of all but the northern limit of the Escollo de Arenas showing prominent sinuous-crested sand waves extending parallel to the axis of the shoal (from Rodriguez and Trias, 1989). See Figure 6 for scale.

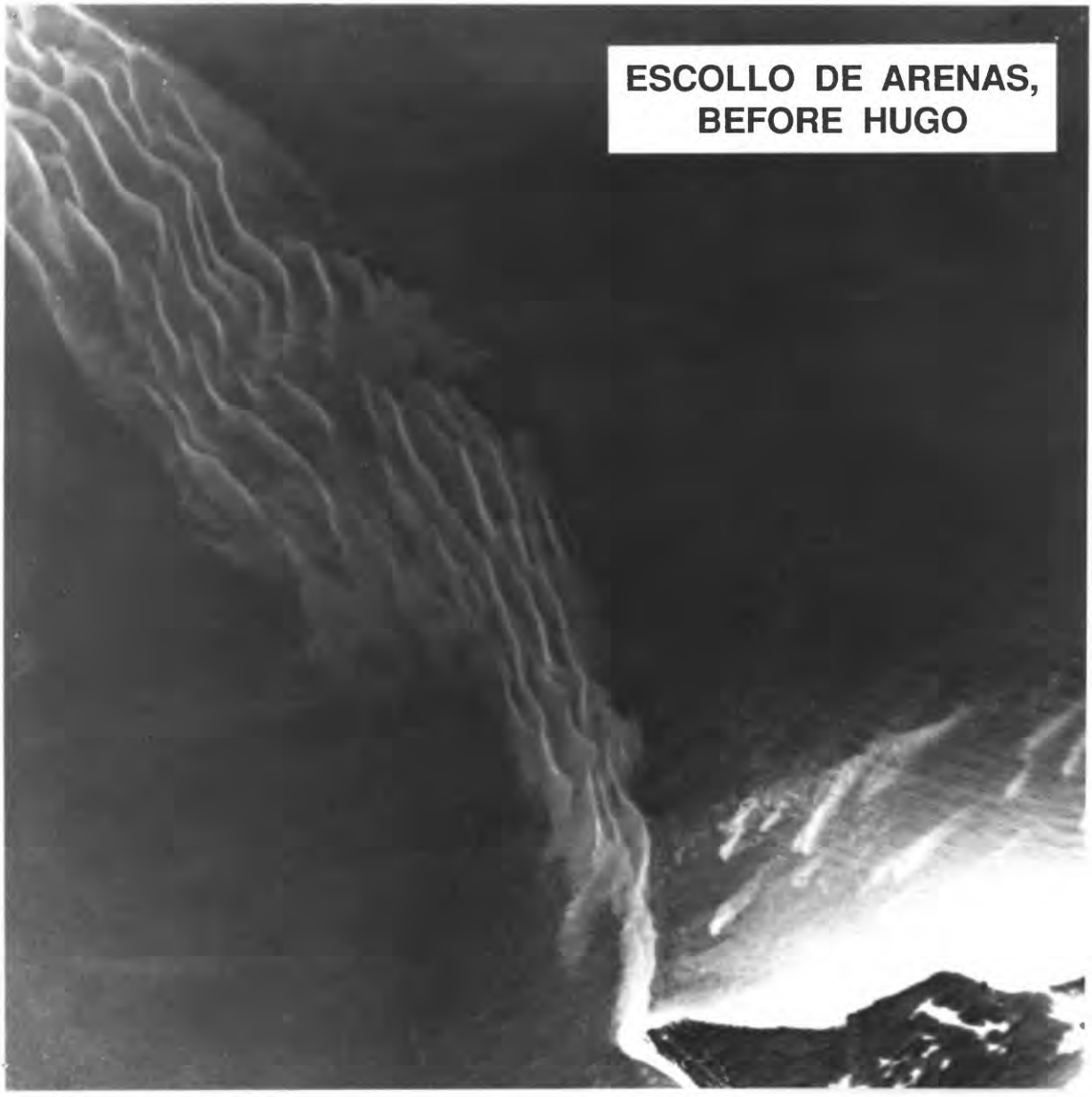
ESCOLLO DE ARENAS,
BEFORE HUGO

Fig. 4. Map showing post-Hugo bathymetry of the Escollo de Arenas (depth in feet in order to compare to pre-Hugo data; Fig. 7). Also shown are sample locations and cross section locations (Fig. 9). Although the overall shape and location of the Escollo de Arenas are the same before and after the hurricane, changes affecting the fine-scale relief have occurred (see Figs. 8 and 9).

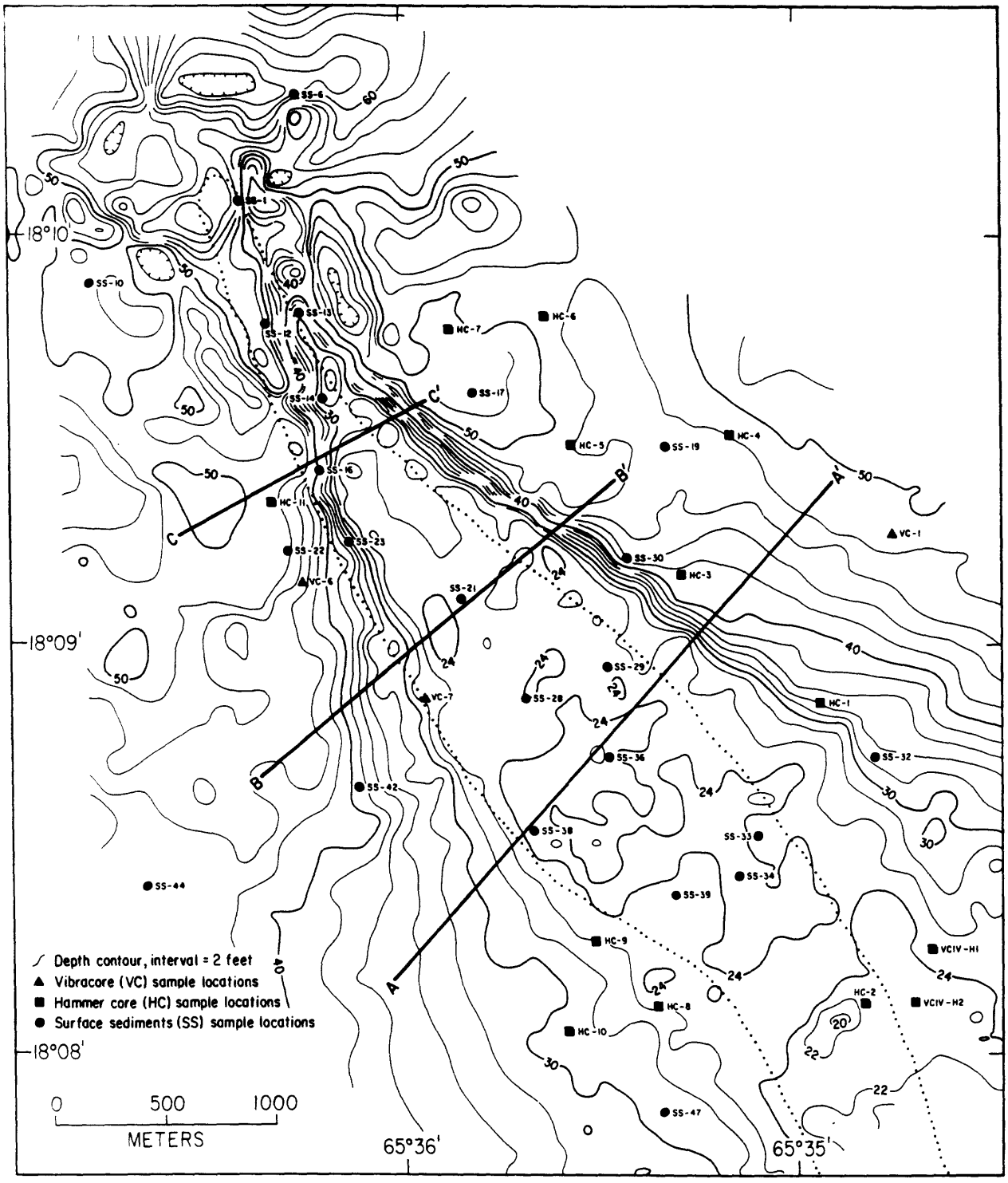
18°10'
18°09'
18°08'
65°36'
65°35'
SS-6
SS-1
SS-10
SS-13
SS-12
SS-14
SS-17
SS-16
SS-22
SS-23
SS-21
SS-30
SS-29
SS-28
SS-36
SS-32
SS-42
SS-38
SS-33
SS-34
SS-39
SS-44
SS-47
HC-7
HC-6
HC-5
SS-19
HC-4
HC-11
HC-3
HC-1
HC-9
HC-8
HC-10
HC-2
VC-1
VC-6
VC-7
VCIV-H1
VCIV-H2
A
A'
B
B'
C
C'
Depth contour, interval = 2 feet
Vibracore (VC) sample locations
Hammer core (HC) sample locations
Surface sediments (SS) sample locations
0
500
1000
METERS

Fig. 5. Isopach map showing thickness, in feet, of Holocene sand and gravel deposit.

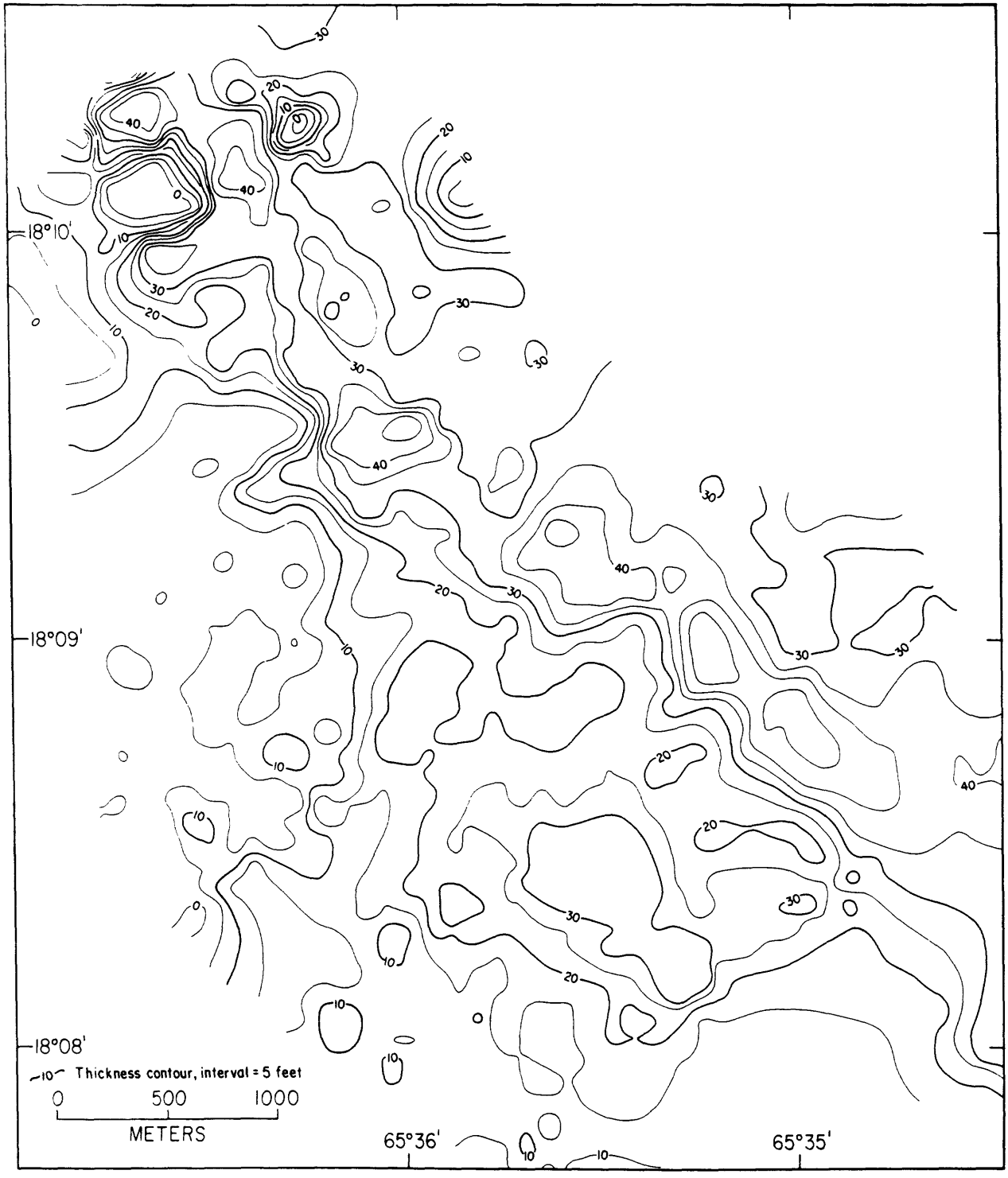
18°10'
18°09'
18°08'
65°36'
65°35'
10 Thickness contour, interval = 5 feet
0 500 1000
METERS

Fig. 6. Map showing the disparity in aerial extent of pre- versus post-Hugo Thalassia grass—sand boundary as suggested by comparison of pre- versus post Hugo aerial photographs (Figs. 2 and 3).

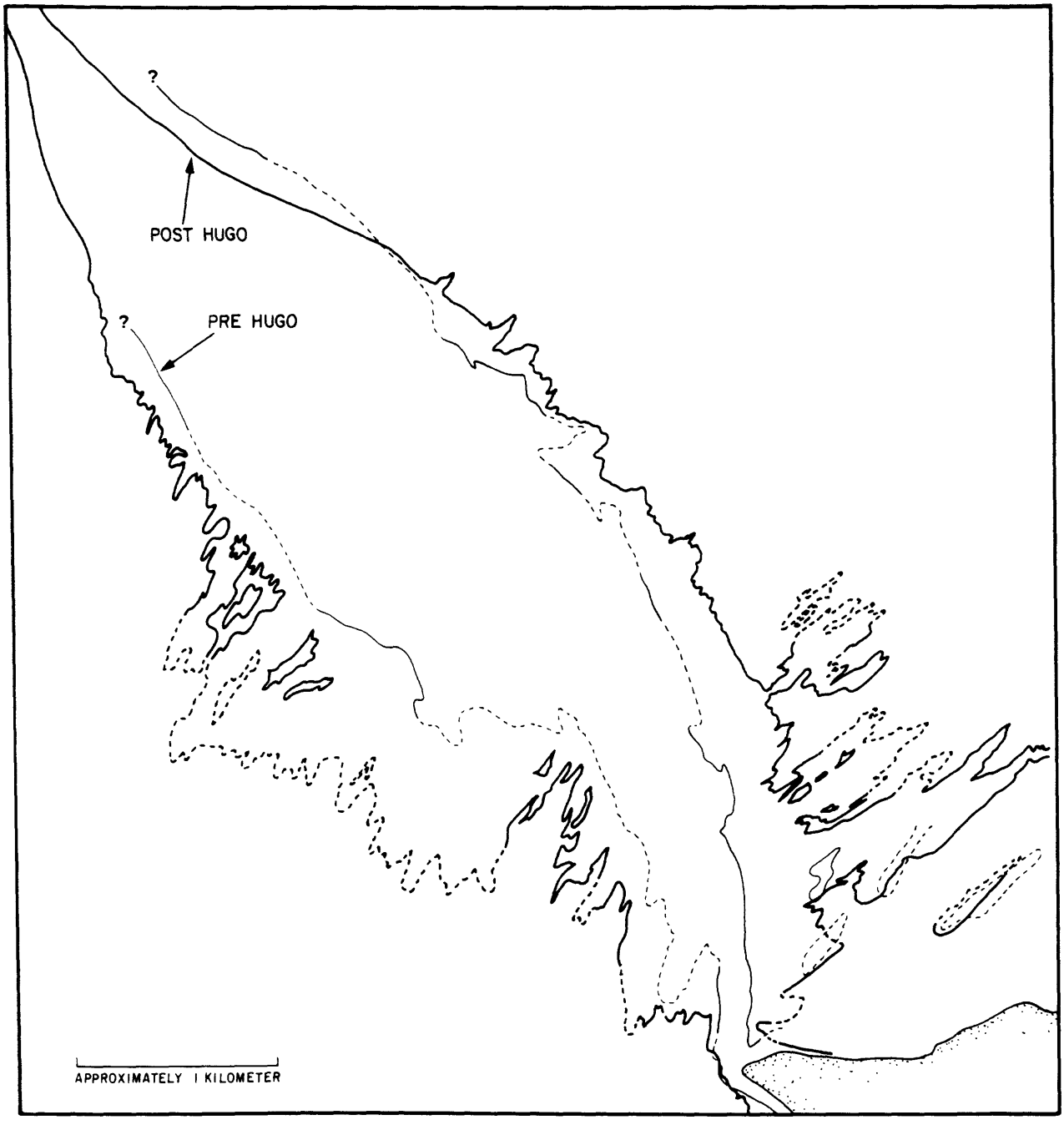
?
POST HUGO
?
PRE HUGO
APPROXIMATELY 1 KILOMETER

Fig. 7. Map showing pre-Hugo bathymetry of the Escollo de Arenas and surrounding area (from Rodriguez and Trias, 1989). Also shown are cross sections locations (Fig. 8).

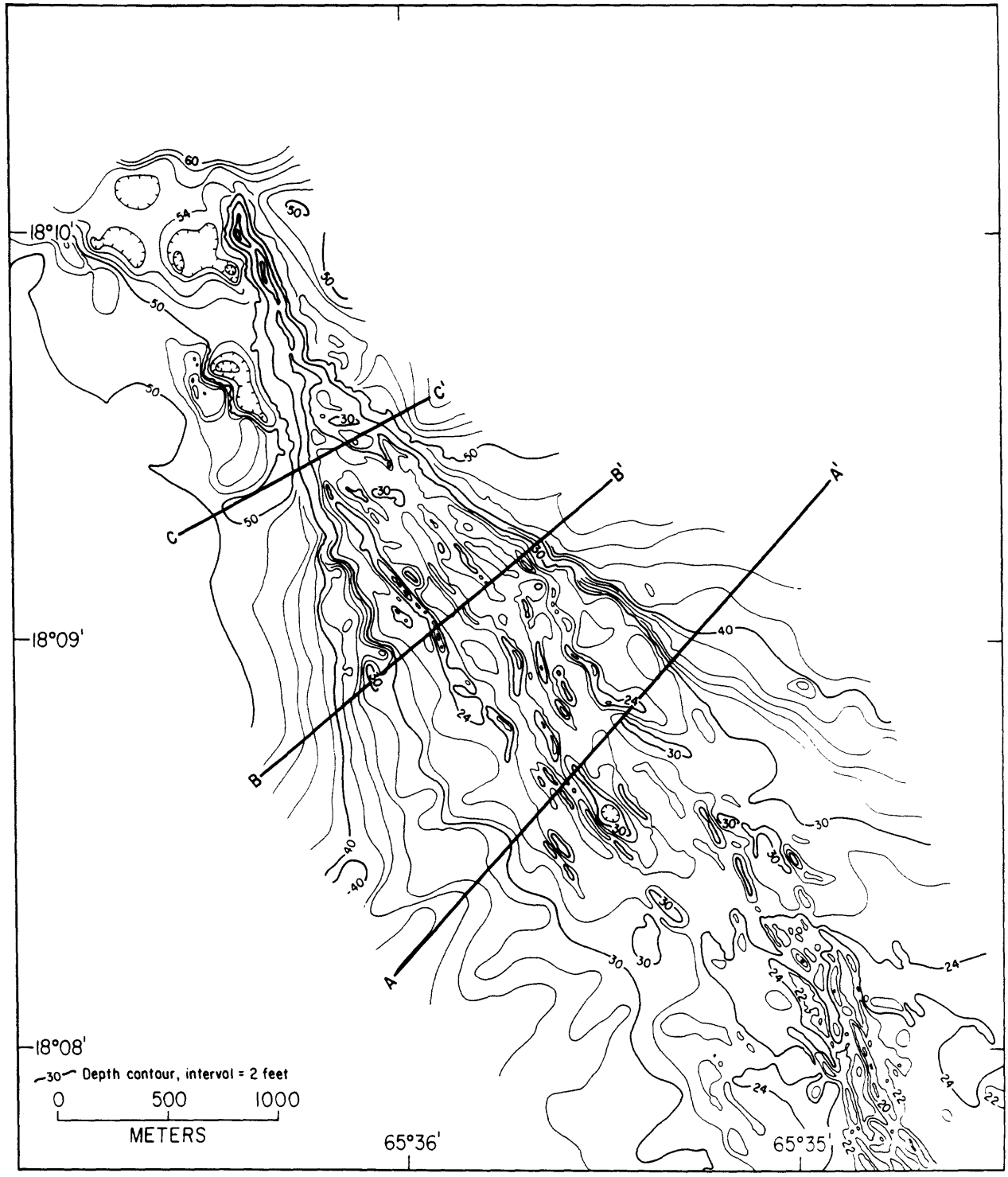
18°10'
18°09'
18°08'
65°36'
65°35'
A
A'
B
B'
C
C'
60
54
50
40
30
24
22
-30- Depth contour, interval = 2 feet
0
500
1000
METERS

Fig. 8. Pre-Hugo geologic cross sections over the Escollo de Arenas. Locations shown on Figure 7. The same cross sections after Hurricane Hugo show a general flattening of sand ridges caused by the storm (Fig. 9).

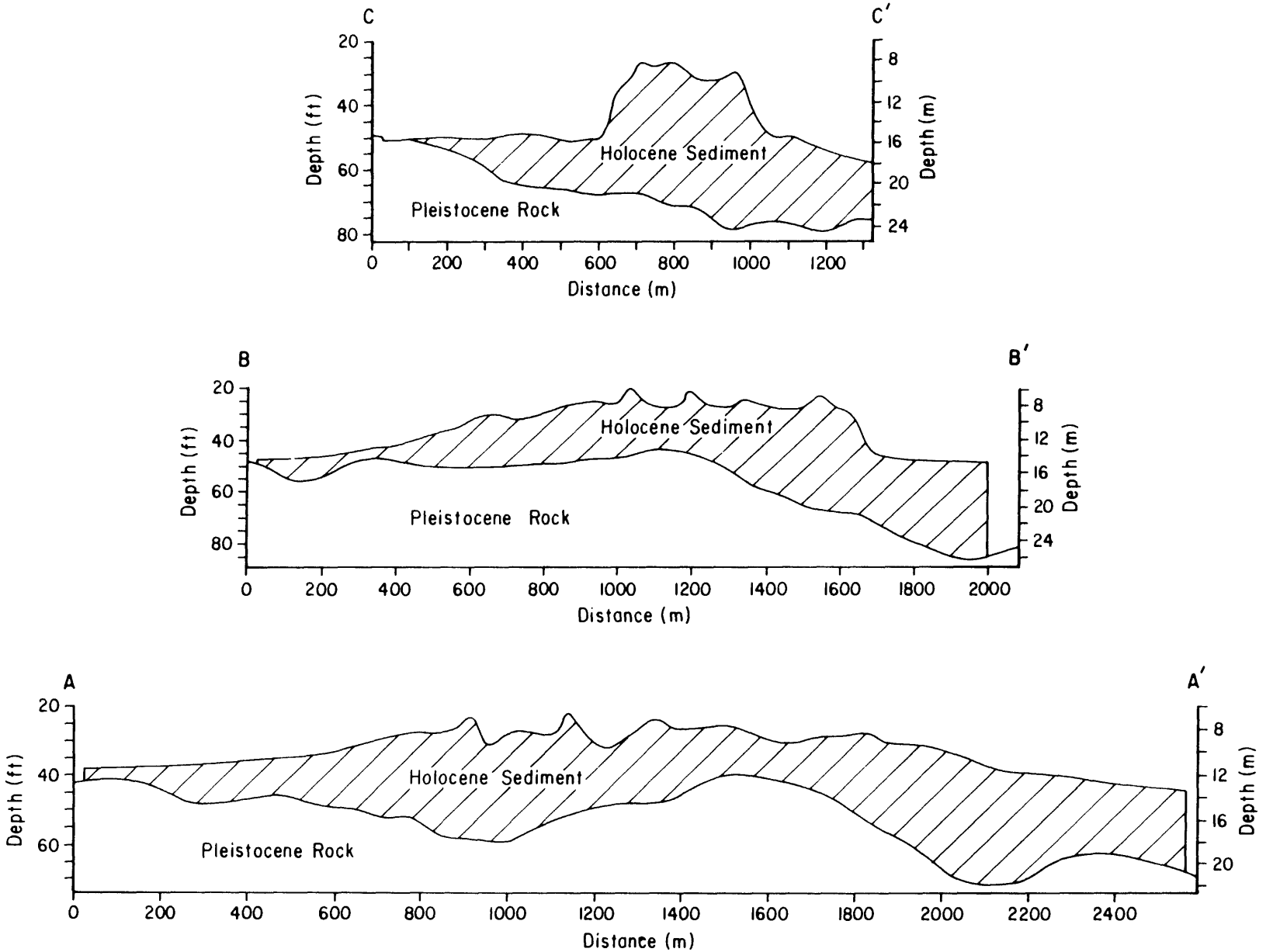
C
C'
Depth (ft)
20
40
60
80
Depth (m)
8
12
16
20
24
Holocene Sediment
Pleistocene Rock
0
200
400
600
800
1000
1200
Distance (m)
B
B'
Depth (ft)
20
40
60
80
Depth (m)
8
12
16
20
24
Holocene Sediment
Pleistocene Rock
0
200
400
600
800
1000
1200
1400
1600
1800
2000
Distance (m)
A
A'
Depth (ft)
20
40
60
Depth (m)
8
12
16
20
Holocene Sediment
Pleistocene Rock
0
200
400
600
800
1000
1200
1400
1600
1800
2000
2200
2400
Distance (m)

Fig. 9 Post-Hugo geologic cross sections over the Escollo de Arenas. Locations shown on Figure 4. Compare to Figure 8 to view changes to the Escollo de Arenas caused by Hurricane Hugo.

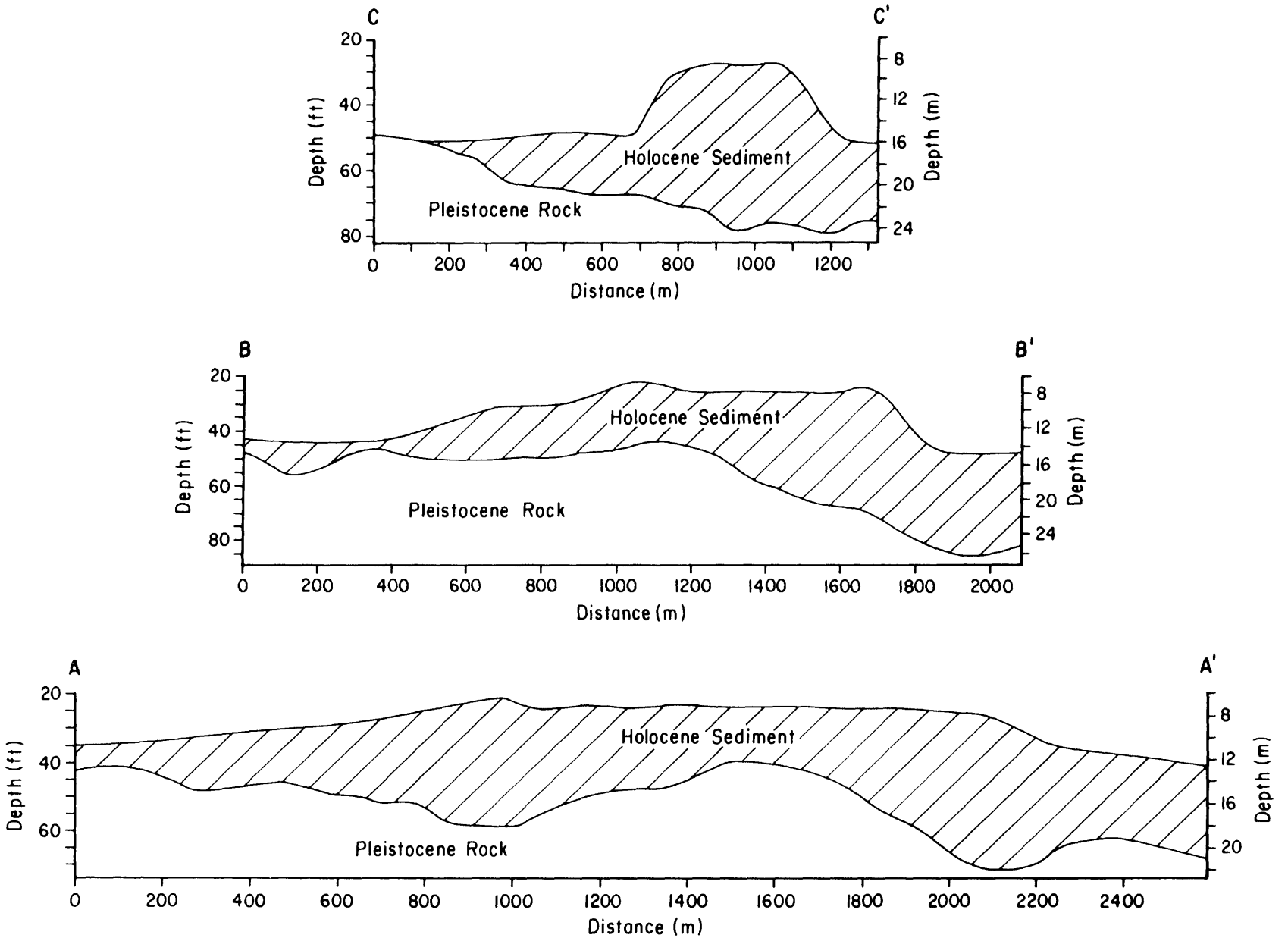
C
C'
Depth (ft)
20
40
60
80
Depth (m)
8
12
16
20
24
Holocene Sediment
Pleistocene Rock
0
200
400
600
800
1000
1200
Distance (m)
B
B'
Depth (ft)
20
40
60
80
Depth (m)
8
12
16
20
24
Holocene Sediment
Pleistocene Rock
0
200
400
600
800
1000
1200
1400
1600
1800
2000
Distance (m)
A
A'
Depth (ft)
20
40
60
Depth (m)
8
12
16
20
Holocene Sediment
Pleistocene Rock
0
200
400
600
800
1000
1200
1400
1600
1800
2000
2200
2400
Distance (m)

Fig. 10. Weight percentage of surficial bottom sediment that is gravel (> 2.0 mm). Heavy contours show the results of this study (post-Hugo); light contours show the pre-Hugo gravel distribution and dashed lines show the outline of the Escollo de Arenas before Hurricane Hugo (from Rodriguez and Trias, 1989).

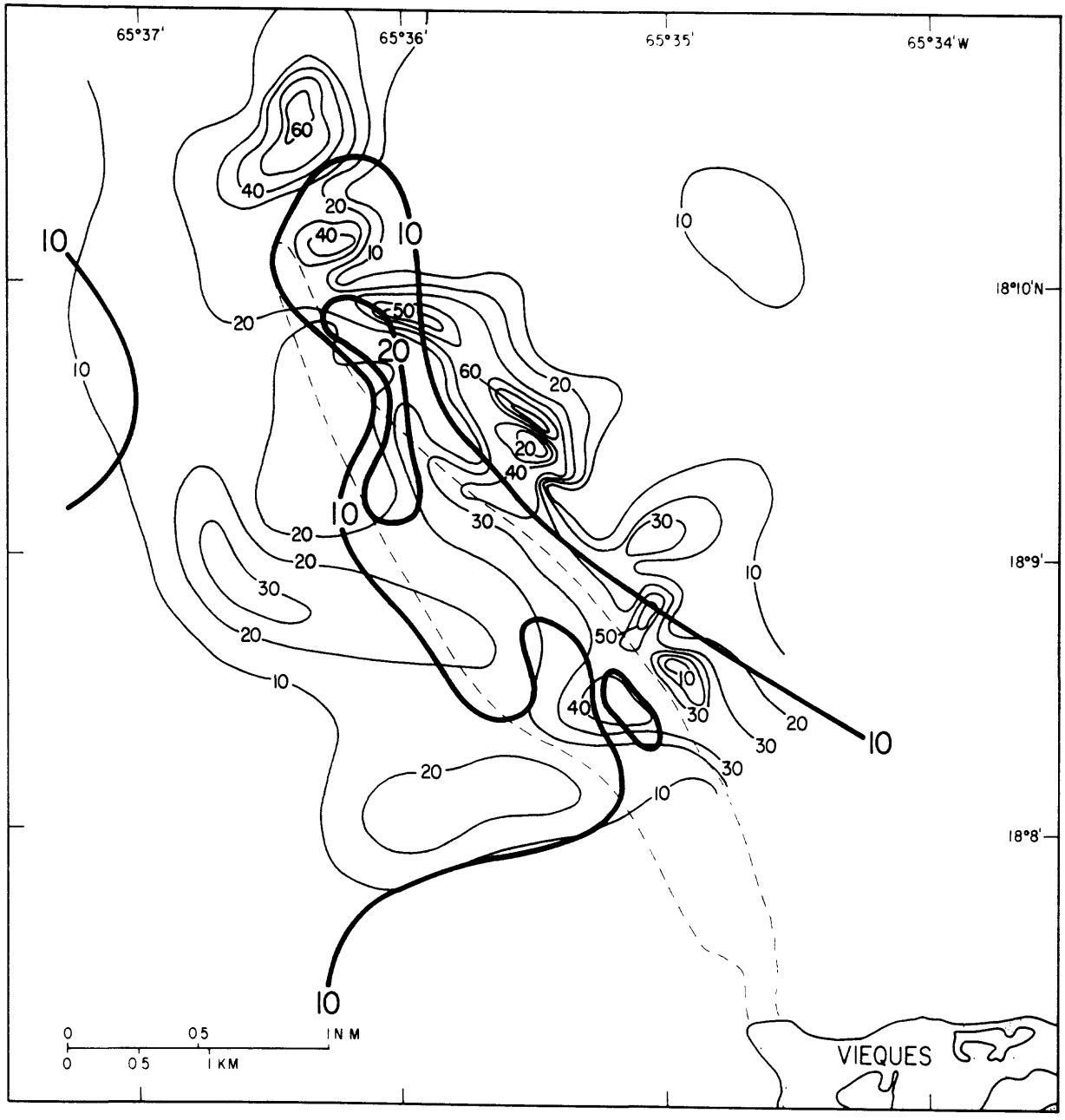
65°37'
65°36'
65°35'
65°34'W
18°10'N
18°9'
18°8'
VIEQUES
0 0.5 1 NM
0 0.5 1 KM

Fig. 11. Weight percentage of surficial bottom sediment that is sand (0.062—2.000 mm). Heavy contours show the results of this study (post-Hugo); light contours show the pre-Hugo sand distribution and dashed lines show the outline of the Escollo de Arenas before Hurricane Hugo (from Rodriguez and Trias, 1989).

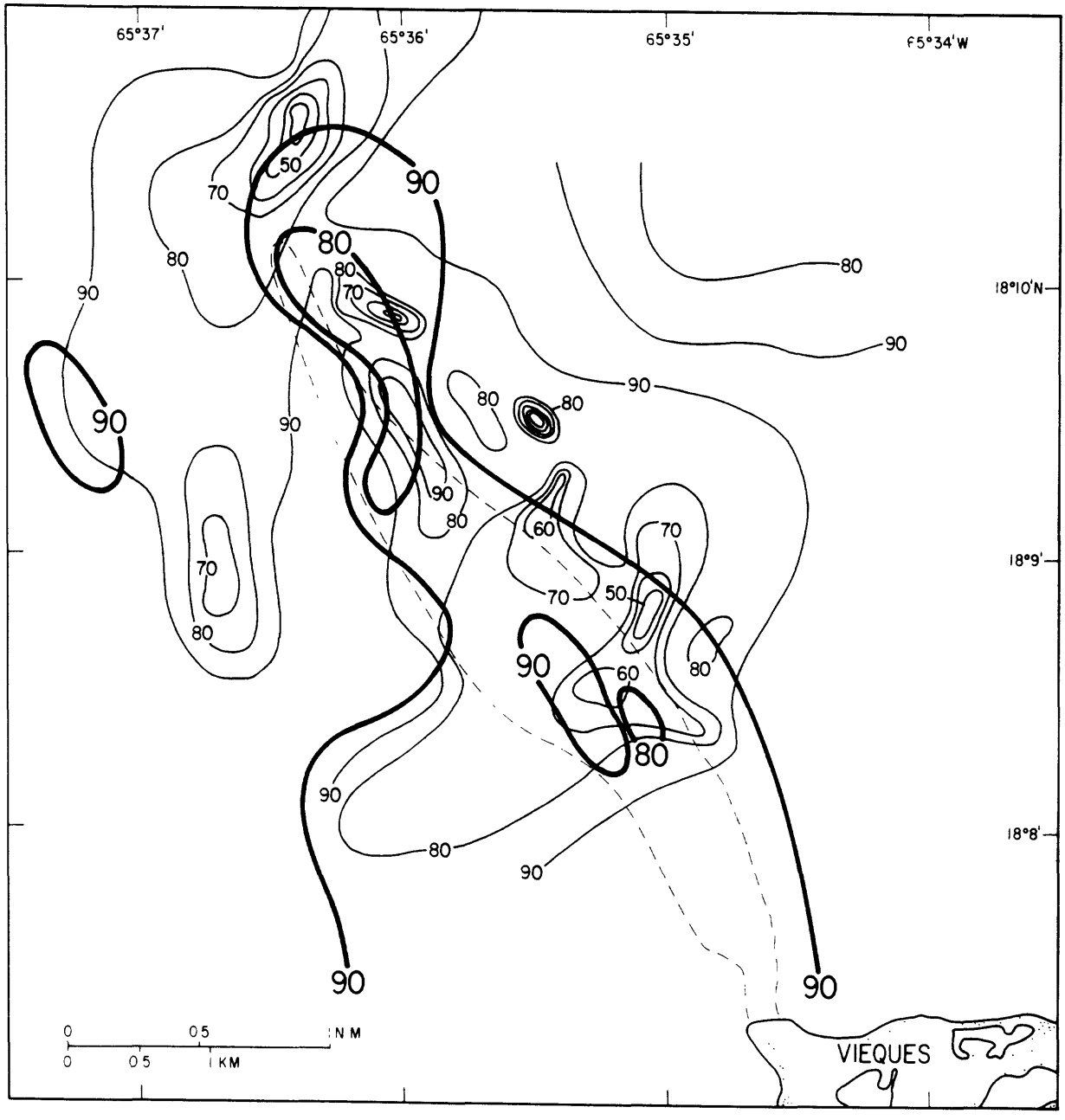
65°37'
65°36'
65°35'
65°34'W
18°10'N
18°9'
18°8'
50
70
80
90
60
0 0.5 1 NM
0 0.5 1 KM
VIEQUES

Fig. 12. Weight percentage of surficial bottom sediment that is silt+clay (< 0.062 mm). Heavy contours show the results of this study (post-Hugo); light contours show the pre-Hugo silt+clay distribution and dashed lines show the outline of the Escollo de Arenas before Hurricane Hugo (from Rodriguez and Trias, 1989).

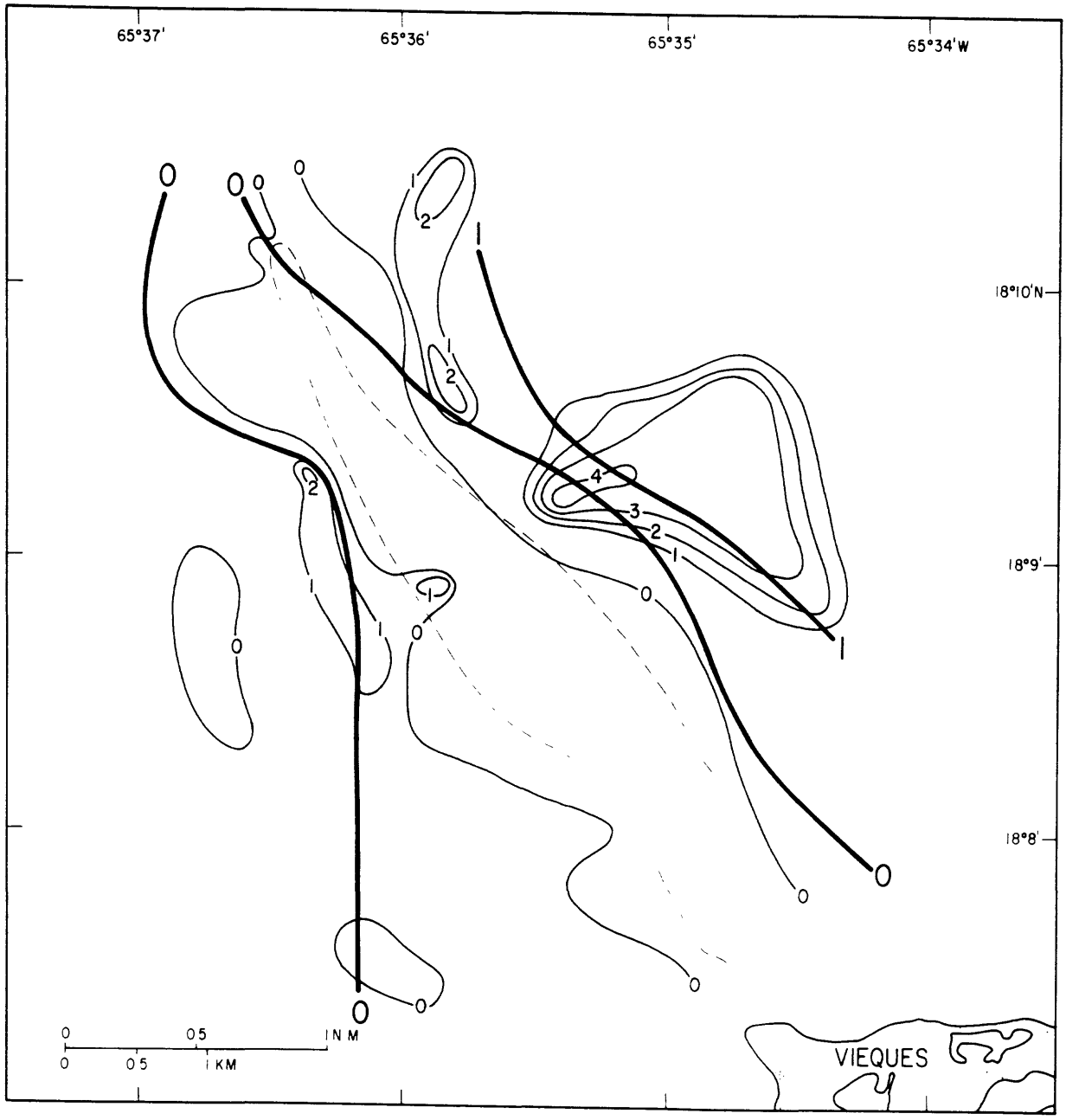
65°37'
65°36'
65°35'
65°34'W
18°10'N
18°9'
18°8'
0
0 0
0
1
2
1
1
2
4
3
2
1
2
1
1
1
0
0
0
0
0
0
0
0
0
0
0 0.5 1 N M
0 0.5 1 KM
VIEQUES

Fig. 13. Carbonate content of surficial sediment in weight percent. Heavy contours show the results of this study (post-Hugo); light contours show the pre-Hugo carbonate content and dashed lines show the outline of the Escollo de Arenas before Hurricane Hugo (from Rodriguez and Trias, 1989).

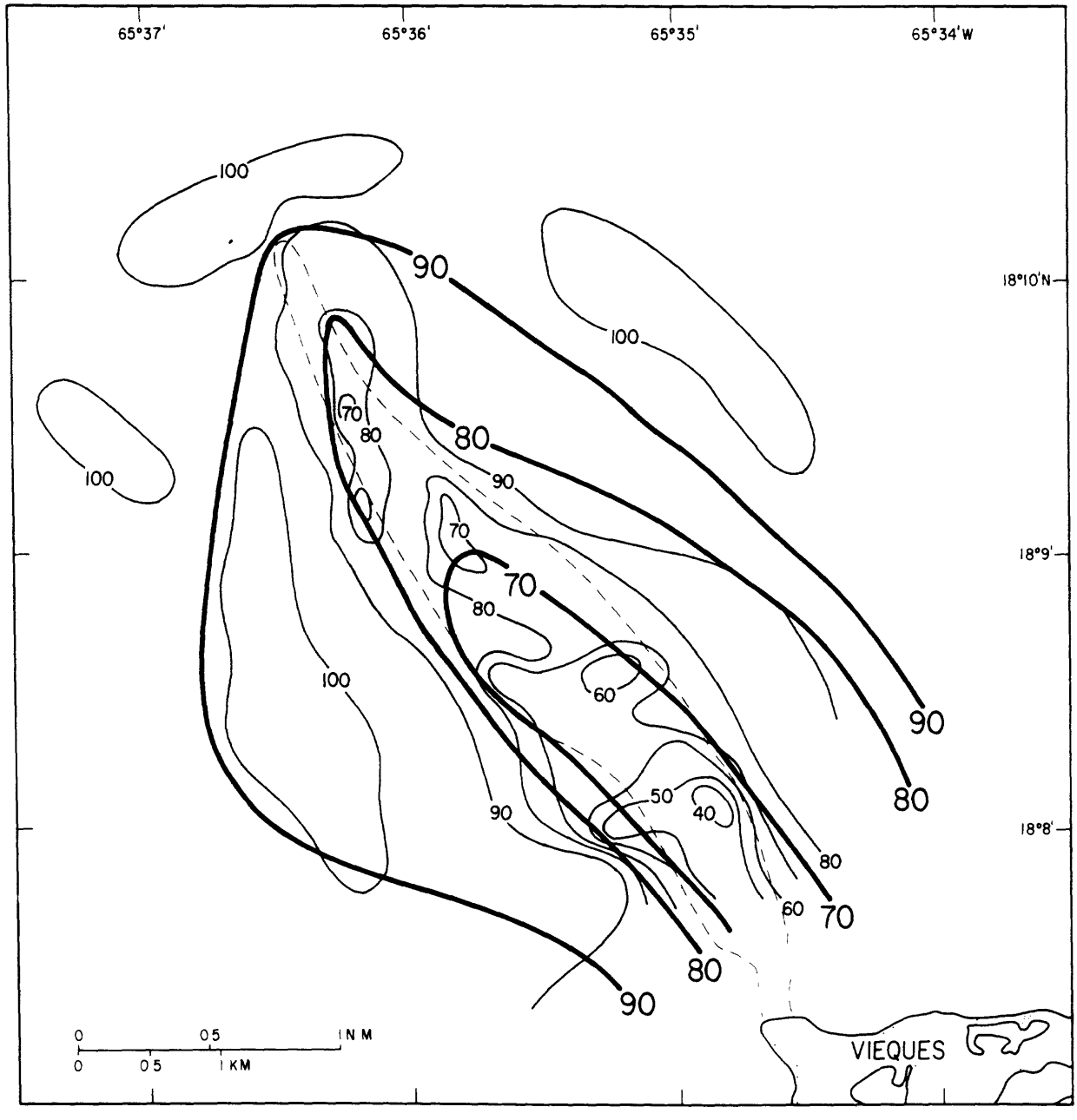
65°37'
65°36'
65°35'
65°34'W
18°10'N
18°9'
18°8'
100
90
80
70
60
50
40
VIEQUES
0 0.5 1 NM
0 0.5 1 KM

Fig. 14. Map showing the location of the hammer and vibracores and thickness of the storm-related surficial coarse-grained layer off the eastern flank of the Escollo de Arenas. Hachured area shows the estimated aerial distribution of the coarse layer. Dashed line shows the outline of the Escollo de Arenas before Hurricane Hugo (from Rodriguez and Trias, 1989).

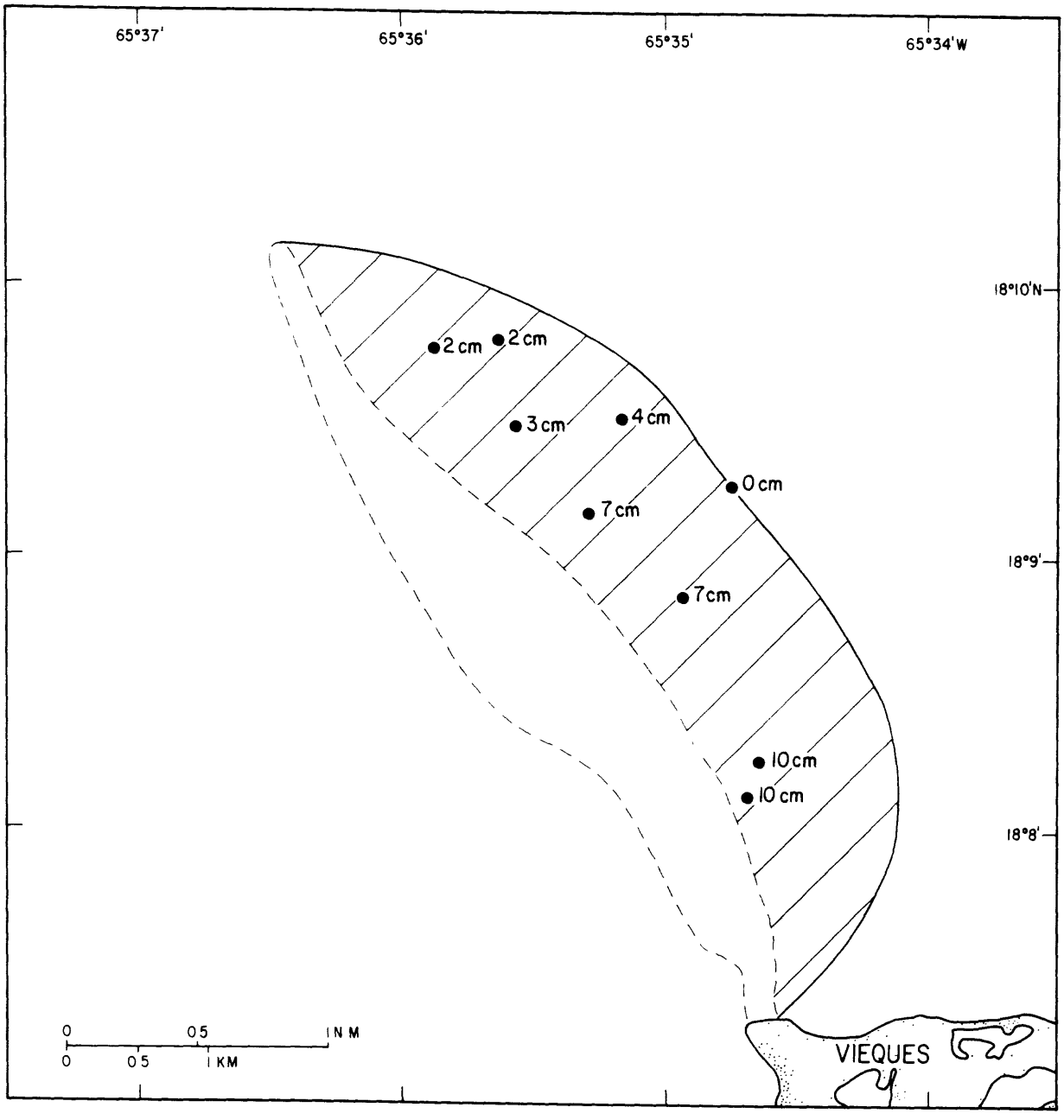
65°37'
65°36'
65°35'
65°34'W
18°10'N
18°9'
18°8'
2 cm
2 cm
3 cm
4 cm
0 cm
7 cm
7 cm
10 cm
10 cm
0 0.5 1 N M
0 0.5 1 KM
VIEQUES

EFFECTS OF MAJOR STORMS ON THE INSULAR SHELF

INSULAR SHELF SEDIMENTOLOGIC PROCESSES: PLAYA DE LUQUILLO

William C. Schwab, William W. Danforth
(U.S. Geological Survey, Woods Hole, Massachusetts)
Rafael W. Rodriguez
(U.S. Geological Survey, San Juan, Puerto Rico)
Marguerite H. Gowen
(Duke University, Durham, North Carolina)
Thomas F. O'Brien
(U.S. Geological Survey, Woods Hole, Massachusetts)

OBJECTIVE

The shoreline of the Luquillo study area was heavily impacted by Hurricane Hugo (Rodriguez and others, this report) and historical shoreline change analysis shows that this shoreline has been eroded (E.R. Thieler, unpublished data). Detailed sea-floor mapping using high-resolution sidescan-sonar, seismic-reflection and bottom sampling, and analysis of the sediment samples was used in order to determine the ultimate fate of the sediment removed from the coastal zone.

RATIONALE

Sediment cover on the narrow insular shelf surrounding Puerto Rico is, in general, patchy and diverse with little continuity (e.g., Pilkey and others, 1987; Trias,1990; Rodriguez and others, 1992). This sediment-cover variability is a reflection of the wide range of physical and biological factors affecting shallow sedimentation in this area. The dominant sediment type on the entire Puerto Rico shelf is calcareous skeletal sand, a potential economic resource. Mapping of the sedimentary environments identifies areas where sediments are most likely to accumulate; these data can be used to find and assess the sources and sinks of offshore sand and gravel needed for beach replenishment and shed light on the processes controlling the distribution of the sediment.

FIELDWORK

Marine geologic surveys were conducted in April/May 1991 aboard the research vessel JEAN A using a sidescan-sonar system, seismic-reflection profiling systems, and a surface grab sampler. Additional bottom samples and sea-floor photographs were collected in June 1992 using the R.V. BORIKEN.

A sidescan-sonar mosaic is an approximate model of the interaction of sound with the sea floor. The level of acoustic backscattering from the sea floor is a function of, among other factors, the sea-floor topography, roughness, and composition (Reed and Hussong, 1989 and references therein). The sidescan-sonar survey over the Luquillo insular shelf was conducted using a 100 kHz Klein sidescan-sonar system; total swath width per trackline was 200 m. The sidescan data were logged digitally using a QMIPS data acquisition system (Danforth and others, 1991) at a sampling rate that resulted in a 0.1 m pixel size in the across track direction. The data were then decimated to a 0.4 m pixel size using a median filtering routine developed by Malinverno and others (1990) and were

processed and mosaicked using procedures developed by Danforth and others (1991). This mosaic was then used as a basemap for the subsequent sampling phase of the investigation. Lighter tones on the sidescan-sonar images represent areas of relatively low acoustic backscatter intensity and darker tones, areas of high backscatter.

Concurrent with the acquisition of the sidescan-sonar imagery, approximately 650 km of 3.5 kHz and Huntec Sea Otter seismic-reflection profiles were collected. These data were recorded using an analog EPC recorder. Bathymetry and Holocene sediment thickness of Holocene-aged sediment were determined from these data.

Bottom sediment samples were obtained using a Shipek grab sampler for the 1991 field work and a Van Veen sampler in 1992. Grain size analysis of the samples was conducted using a combination of wet sieve and Coulter counter techniques following the methodology of Poppe and others (1985). Analyses of calcium carbonate content were performed at Puerto Rico's Department of Natural Resources sedimentological laboratories using methods described by Rodriguez and Trias (1989).

Ship navigation was conducted using a shore-base Miniranger Falcon IV transponder navigation system for the 1991 investigation and a Global Positioning System (GPS) satellite navigation system in 1992. Using these navigation data, the seismic-reflection profiles and 1991 bottom sample locations are accurate to within 4 m. The sidescan towfish, however, was not navigated independently of the ship, thus, an additional maximum error from 15 m in shallow water to approximately 100 m in deeper areas exists along-track in the sidescan imagery.

RESULTS

Maps have been completed in a 105 km^2 area of the Luquillo insular shelf (Fig. 1). These maps show sidescan-sonar imagery, bathymetry and bottom sample locations, Holocene sediment thickness, and a Pleistocene structural horizon. These maps were used to select sediment sample sites. The maps demonstrate a complex sea floor displaying a fine-scale of spatial variability (Fig. 2), in places blanketed by sediment deposits of varied thickness (Fig. 3).

The sea floor in the study area is dominated by a series of eolianite ridges which are clearly expressed on the sidescan imagery (Fig. 4) as areas of high acoustic backscatter intensity with a high degree of variance (dark tones indicating high backscatter and light tones representing acoustic shadows). These ridges trend roughly east-west across the study area. Although samples of these rock ridges were not collected, they are thought to be eolianite formed during the Pleistocene during a time when sea level was lower. Similar eolianite dunes are common along the northern coast of Puerto Rico and crop out to the east on the islands northeast of Cabo San Juan (Fig. 1) (Kaye, 1959). Using seismic-reflection profiles, this Pleistocene surface can be traced as a strong reflector under the Holocene sediments (Fig. 3) which, in turn, fill in depressions on the surface.

The surficial sediment can be subdivided into four acoustic facies (Fig. 2) based on relative degree of backscatter shown on the sidescan images (Fig. 4) and sediment texture (Fig. 5). These are: 1) low backscatter sand — relatively fine-grained sand found in the nearshore region of the study area in areas of relatively low backscatter; 2) high backscatter sand — relatively coarse-grained reefal-derived sands and gravelly sands found in areas of relatively high acoustic backscatter; 3) low backscatter silt — silt to sandy silt found in areas of low backscatter on the outer shelf; and 4) intermediate backscatter sandy silt — sandy silt to silty sand found in an area of relatively high backscatter along the shelfbreak.

The composition of the sand fraction of the sediment distributions is summarized on Figures 6 to 8. The samples were analyzed for their skeletal carbonate (corralline algae, Halimeda, Echinoderm, coral fragments, Porifera, Mollusk, Gorgonian, Annelid, Bryzoan, and Foraminifera), non-skeletal carbonate (ooid, aggregate, and peloid), and terrigenous (quartz, feldspar, and rock fragment) components.

The composition of the low backscatter sand is presented on Figure 6 and is subdivided into samples collected from the nearby beaches, from the inner shelf, and from areas of low backscatter in close proximity to the eolianite (referred to as reefal sands). The increase of the coral fragment component in samples from the beach and from areas in close proximity to the eolianite in comparison to that of the inner shelf sand is probably due to the relative proximity of the sediment to coral reefs that fringe the coast and corals that are growing on the eolianite. However, the compositional (Fig. 6) and textural (Fig. 5) similarity of the low backscatter sand from the beach to the eolianite suggests that they are the same deposit.

The composition of the high backscatter sand (Fig. 7) is similar to the composition of low backscatter sand with an expected increase in the Halimeda component (Halimeda grows on the eolianite) and an unexplained minor reduction in the Echinoderm and Porifera components. The similarity of the composition of the low backscatter sand and high backscatter reefal sand strongly suggests that the relative backscatter intensity displayed on the sidescan-sonar imagery is a function of sediment texture (Fig. 5); quantitative analysis of the sidescan imagery supports this hypothesis (Gowen and others, this report).

Chemical analyses of the low and high backscatter sand shows that the samples are all greater than 85 percent calcium carbonate with all but two samples greater than 93 percent (Fig. 9). This indicates that there is little input of terrigenous sandy sediment into this area from the local rivers and that most of the sandy sediment is locally (biologically) derived from carbonate-producing organisms which grow on the local hardgrounds (from the reefs that fringe the nearby coast and the eolianite outcrops). Any terrigenous deposition in the study area appears to be concentrated in the high-backscatter silt found on the outer insular shelf and is expressed by the relative increase of the terrigenous component of this sediment's composition (Fig. 8) and an average calcium carbonate concentration of 49 percent (Fig. 9).

Compositional and textural data augmented with the sidescan imagery and sediment isopach maps suggest that sediment derived from the local hardgrounds and any sediment removed from the shoreline resides on the inner shelf, generally inshore of the eolianite. Seismic-reflection profiles show a sand deposit, in places up to 20 m thick, has formed landward of the eolianite; a potential economic resource. In addition, a series of "channels" across the eolianite (most likely subaerially formed) have been partially filled by the low backscatter sand (Fig. 2).

An offshore-directed storm-induced sediment transport direction is suggested by the elongate deposits of high backscatter sand lying atop the low backscatter silt of the outer insular shelf (Fig. 2). These high backscatter "wisps" on the sidescan images are composed of relatively coarse-grained sediment derived from the eolianite and transported in a general offshore (north-northwest) direction. It is probably realistic to think that these high-backscatter deposits are the result of a combined wave/current effects, largely owing to storm conditions where downwelling and high wave energies are dominant (e.g., Cacchione and others, 1984). Although the oceanographic processes responsible for this offshore net transport direction are unknown, the sidescan imagery shows that it is

dominant throughout the study area (Fig. 2).

FUTURE PLANS

Examination of the sidescan data in conjunction with the seismic-reflection profiles and sediment samples suggest that a net offshore transport of sediment occurs during storms on the insular shelf off of Luquillo. A series of bottom samples were collected over the study area in July, 1992. These samples will be analyzed and compared to the existing data base to attempt to ascertain whether any changes have occurred since the original survey in 1991. These data will be combined with the existing data and published as a series of U.S. Geological Survey Miscellaneous Field Studies Map in 1993. All of the geophysical data and interpretive mapping products are in digital format. It is planned that these data and derivative products will be released on CD ROM in 1994.

Fig. 1. Map showing location of sidescan-sonar mosaic and location of Map 1 (Fig. 4) and seismic-reflection profile (Fig. 3).

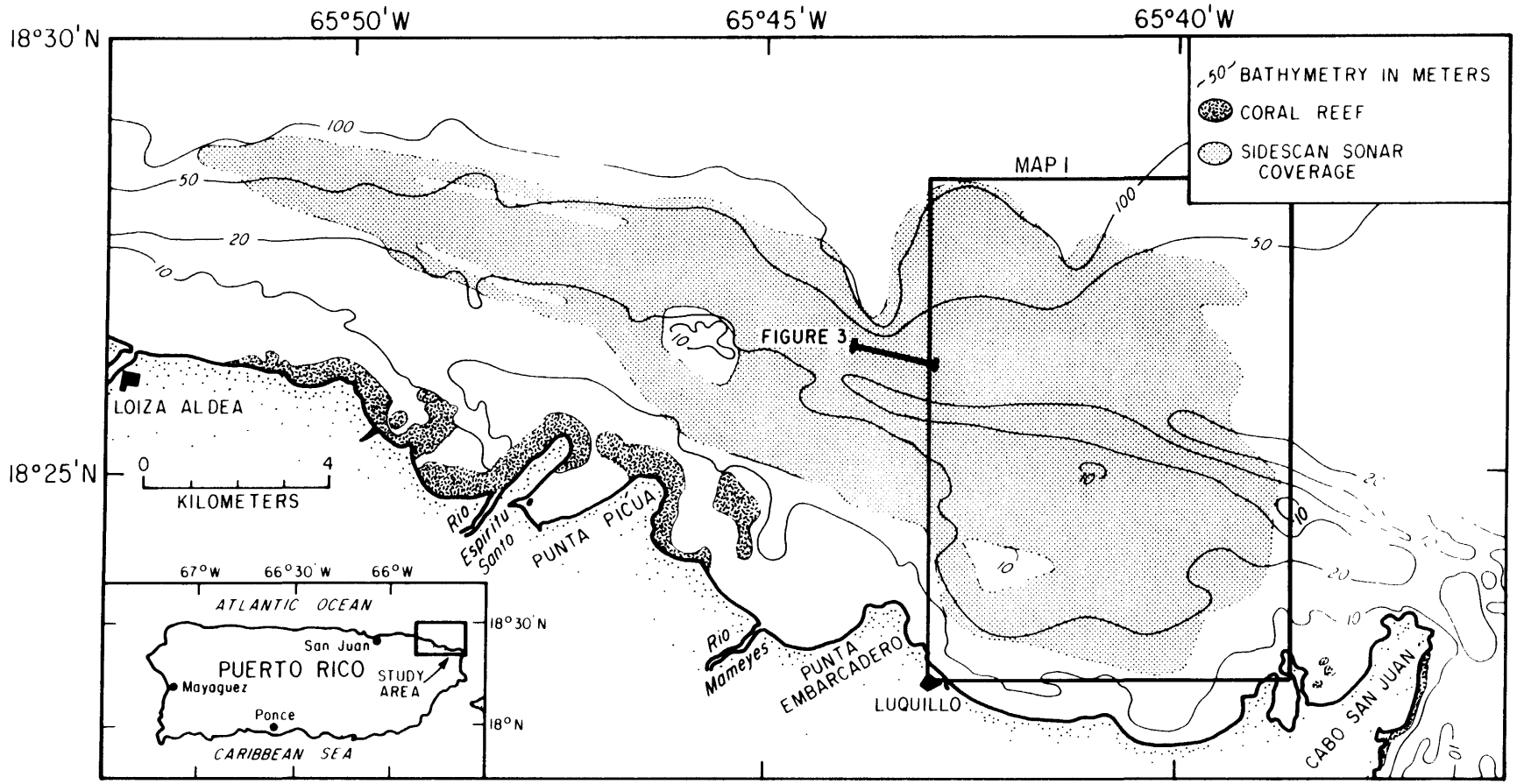
18°30'N
65°50'W
65°45'W
65°40'W
50 BATHYMETRY IN METERS
CORAL REEF
SIDESCAN SONAR COVERAGE
MAP I
FIGURE 3
100
50
20
10
LOIZA ALDEA
18°25'N
0
4
KILOMETERS
Rio Espiritu Santo
PUNTA PICUA
Rio Mameyes
PUNTA EMBARCADERO
LUQUILLO
CABO SAN JUAN
67°W
66°30'W
66°W
ATLANTIC OCEAN
San Juan
PUERTO RICO
STUDY AREA
Mayaguez
Ponce
CARIBBEAN SEA
18°30'N
18°N

64a

Fig. 2. Generalized interpretative map of Luquillo shelf study area. The sea floor is dominated by outcropping eolianite. Sand lost from the beach front moves offshore forming, in part, the low backscatter sand deposit. The orientation of the high backscatter sand deposit seaward of the eolianite ridges is interpreted to indicate a net offshore sediment transport direction during storms.

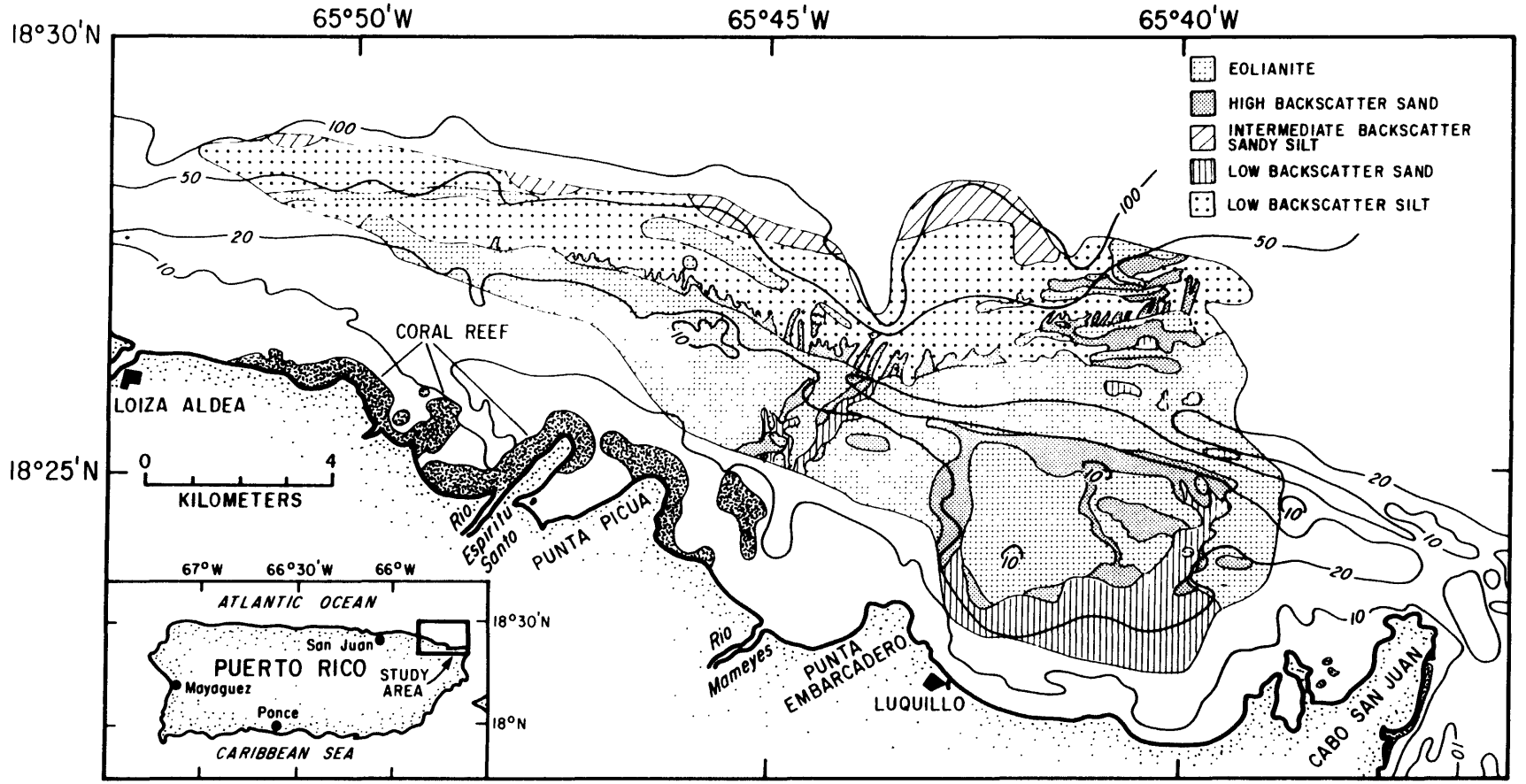
18°30'N
65°50'W
65°45'W
65°40'W
EOLIANITE
HIGH BACKSCATTER SAND
INTERMEDIATE BACKSCATTER SANDY SILT
LOW BACKSCATTER SAND
LOW BACKSCATTER SILT
100
50
20
10
CORAL REEF
LOIZA ALDEA
18°25'N
0
4
KILOMETERS
Rio Espiritu Santo
PUNTA PICUA
Rio Mameyes
PUNTA EMBARCADERO
LUQUILLO
CABO SAN JUAN
67°W
66°30'W
66°W
ATLANTIC OCEAN
18°30'N
San Juan
PUERTO RICO
STUDY AREA
Mayaguez
Ponce
18°N
CARIBBEAN SEA

65a

Fig. 3. Seismic-reflection profiles and interpretation (for location see Fig. 1).

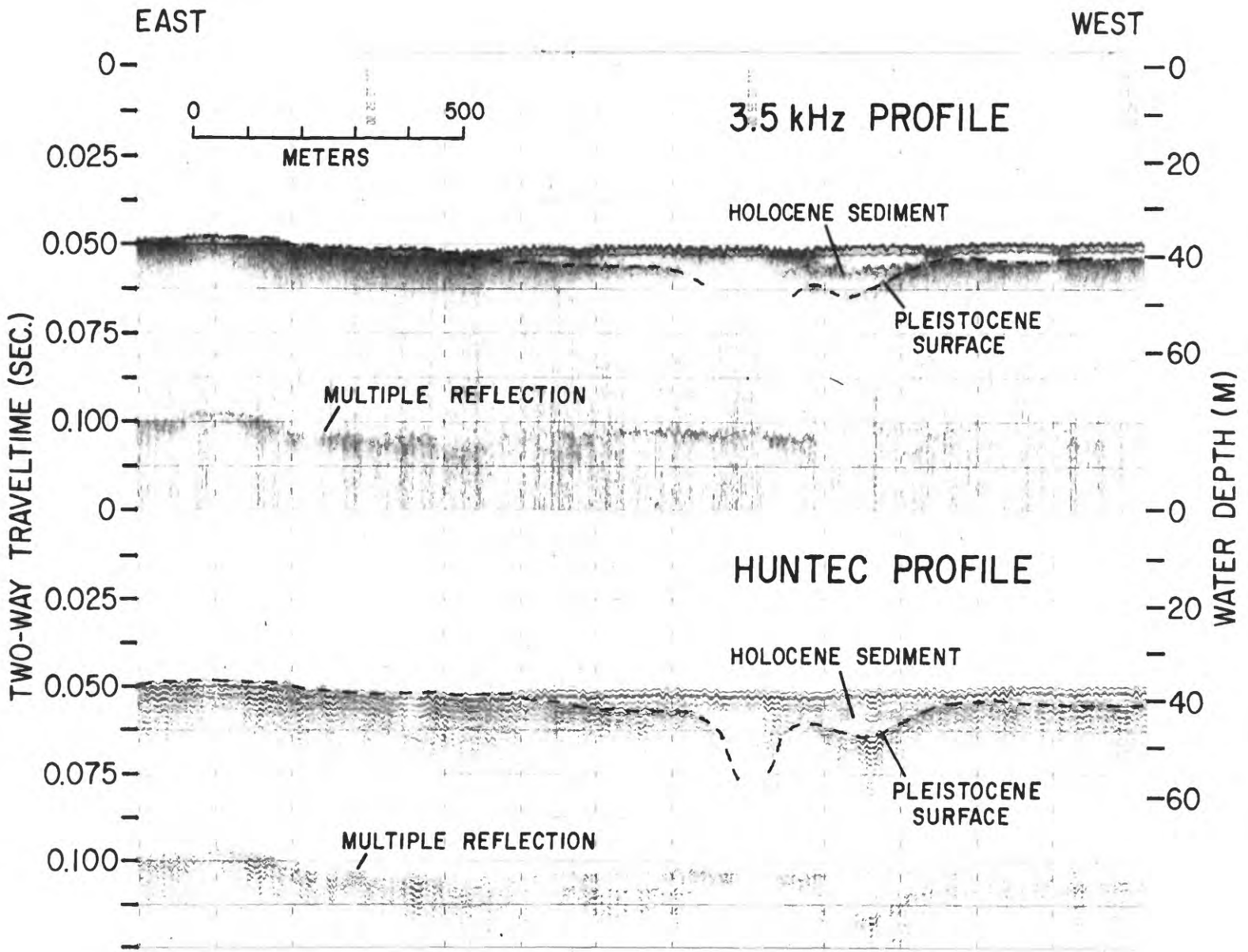
EAST
WEST
0
500
METERS
3.5 kHz PROFILE
HOLOCENE SEDIMENT
PLEISTOCENE SURFACE
MULTIPLE REFLECTION
HUNTEC PROFILE
HOLOCENE SEDIMENT
PLEISTOCENE SURFACE
MULTIPLE REFLECTION
TWO-WAY TRAVELTIME (SEC.)
0
0.025
0.050
0.075
0.100
WATER DEPTH (M)
0
20
40
60

Fig. 4. Map 1 showing the sidescan-sonar imagery of the eastern segment of the insular shelf off Luquillo. See Figure 1 for location.

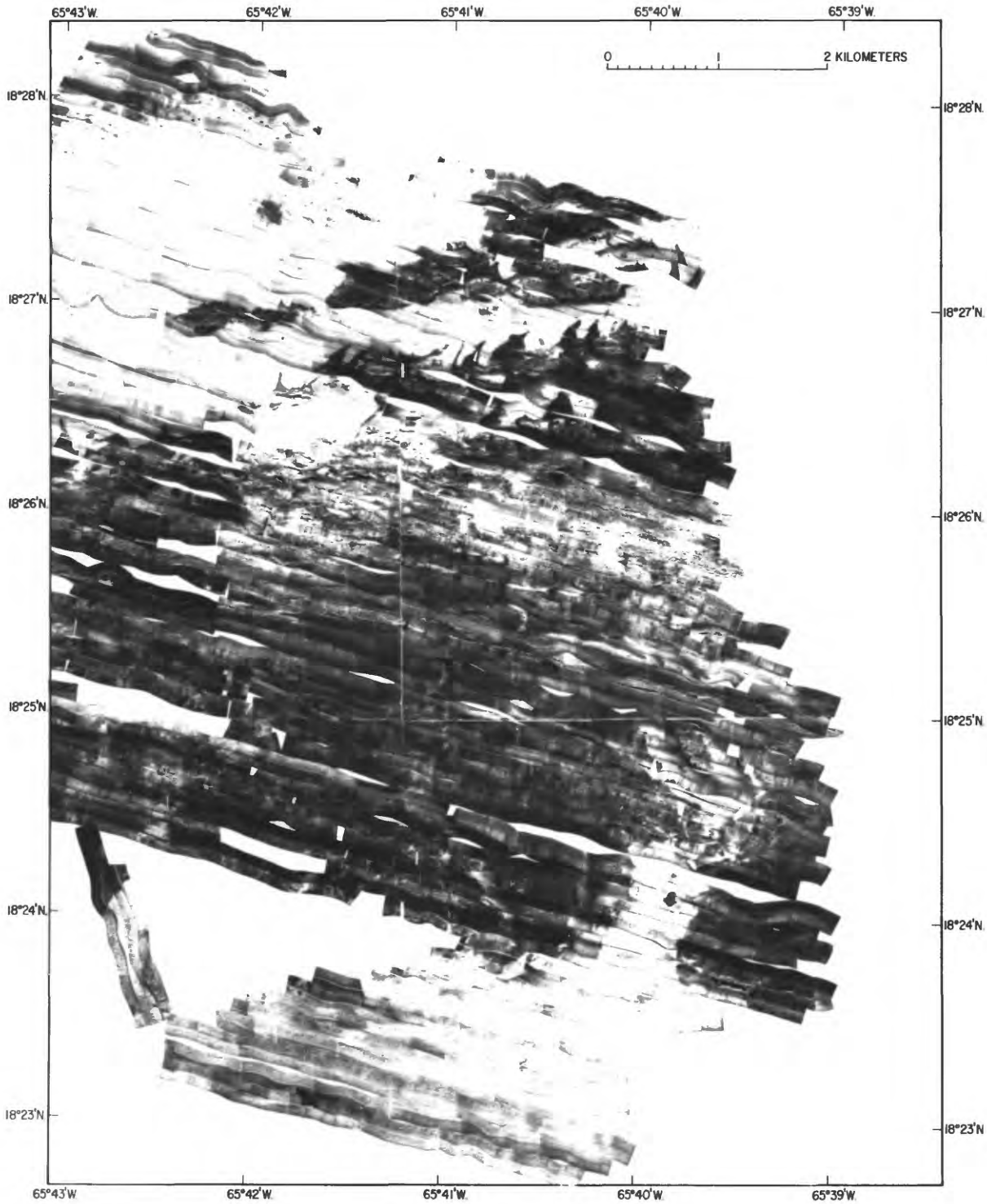
65°43'W.
65°42'W.
65°41'W.
65°40'W.
65°39'W.
0
1
2 KILOMETERS
18°28'N.
18°27'N.
18°26'N.
18°25'N.
18°24'N.
18°23'N.

Fig. 5. Relation between mean grain size (in phi-units) and standard deviation of the sediment distribution showing the four major acoustic facies.

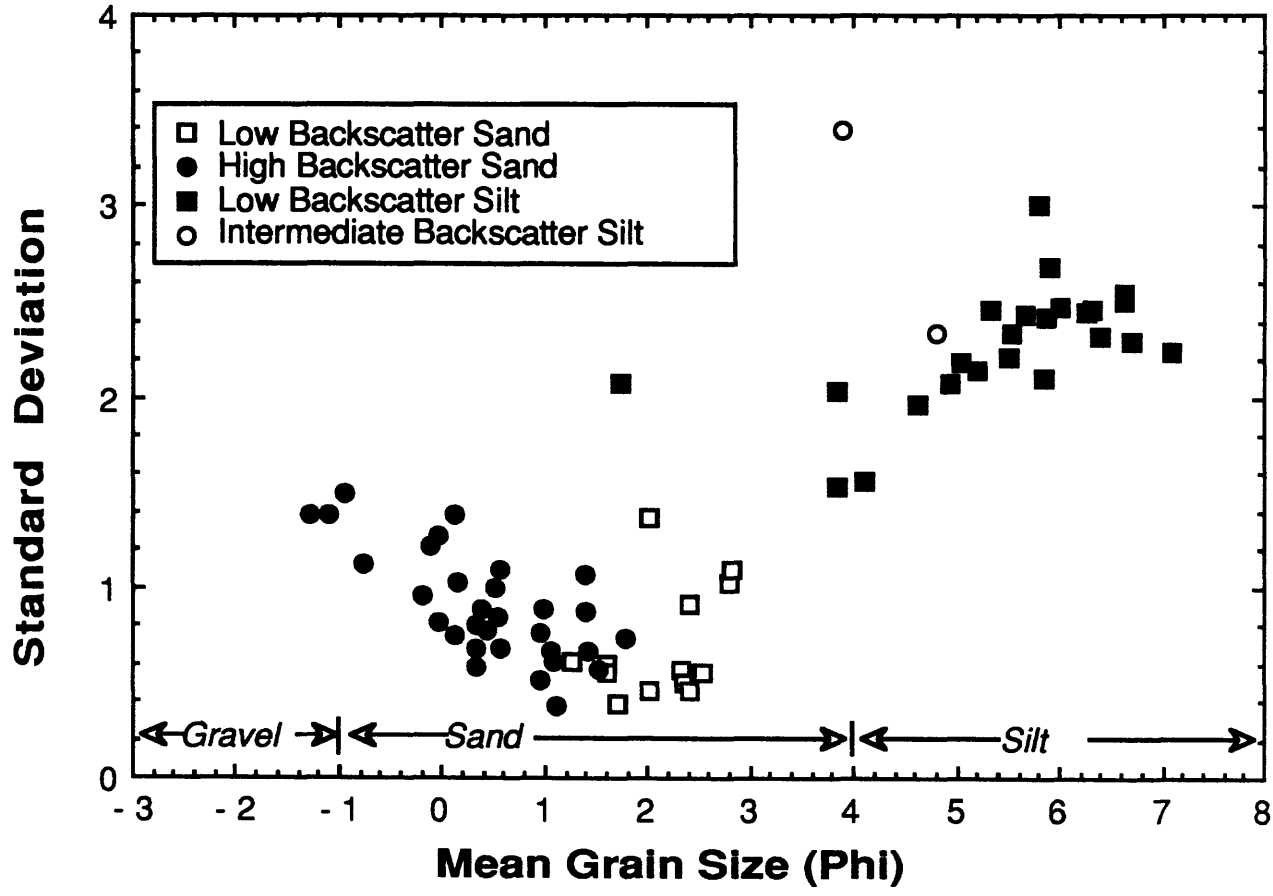
Low Backscatter Sand
High Backscatter Sand
Low Backscatter Silt
Intermediate Backscatter Silt
Standard Deviation
Mean Grain Size (Phi)
Gravel
Sand
Silt
0
1
2
3
4
- 3
- 2
- 1
0
1
2
3
4
5
6
7
8

Fig. 6. Composition of the sand fraction for beach and low backscatter sands. These sediments are extremely similar and are predominantly composed of skeletal carbonate material.

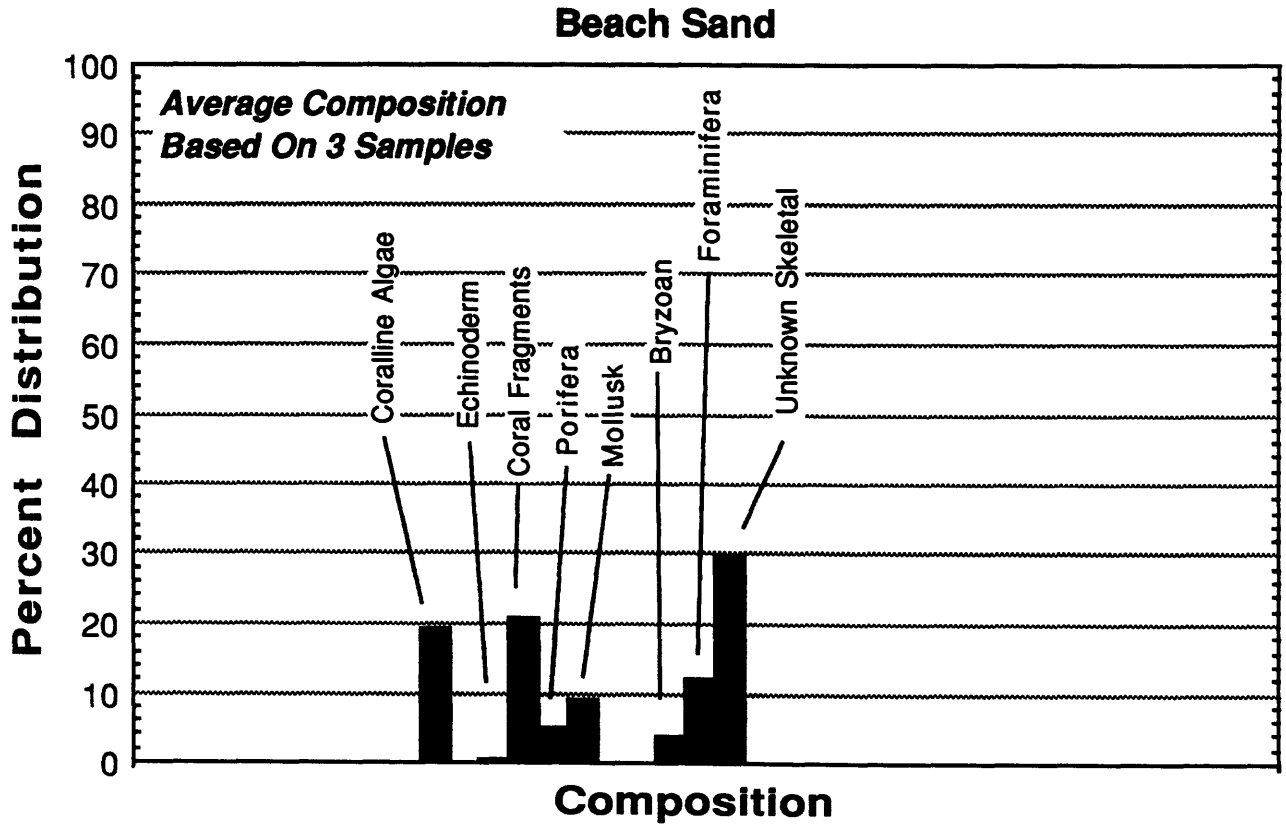
Beach Sand
Average Composition
Based On 3 Samples
Percent Distribution
100
90
80
70
60
50
40
30
20
10
0
Coralline Algae
Echinoderm
Coral Fragments
Porifera
Mollusk
Bryzoan
Foraminifera
Unknown Skeletal
Composition

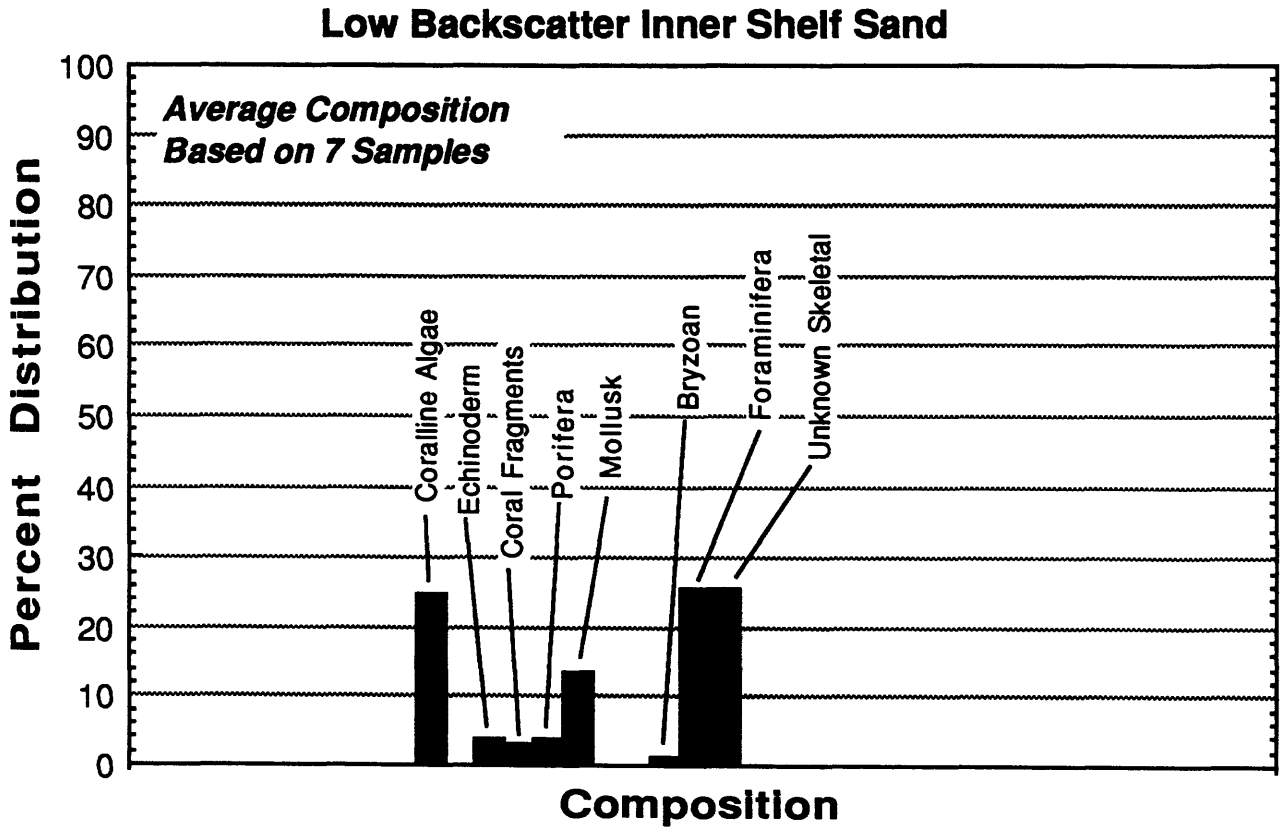
Low Backscatter Inner Shelf Sand
Average Composition
Based on 7 Samples
Percent Distribution
100
90
80
70
60
50
40
30
20
10
0
Coralline Algae
Echinoderm
Coral Fragments
Porifera
Mollusk
Bryzoan
Foraminifera
Unknown Skeletal
Composition

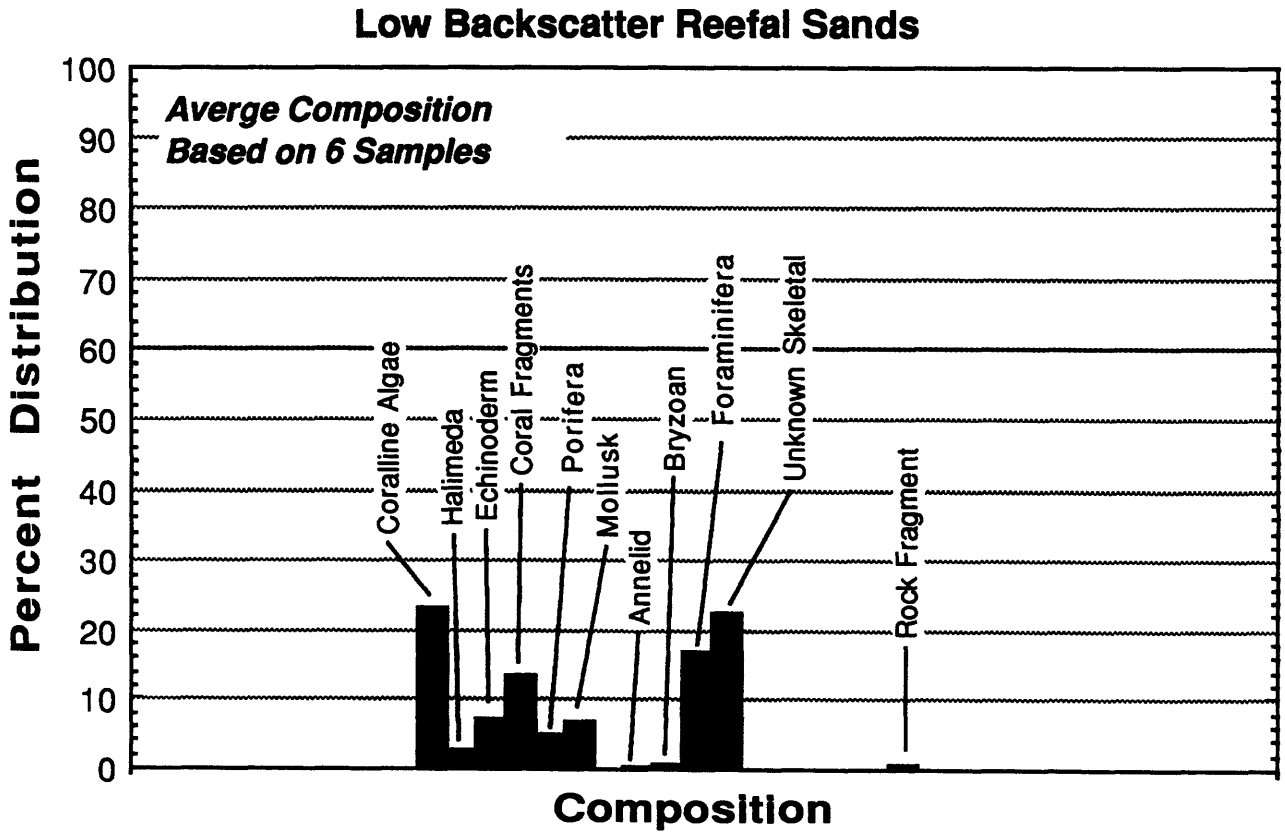
Low Backscatter Reefal Sands
Averge Composition
Based on 6 Samples
Percent Distribution
100
90
80
70
60
50
40
30
20
10
0
Coralline Algae
Halimeda
Echinoderm
Coral Fragments
Porifera
Mollusk
Annelid
Bryzoan
Foraminifera
Unknown Skeletal
Rock Fragment
Composition

Fig. 7. Composition of the sand fraction for high backscatter sands. Composition is similar to the beach and low backscatter sand (Fig. 5).

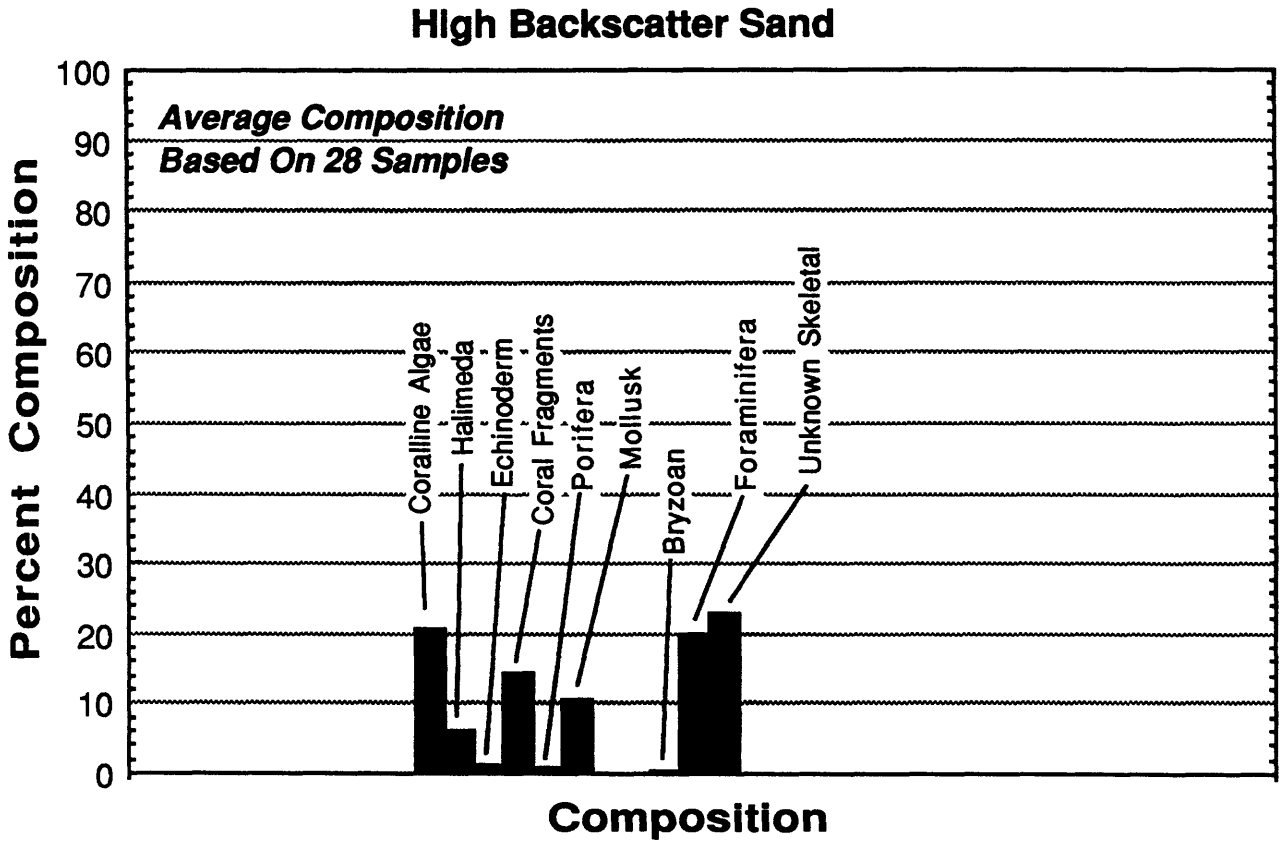
High Backscatter Sand
Average Composition
Based On 28 Samples
Percent Composition
100
90
80
70
60
50
40
30
20
10
0
Coralline Algae
Halimeda
Echinoderm
Coral Fragments
Porifera
Mollusk
Bryzoan
Foraminifera
Unknown Skeletal
Composition

Fig. 8. Composition of the sand fraction for low backscatter silt. These sediments composition has a high terrigenous component in comparison to the sands shown in Figures 6 and 7 (also see Figure 8).

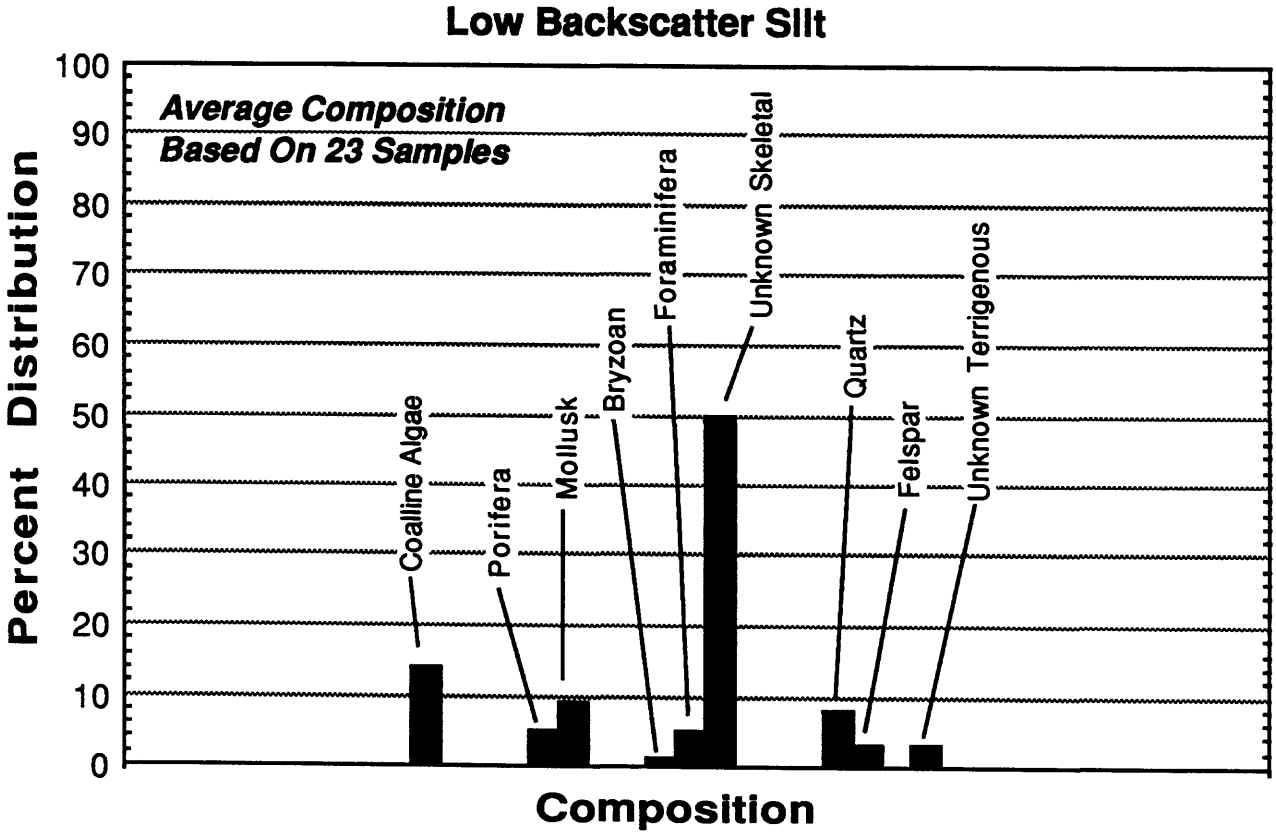
Low Backscatter Silt
Average Composition
Based On 23 Samples
Percent Distribution
100
90
80
70
60
50
40
30
20
10
0
Coalline Algae
Porifera
Mollusk
Bryzoan
Foraminifera
Unknown Skeletal
Quartz
Felspar
Unknown Terrigenous
Composition

Fig. 9. Relation of sediment mean grain size and calcium carbonate concentration.

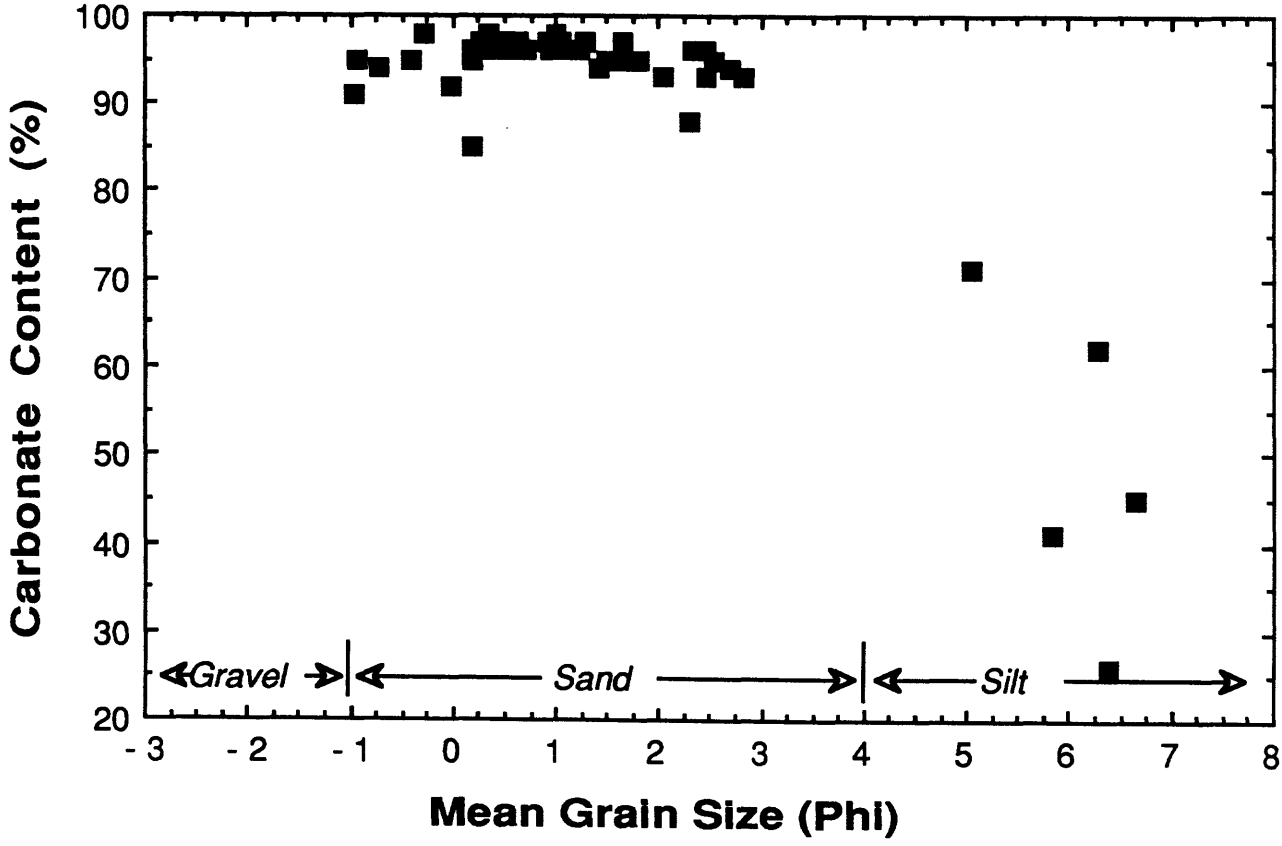
Carbonate Content (%)
100
90
80
70
60
50
40
30
20
Gravel
Sand
Silt
- 3
- 2
- 1
0
1
2
3
4
5
6
7
8
Mean Grain Size (Phi)

QUANTITATIVE ANALYSIS OF SIDESCAN SONAR IMAGERY

Marguerite H. Gowen
(Duke University, Durham, North Carolina)
William C. Schwab, William W. Danforth
(U.S. Geological Survey, Woods Hole, Massachusetts)

OBJECTIVE

High-resolution sidescan-sonar images provide a reconnaissance view of the sea floor. A subset of the data collected on the insular shelf off Luquillo was quantitatively analyzed to assess what properties of the sea floor fundamentally control relative backscatter intensity.

RATIONALE

Sidescan-sonar data collection and digital processing techniques produce photograph-like images of the sea floor. However, a sidescan-sonar image does not represent what the sea floor would look like if the water were removed; it is a graphical representation of how the sea floor interacts with sound (see Johnson and Helferty, 1990). Sidescan-sonar images constitute the primary data base for the insular shelf mapping component (this study), but correct geologic interpretation requires a quantitative evaluation of factors that control the level of acoustic backscatter. Recent developments in data acquisition and computer processing and enhancement allow at least a semi-quantitative analysis of the causes of relative backscatter; the limit is the non-quantitative nature of sidescan-sonar systems presently in use.

FIELDWORK

Marine geologic surveys were conducted in April/May 1991 aboard the research vessel JEAN A using a sidescan-sonar system and surface grab sampler (Schwab and others, this report). Additional bottom samples and sea-floor photographs were collected in June 1992 using the R.V. BORIKEN. The sidescan-sonar survey over the Luquillo insular shelf (Fig. 1) was conducted using a 100 kHz Klein sidescan system; the total swath width per trackline was 200 m. The sidescan data were logged digitally following the methodology of Danforth and others (1990) at a sampling rate that resulted in a 0.1 m pixel size in the across-track direction. A subset of these sidescan-sonar data that exhibits a broad range of backscatter intensities viewed throughout the study area was selected for analysis. This subset of the imagery data was compressed to a 0.4 m pixel size using a median filter routine developed by Malinverno and others (1990), processed using techniques modified from Chavez (1986) and Malinverno and others (1990), and digitally mosaicked using procedures developed by Chavez (EEZ-SCAN 85 Scientific Staff, 1987). Here, a relative backscatter intensity is expressed as a Digital Number (DN). The full range of possible backscatter is divided into 256 gray-scale levels. A value of DN=0 is equivalent to no backscatter, expressed as true black on the digital sidescan image (Fig. 2), while DN=255 is equivalent to complete backscatter, expressed as true white on the image.

Bottom sediment samples were obtained using a Shipek grab sampler for the 1991 field work (Fig. 2) and a Van Veen sampler in 1992. Grain size analysis of the samples was conducted using a combination of wet sieve and Coulter counter techniques following the methodology of Poppe and others (1985). Analyses of calcium carbonate content were

performed by Puerto Rico's Department of Natural Resources sedimentological laboratories using methods described by Rodriguez and Trias (1989).

Ship navigation was conducted using a shore-based Miniranger Falcon IV transponder navigation system. Using these navigation data, ship-trackline and bottom sample locations are accurate to within 5 m. The sidescan-sonar towfish, however, was not navigated independently of the ship, thus, an additional maximum error of approximately 15 m exists in the sidescan imagery.

RESULTS

The vast majority of backscattered sound acquired by a sidescan-sonar receiver is diffracted from the sea floor rather than directly reflected (Chavez, 1980). Only those areas of the sea floor that have a bottom roughness of the appropriate scale and an acoustic impedance significantly different than water will produce backscatter energy (Johnson and Helferty, 1990). Thus, the relative backscatter intensity is controlled by a variety of factors including: the acoustic impedance contrast between the sea floor and the water, the angle of incidence of the sound wave front and the sea floor, and sea-floor topography and microtopography.

Sidescan-sonar imagery was used to guide the sampling phase of data collection and to assess sediment transport processes on the Luquillo shelf segment (Schwab and others, this report). Four acoustic facies based on relative degree of backscatter and sediment texture were identified and mapped: (1) low backscatter sand; (2) high backscatter sand; (3) low backscatter silt; and (4) intermediate backscatter sandy silt. To verify these interpretations, statistical parameters of DN values in varied acoustic backscatter regimes were analytically compared to the textural, compositional, and geochemical properties of the associated sediment samples.

Eolianite outcrops produce local relief which generates areas of high variance in acoustic backscatter. However, in the remainder of the study area, sedimentation has resulted in a relatively flat sea floor. Thus, the sea floor slope is not a major factor in controlling the backscatter intensity over areas of sediment cover. Sediment composition, predominantly skeletal carbonate sand, is extremely similar throughout the digitally mosaicked area. Because acoustic backscatter varies where sediment composition does not, we conclude that the composition of the sediment is not a major factor controlling acoustic backscatter differences. The only significant variable in the study area found to control the relative backscatter intensity is sediment texture: mean grain-size correlates extremely well with mean DN value (Fig. 3). The standard deviation of the sediment distribution (sediment sorting) only affects the acoustic backscatter in the fine-grained sediment (silt and finer) where increased values of standard deviation result in suppressed relative backscatter intensity (Fig. 4).

The direct relation of increasing mean grain size with increasing DN value (Fig. 3) verifies the mapping interpretations of sediment distribution on the Luquillo insular shelf proposed by Schwab and others (this report). Sedimentary facies, indicated by the acoustic facies, can be mapped with a high level of confidence using the sidescan-sonar imagery.

FUTURE PLANS

The findings of this study were based on a limited number of sediment samples. Additional bottom samples were collected over the study area in July, 1992 (Map 6). These samples will be analyzed and compared to the existing data base in an attempt to

increase the level of confidence in the relation between texture and relative backscatter intensity. It is planned that these data and derivative products will be released on CD ROM in 1993/94.

Fig. 1. Map showing the location of the sidescan-sonar image collected over the insular shelf off Luquillo and the portion of the imagery used in this study (Fig. 2).

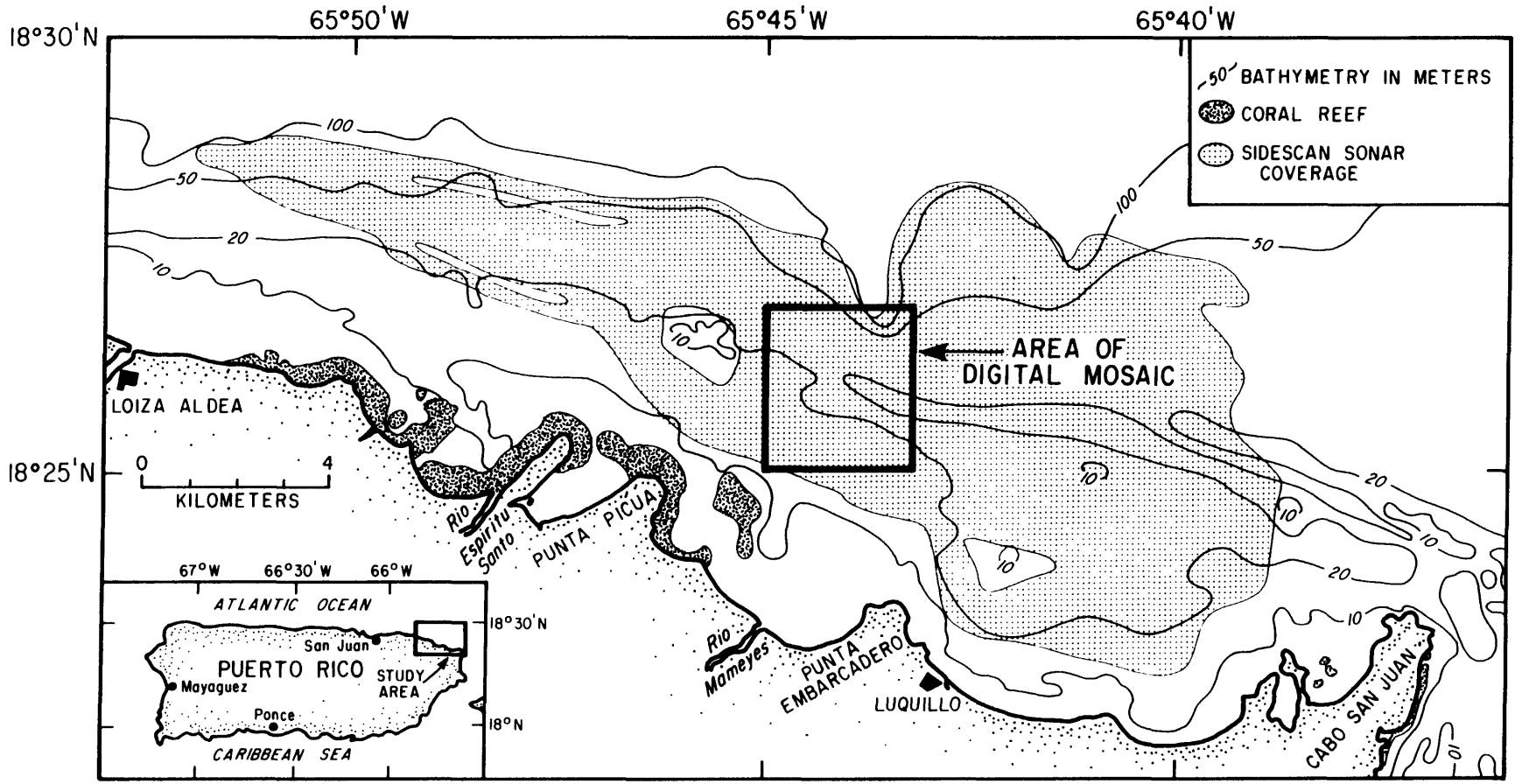
18°30'N
65°50'W
65°45'W
65°40'W
50 BATHYMETRY IN METERS
CORAL REEF
SIDESCAN SONAR COVERAGE
AREA OF DIGITAL MOSAIC
LOIZA ALDEA
18°25'N
0
4
KILOMETERS
Rio Espiritu Santo
PUNTA PICUA
Rio Mameyes
PUNTA EMBARCADERO
LUQUILLO
CABO SAN JUAN
67°W
66°30'W
66°W
ATLANTIC OCEAN
18°30'N
San Juan
PUERTO RICO
STUDY AREA
Mayaguez
Ponce
18°N
CARIBBEAN SEA

76a

Fig. 2. Digitally processed and enhanced sidescan-sonar mosaic of a portion of the insular shelf off Luquillo showing the bathymetry in 2 meter contour intervals and sample locations. Note the channel partially filled with sediment cutting across the eolianite ridges in the center of the image.

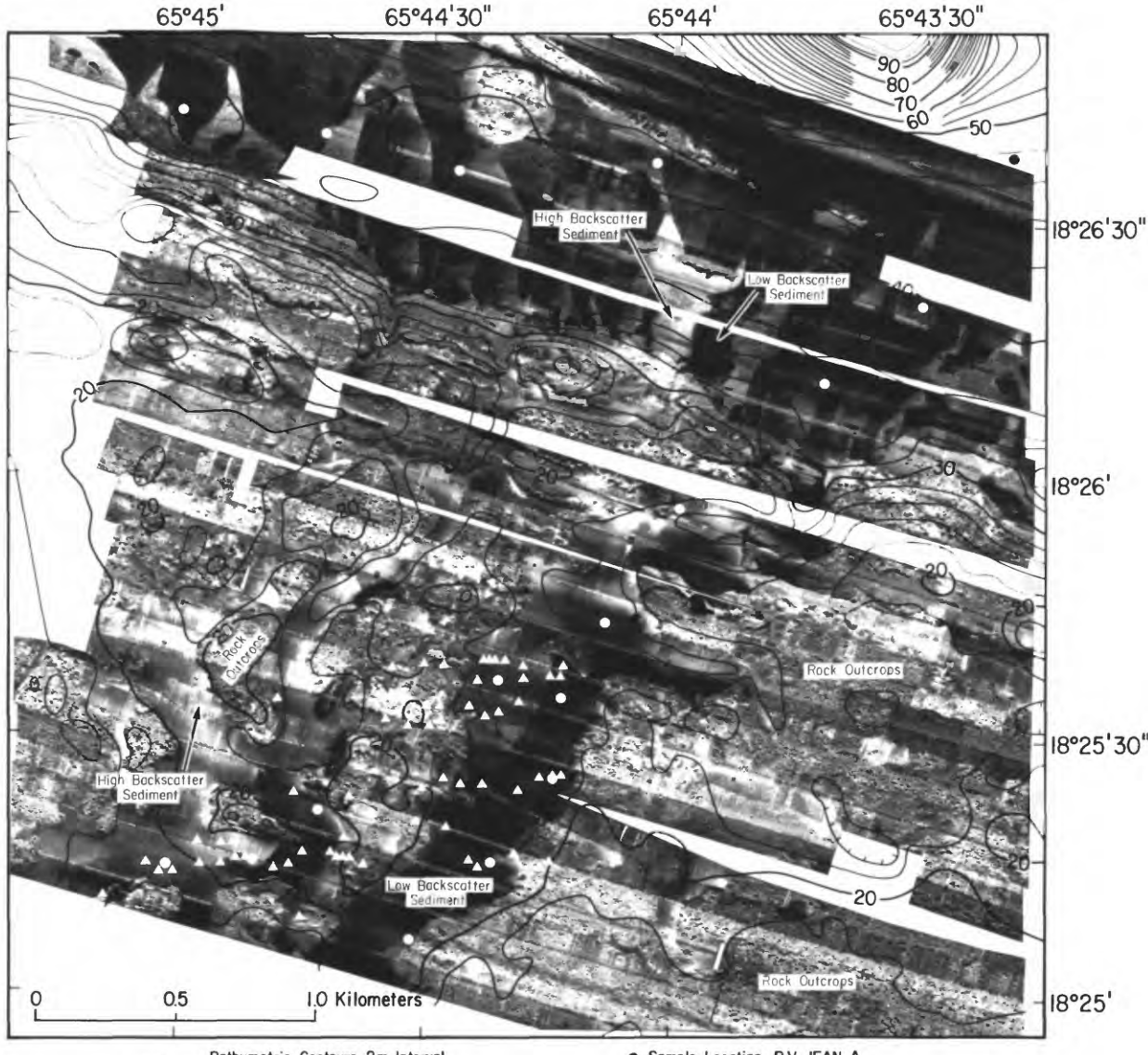
65°45'
65°44'30"
65°44'
65°43'30"
18°26'30"
18°26'
18°25'30"
18°25'
90
80
70
60
50
30
20
High Backscatter Sediment
Low Backscatter Sediment
Rock Outcrops
Rock Outcrops
Rock Outcrops
High Backscatter Sediment
Low Backscatter Sediment
Rock Outcrops
0
0.5
1.0 Kilometers
—20— Bathymetric Contours, 2m Interval
Hachures Indicate Direction of Dip
● Sample Location, R.V. JEAN A
▲ Sample Location, R.V. BORIKEN

Fig. 3. Relation between relative acoustic backscatter intensity (DN) and sediment mean grain size (GS) where R^2 is the correlation coefficient.

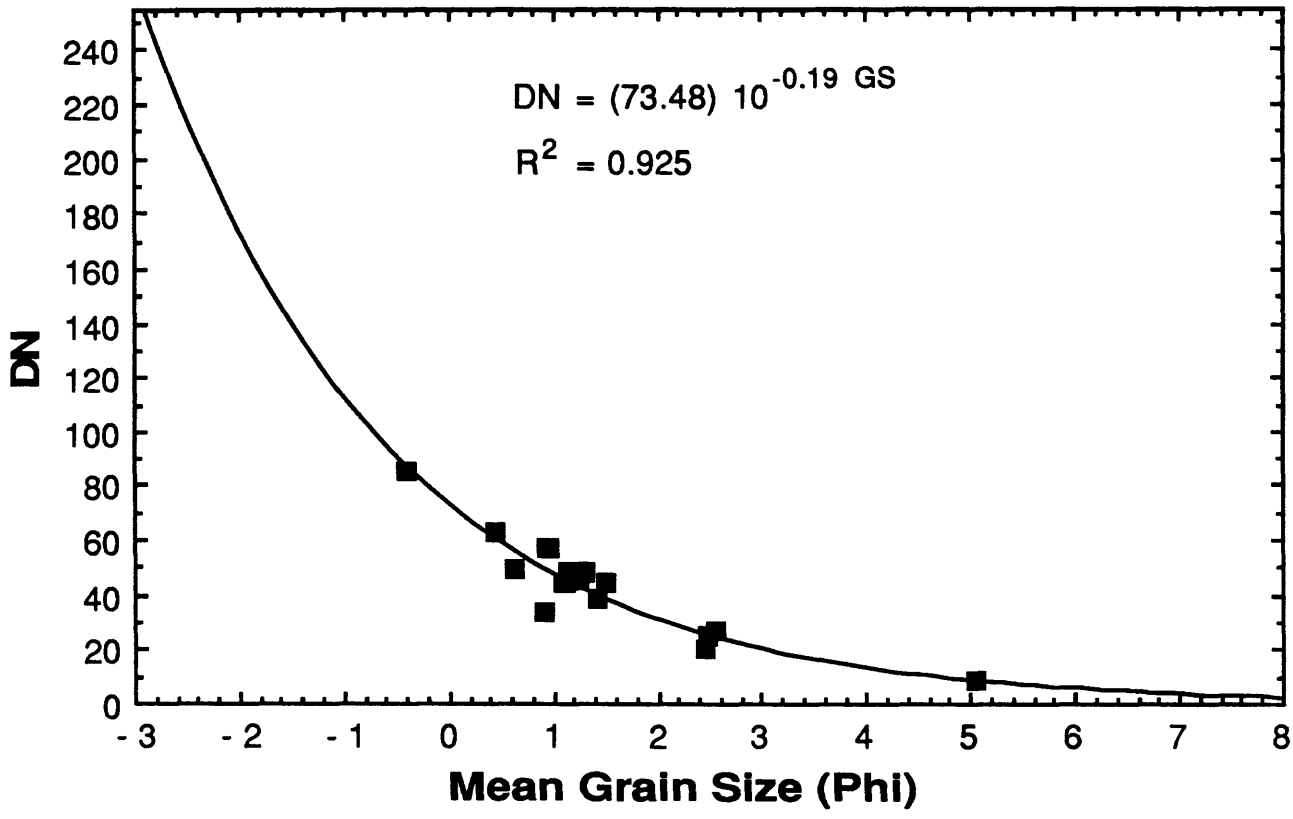
DN = (73.48) 10^-0.19 GS
R^2 = 0.925
DN
240
220
200
180
160
140
120
100
80
60
40
20
0
-3
-2
-1
0
1
2
3
4
5
6
7
8
Mean Grain Size (Phi)

Fig. 4. Relation between relative acoustic backscatter intensity (DN) and the standard deviation (SD) of the sediment grain size distribution for the silt-size component of the distribution (from 2 to 6 phi) and sand-size component (from -1 to 2 phi).

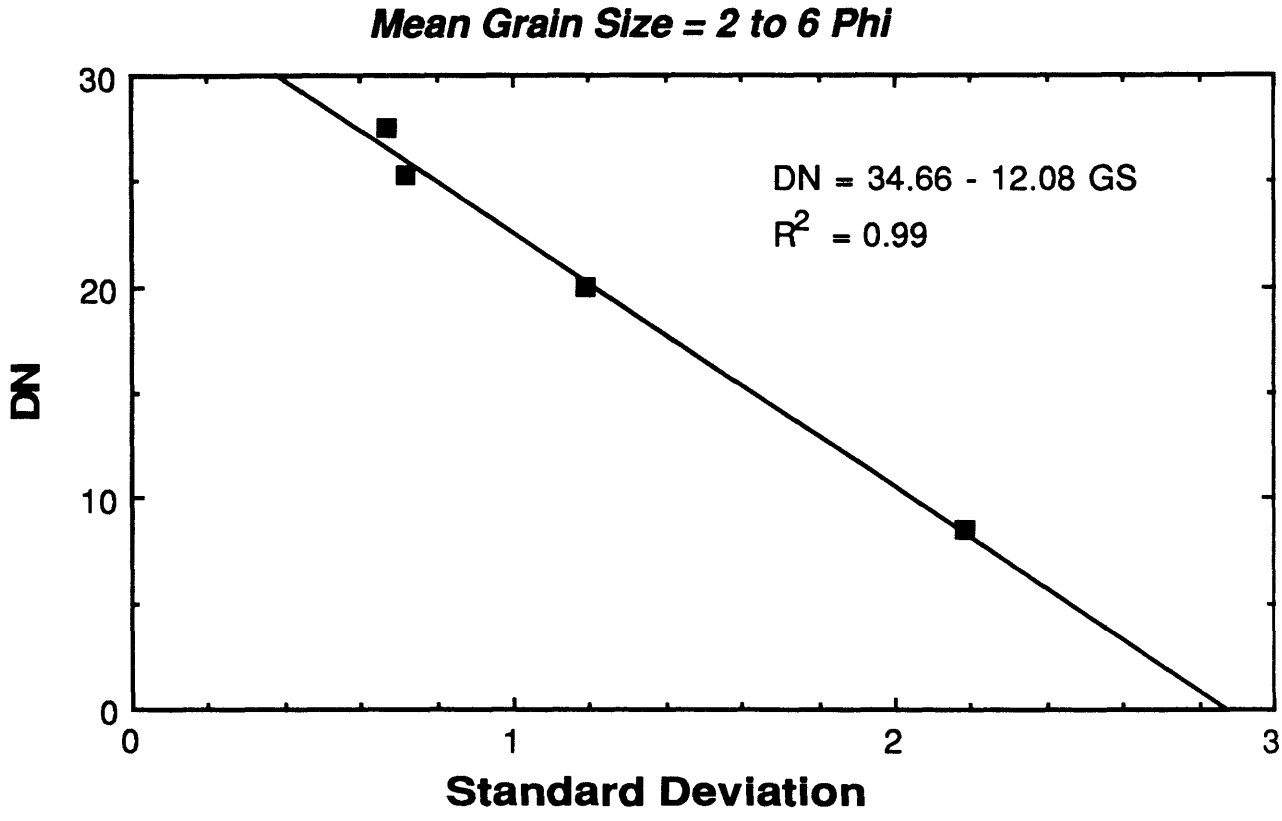
Mean Grain Size = 2 to 6 Phi
DN = 34.66 - 12.08 GS
R2 = 0.99
DN
Standard Deviation
0
10
20
30
0
1
2
3

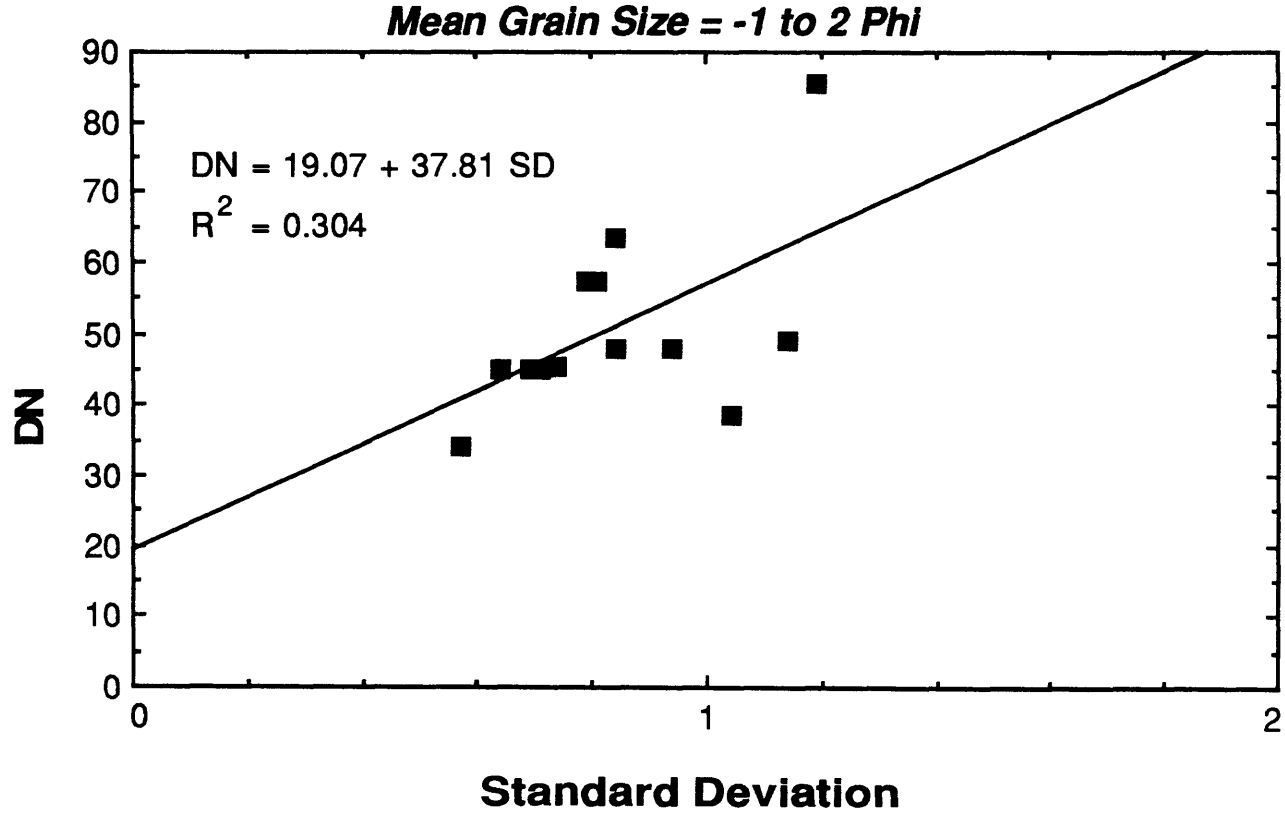
Mean Grain Size = -1 to 2 Phi
DN = 19.07 + 37.81 SD
R2 = 0.304
DN
Standard Deviation
0
10
20
30
40
50
60
70
80
90
0
1
2

ASSESSMENT OF DAMAGE TO CORAL REEFS

Eugene. A. Shinn, Robert.B. Halley
(U.S. Geological Survey, St. Petersburg, Florida)

OBJECTIVE

This study is designed to document the effect of Hurricane Hugo on coral reefs using the reef complexes around the island of Culebra as a model. An additional objective was to establish a series of "coral growth stations" to monitor future coral growth.

RATIONALE

Coral reefs around the island of Puerto Rico are sources of carbonate sand production, act as buffers to storm-wave induced coastal erosion, are sites of high biologic productivities (important to local fisheries), and are a tourist attraction. Thus, a living "healthy" reef is a resource in itself. Also, because coral reefs are living biological communities, they are sensitive to marine pollution and have the potential of being used as an "early warning" system in the case of widespread or significant pollution problems.

FIELDWORK

In July, 1991 a team of two USGS scientists and two technicians, working in conjunction with personnel of the USGS Puerto Rico office, spent three weeks on the island of Culebra (Fig. 1) recording damage inflicted on reefs by Hurricane Hugo, which struck September 18, 1989 with wind gusts up to 240 km/hr (Rodriguez and others, this report). Deep cores were drilled to determine the geologic history of reefs affected by Hugo. Cores of individual living corals were taken to study growth rate and evaluate the effect of Hugo and pollution on coral growth rate. Three permanent coral growth stations were established to monitor future coral growth and reef recovery. The permanent stations were sited on windward reefs devastated by Hugo, leeward reefs that sustained little damage, and a reef off the southern coast, where pollution is apparent and likely to increase.

RESULTS

Direct observations by towed divers (Fig. 1) and photographic documentation showed hurricane damage to be extensive on the east and southeast sides of Culebra. The most obvious effect of the storm was the nearly total destruction of the elkhorn coral *Acropora palmata*, the principal builder of reefs in the Caribbean (Fig. 2). The extent of damage was similar to that documented on the reefs of St. Croix by Hubbard and others (1991). Virtually all colonies larger than 1 m in diameter were overturned and fragmented. Evidence of regeneration from broken pieces of this species was rare. Rather, new growth was apparent as small colonies on otherwise dead fragments, suggesting recruitment. An obvious exception were colonies of *Dendrogyra cylindrus* that always exhibit new growth from still living, but toppled columnar colonies (Fig. 3). Considering the common "organ pipe" morphology of this species, we speculate that such multi-columnar forms may commonly arise after continued growth from fallen individual columns.

The second most obvious effect was breakage of the finer coral *Porites porites* (Fig. 4) and staghorn coral *Acropora cervicornis*. Large quantities of these delicate branching corals had been reduced to gravel-size rubble and transported and deposited, as

small banks 2-3 m high. As with *Acropora palmata*, almost no regeneration was apparent from fragmented pieces of these species. On the leeward side of several reefs, the fragments formed steep (20° to 30°) avalanche slopes 2 to 3 m high that buried boulder corals such as *Montastraea annularis* (Fig. 5).

The west side of Culebra is relatively more protected from large storm waves because of the shallow shelf and small islands that extend westward to the main island of Puerto Rico. Consequently, reefs there showed less damage. On the west side, the coral community consists mainly of the massive star or boulder coral *Montastraea annularis*. Although this species is morphologically variable, the dominant form of *Montastraea annularis* at Culebra grows in a columnar fashion and is similar to morphotype 1 of Knowlton and others (1992). This morphotype breaks apart into component club-like columns scattered about the original growth place of the coral. Morphotype 2, a more massive form, also occurs at Culebra, and forms compact boulders that remain rounded when tumbled and have more tendency to roll through the reef than morphotype 1, causing damage to other coral colonies. Less than 1 percent were spared because: 1) they are more wave resistant than elkhorn coral; 2) they thrive in protected environments (where they are less prone to overgrowth by the more rapidly growing elkhorn coral); and 3) wave action was less severe on the west side of the island compared to that on the windward east side, which is fronted by deep water.

Most toppled columns of *Montastraea annularis* on the leeward western reefs have continued to grow at their tips (Fig. 6). New growth is turned upward, similar to that of a fallen tree. Several examples were collected and slabbed for sclerochronological study. Growth bands in all examples studied to date indicate these corals fell in late summer of 1989, thus confirming disturbance at the time of Hurricane Hugo (Fig. 7). Although damage occurred on the west side of Culebra, it was minimal compared to that on the east coast. The widespread destruction of *Montastraea annularis* observed by Edmunds and Witman (1991) at Greater Lameshur Bay, St. John, U.S. Virgin Islands was not observed at Culebra. Therefore, the changes anticipated within the framework community by Edmunds and Witman (1991) are not expected to occur in Culebra reefs dominated by *Montastraea annularis*.

Despite extensive damage to *Acropora palmata* reefs, abundant evidence of post-hurricane recruitment and regrowth was noted during the study. Many new colonies, up to 15 cm in diameter, were observed growing on what is considered hurricane-derived rubble. In order to document recovery rates and test the theory that recruitment post-dated the storm, divers made measurements of colony dimensions for *Acropora cervicornis*, *Acropora palmata*, the fire coral *Millepora* sp. and mustard coral *Porites astreoides*. Comparison of the results of these measurements (Fig. 8) with published growth rates for the species supports our contention that recruitment and growth occurred after Hurricane Hugo. On the basis of these observations, together with the healthy condition of new recruits, lack of algal incrustations, abundance of the long-spined herbivorous sea urchin *Diadema* sp., and general lack of pollution except near the only small town, it is thought recovery will occur within the next 5 years. Coral diseases, however, wiped out most of the recovering corals after Hurricane Allen devastated reefs in Jamaica in 1980 (Knowlton and others, 1981). Thus, rapid recovery such as that documented in Florida and the Persian Gulf by Shinn (1974) should proceed unless devastating blight or disease breaks out.

Diadema sp., which benefit corals by grazing algae that can overgrow entire reefs,

experienced a Caribbean-wide "die-off" of unknown causes in 1983 (Lessios and others, 1984). A consequence of this die-off is that many reefs around the Caribbean and Florida are currently being overgrown by fleshy algae and the calcareous algae Halimeda. The abundance of *Diadema* sp. observed around Culebra is considered to be similar to pre-1983 abundance.

A consistent observation made by the USGS team at Culebra and by a group examining Hurricane Hugo's effects at St. Thomas (Rogers and others, 1990) was the patchiness of storm damage. Delicate corals were often seen standing unbroken adjacent to or within areas of extreme devastation. These observations led to the conclusion that much damage was caused by a domino effect, when one dislodged coral struck another and so on, rather than by direct damage by waves and currents. In some instances large coral colonies acted as "tools" in the waves and were pushed along plowing down everything in their path. These cases were evident by trenches in the reef still occupied by the coral that made them.

Two *Acropora* reefs on the windward side of the island were cored to a depth of 5.5 m and the *Montastraea* reef on the leeward side was cored to a depth of 6.5 m. Cores from the seaward reefs indicate they were initiated by the finger coral *Porites porites*. The finger coral, which is "in-place" and cemented by grey mud-textured Mg-calcite to form a hard limestone, is overlain by 1-2 m of white uncemented *Acropora palmata* rubble. The rubble is a result of both Hurricane Hugo and previous large storms. Dozens of pinnacle reefs off the east side of Culebra were also examined by diving. *Acropora palmata* had been stripped from these pinnacles by Hugo, exposing a base composed of cemented *Porites* framework, suggesting that most *Acropora* reefs on the seaward side initiated growth on *Porites* reefs.

A core drilled into the *Montastraea*-dominated reef on the leeward side of Culebra (located in the center of monitoring site C) penetrated the entire 6.5-m-thick Holocene section and consists of the same coral species that presently live there. *Porites porites*, which underlies the windward reefs, was never a reef builder here and there is no obvious submarine cementation. The absence of cementation is consistent with the lack of wave pumping which is most pronounced on the windward reefs. Though the base of the Holocene section was not reached on the windward reefs, it is considered likely that the reef accumulation on windward reefs is thicker than the leeward reefs because windward reefs are composed of much faster growing species.

FUTURE PLANS

Both recovery and deterioration of Culebra's reefs can be quantitatively monitored in the future at three strategic sites. At each of three sites, 13 numbered, 3/4-inch-diameter stainless steel stakes were driven and cemented into the reef. The stakes are spaced 10 m apart and arranged to form two 60-m-long transects. These transects share a central stake and are arranged at 90° to form a cross. A 3/8-inch-diameter line, marked each meter with bright red tape, was stretched between the stakes and all the corals beneath the line were recorded with continuous underwater video. The lines can be quickly attached in the future and the transects photographed or documented with video for comparison with the original images. A vertical photograph was also taken at each stake using the stake as the center of the photograph. Each vertical photograph was taken with north at the top and contains a location number in the view. Photographs were taken exactly 3 m from the bottom to insure uniformity of scale and to allow quantification and comparison of future changes.

These data are stored at the USGS office in St. Petersburg, Florida.

The three monitoring stations (locations of stations C, D, and E are shown in Figure 1) were selected to show changes on a windward *Acropora* reef, a leeward *Monastraea* reef and a suspected polluted reef off the south shore near the canal that runs through the village of Culebra. The location of the central stake at each site was determined by taking three to four compass bearings on permanent island features. The suspected polluted site is located just south of the town and directly off the artificial channel that drains Ensenada Honda lagoon.

The lagoon, a classic cul de sac, receives both treated and untreated sewage and other wastes generated by the surrounding human and animal population. This site was selected because it was observed to be bathed in murky water at low tide when lagoon waters flow southward from the western mouth of the canal. Corals at this site were less abundant and pale in color. Abundant fleshy algal growth at this site suggests nutrient enrichment, probably from lagoon water emanating from the canal. Future monitoring of all three sites should be sufficient to determine the general health and well being of coral reefs around Culebra.

Fig.1. Map of Isla de Culebra showing areas examined by divers, location of monitoring stations C, D, and E, and the three deep cores taken with a diver-operated hydraulic coring device. Prevailing easterly trade winds tend to push water into Ensenada Honda lagoon, causing flow of water through the artificial canal (located near the town) and toward monitoring station D.

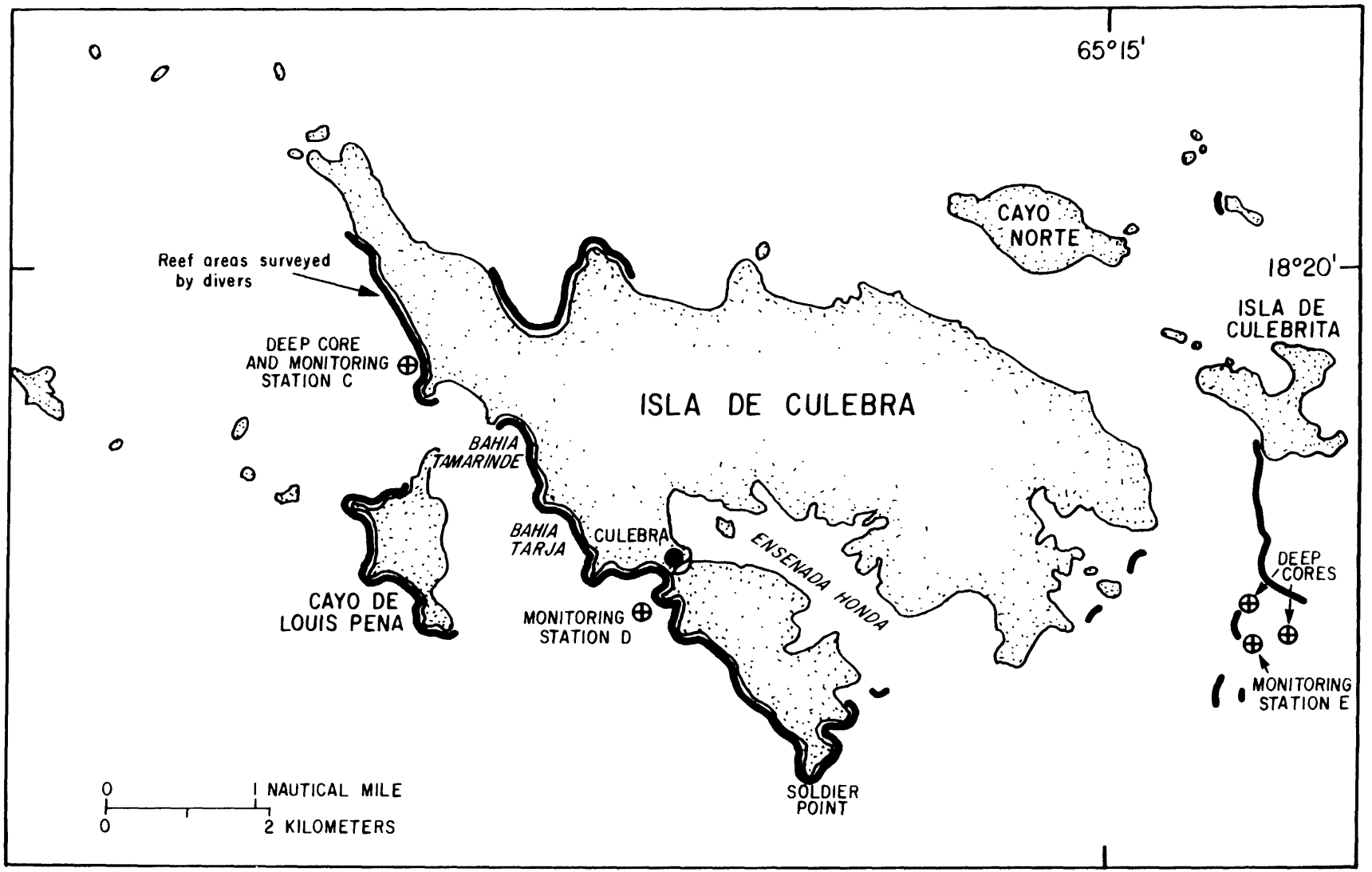
65°15'
18°20'
CAYO NORTE
ISLA DE CULEBRITA
Reef areas surveyed by divers
DEEP CORE AND MONITORING STATION C
ISLA DE CULEBRA
BAHIA TAMARINDE
BAHIA TARJA
CULEBRA
ENSENADA HONDA
CAYO DE LOUIS PENA
MONITORING STATION D
DEEP CORES
MONITORING STATION E
SOLDIER POINT
0 1 NAUTICAL MILE
0 2 KILOMETERS

Fig. 2. Typical underwater views of damage to the principal reef building coral *Acropora palmata* on the east side of Culebra near station E (Fig. 1). All of these dead corals have been coated with encrusting algae.

Fig. 3. Overturned Pillar coral, *Dendrogyra cylindrus* on the windward side of Culebra near station E (Fig. 1). This species is less common on the leeward side of the island near station C. Note upward directed knobs. Similar-sized growth knobs were observed on all overturned colonies. Amount of new growth is consistent with the known growth rate and period of time since Hugo struck.

Fig. 4. (A) Healthy, unbroken colonies of *Porites porites* on the seaward (eastern side of Culebra. Here they form the underpinning of the *Acropora palmata*-capped. pinnacle reefs. Such reefs were absent on the western (leeward) side of Culebra (B) Gravel produced by breakage of *Porites porites* during Hurricane Hugo. Such scenes were present on numerous reefs east of Culebra and on the reefs along the south side of Esenada Honda.

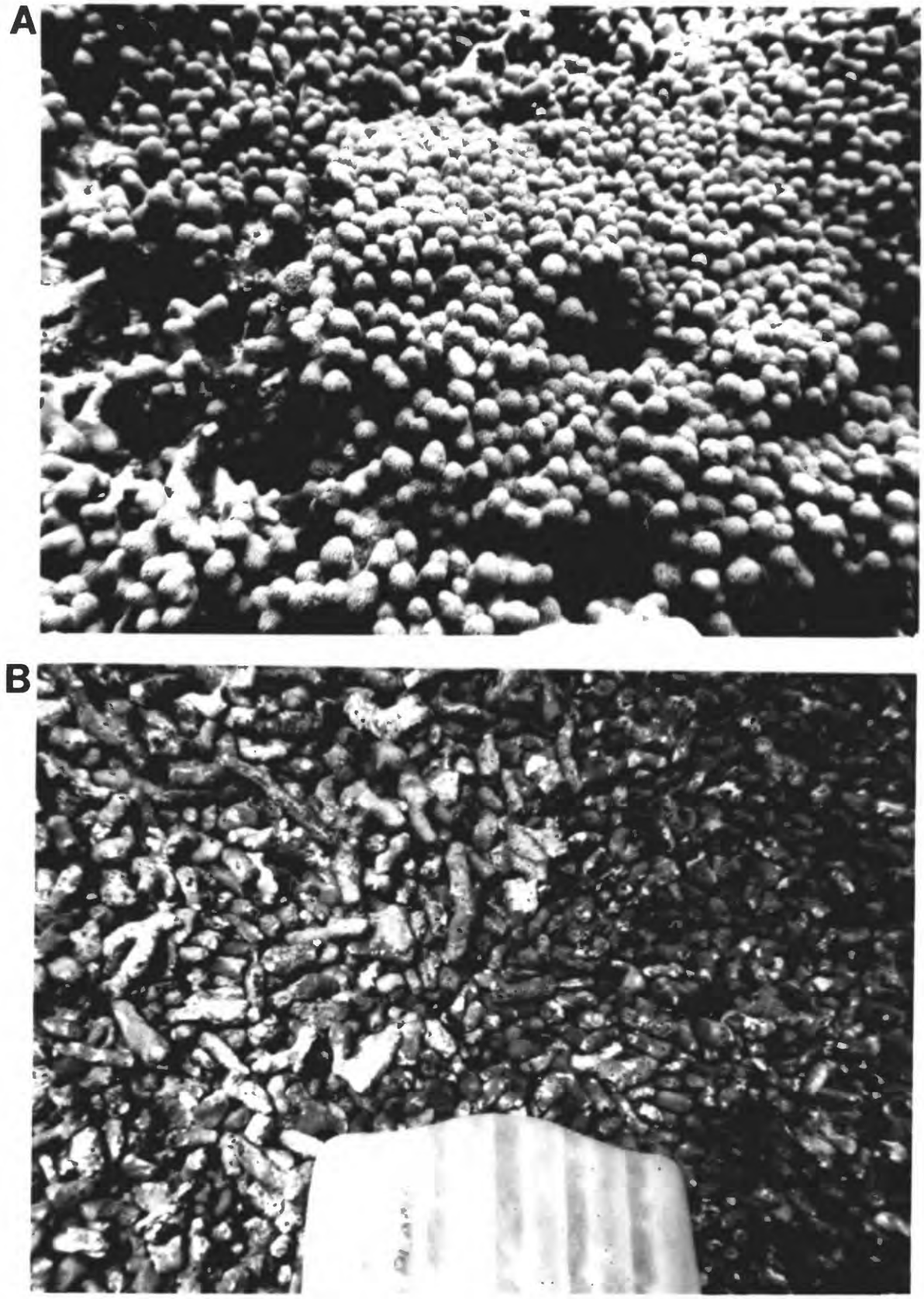
A
B

Fig. 5. Views of back reef "overwash" of *Porites porites* and *Acropora cervicornis* gravel covering live *Montastrea annularis* heads. These photographs were taken on the back side of a reef, northwest of station E (Fig. 1). Similar observations were made on the leeward side of all the north-south oriented linear reefs on the east side of Culebra.

Fig. 6. Broken columns of the head coral *Montastrea annularis* from the west side of Culebra near station D (Fig. 1). Notice that tips of columns are living.

Fig. 7. X-radiograph of a slab cut from tip of a broken *Montastrea annularis* column as shown in Figure 6 collected at station C (Fig. 1). Annual growth bands in upward directed growth suggests that the column was broken and became horizontal at the time of Hurricane Hugo. Similar upward growth was seen on nearly all broken *Montastrea annularis* heads.

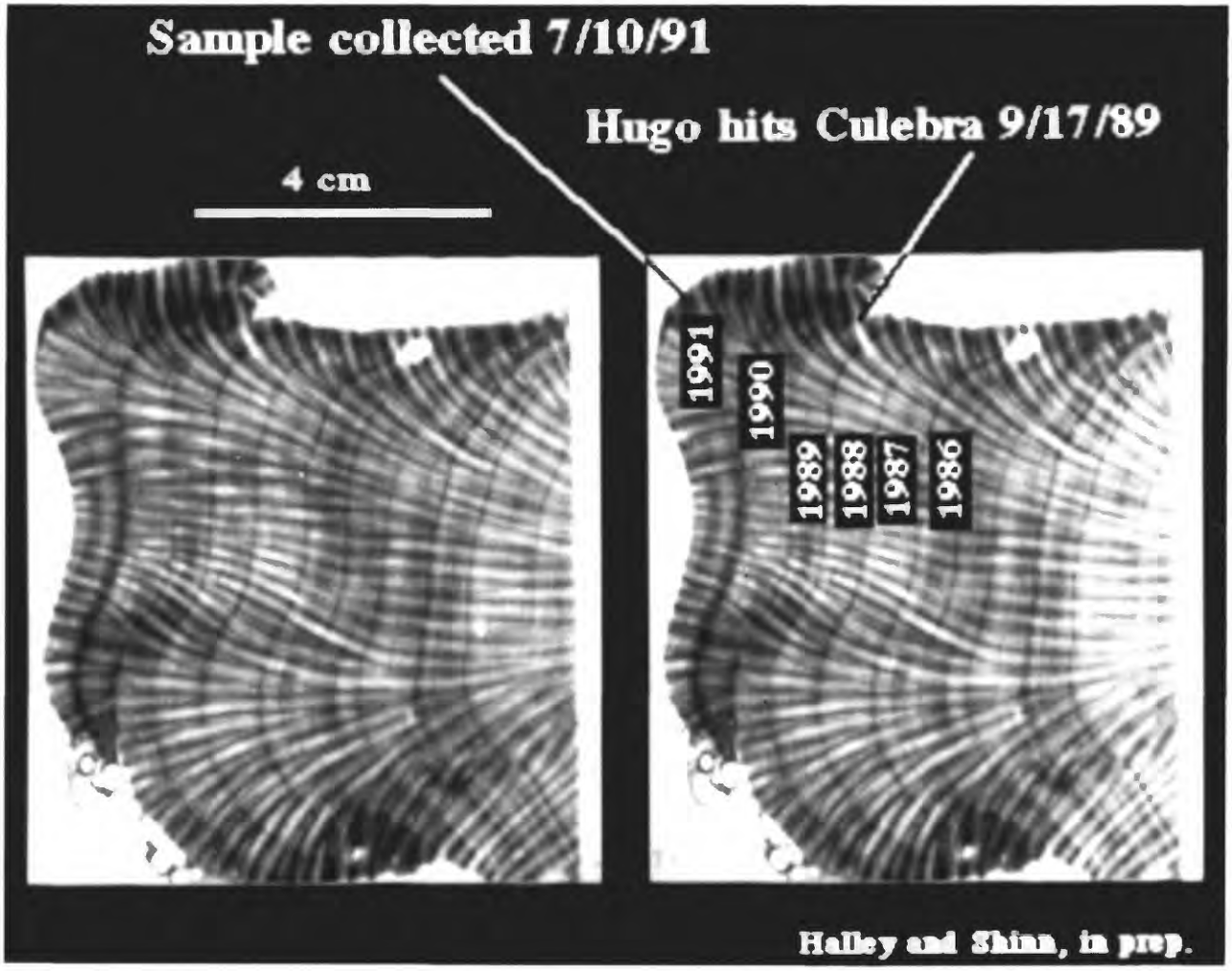
Sample collected 7/10/91
Hugo hits Culebra 9/17/89
4 cm
1991
1990
1989
1988
1987
1986
Halley and Shinn, in prep.

Fig. 8. Histograms of coral height or diameter measurements made near station E (Fig. 1). Most colonies were growing on fragments of larger corals killed by Hurricane Hugo. Amount of growth for (A) *Acropora cervicornis*, (B) the encrusting coral *Porites astreoides*, (C) the hydrocoral *Millepora* sp., and (D) *Acropora palmata* is consistent with published rates and the 22-month period since Hurricane Hugo. These data confirm that colonies post-date Hurricane Hugo and lend support to our contention that the dead corals on which they are growing were killed by Hugo. Only the maximum diameter was measured for the irregular low-profile encrusting coral *Porites astreoides*.

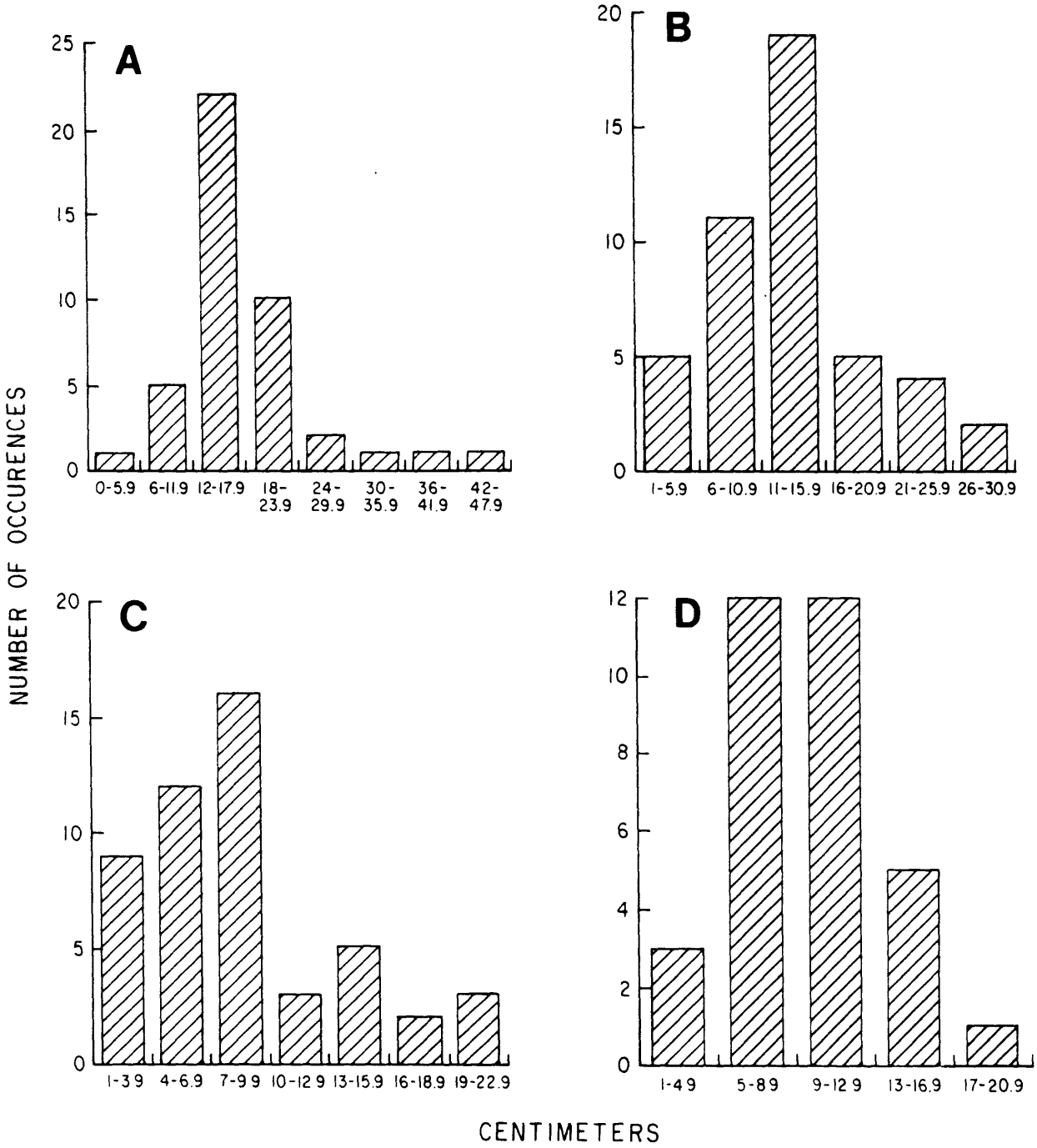
A
B
C
D
NUMBER OF OCCURENCES
CENTIMETERS
0-5.9
6-11.9
12-17.9
18-23.9
24-29.9
30-35.9
36-41.9
42-47.9
1-5.9
6-10.9
11-15.9
16-20.9
21-25.9
26-30.9
1-3.9
4-6.9
7-9.9
10-12.9
13-15.9
16-18.9
19-22.9
1-4.9
5-8.9
9-12.9
13-16.9
17-20.9

ACKNOWLEDGEMENTS

The success of this program is based on the broad range of technical support provided by the USGS Puerto Rico Marine Geology Program. The Program for the Study of Developed Shorelines directed by Orrin H. Pilkey, Duke University provided additional support. Richard Webb initiated the beach profile monitoring program in the San Juan area and was instrumental in the initial phases of this project. He also kindly provided access to the early profile data and is gratefully acknowledged for his support. The training of technical support personnel in state-of-art beach surveying techniques and data reduction was conducted by Thomas Reiss and Roberto Anima. Navigation support of offshore surveys was provided by Barry Irwin, electronics support was provided by Ken Parolski, and diver assistance was provided by Dann Blackwood. All illustrations were prepared by Jeff Zwinakis and Dann Blackwood. In addition, we appreciate the cooperation of the captain and crew of the research vessel JEAN A, provided by the Department of Natural Resources, Commonwealth of Puerto Rico. Funding for this program was provided by the office of the U.S. Secretary of the Interior, the Honorable Manuel Lujan.

REFERENCES CITED

Brennan, J.W., 1991, Meteorological summary of Hurricane Hugo: Journal of Coastal Research, Special Issue No. 8, p. 1-12.

Bush, D.M., 1991, Impact of Hurricane Hugo on the rocky coast of Puerto Rico: Journal of Coastal Research, Special Issue No. 8, p. 46-69.

Cacchione, D.A., Drake, D.E., Grant, W.D., Tate, G.B., 1984, Rippled scour depressions on the inner continental shelf off central California: Journal of Sedimentary Petrology, v. 54, P. 1280-1291.

Chavez, P.S., 1980, Automated shading correction and speckle noise removal mapping techniques for radar image data: Radar Geology, An Assessment, Jet Propulsion Laboratory Publication 80-61, p. 251-264.

Chavez, P.S., 1986, Processing techniques for digital sonar images from GLORIA: Photogrammetric Engineering and Remote Sensing, v. 52, p. 1133-1145.

Corson, S.D., Resio, D.T., Brooks, R.M., Ebersole, B.A., Jensen, R.E., Ragsdale, D.S., and Tracy, B.A., 1981, Atlantic coast hindcast, deepwater, significant wave information: U.S. Army Corp of Engineers Waterways Experiment Station, WIS Report 2.

Danforth, W.W., O'Brien, T.F., and Schwab, W.C., 1991, USGS image processing system: Near real-time mosaicking of high-resolution side scan SONAR data: Sea Technology, v. 32, p. 54-59.

Danforth, W.W., and Thieler, E.R., 1992a, Digital Shoreline Mapping System (DSMS) user's guide, version 1.0: U.S. Geological Survey Open File-Report 92-240, 33 p.

Danforth, W.W., and Thieler, E.R., 1992b, Digital Shoreline Analysis System (DSAS) users guide, version 1.0: U.S. Geological Survey Open-File Report 92-355, 41 p.

Dean, R.G., 1991, Equilibrium beach profiles: characteristics and applications: Journal of Coastal Research, v. 7, p. 53-84.

Dolan, Robert, Fenster, M.S., and Holme, S.J., 1991, Temporal analysis of shoreline recession and accretion: Journal of Coastal Research, v. 7, no. 3, p. 723-744.

Dolan, Robert, Hayden, B.A., and Heywood, J.A., 1978, A new photogrammetric method for determining shoreline erosion: Coastal Engineering, v. 2, p. 21-39.

Edmunds, P.J., and Witman, J.D., 1991, Effect of Hurricane Hugo on the primary framework of a reef along the south shore of St. John, U.S. Virgin Islands: Marine Ecology Progress Series, v. 78, p. 201-204.

EEZ-SCAN 85 Scientific Staff, 1987, Atlas of the U.S. Exclusive Economic Zone, Gulf of Mexico and eastern Caribbean areas: U.S. Geological Survey Miscellaneous Investigation I-1864-A, 104 p.

Elassal, A.A., and Malhotra, R.C., 1987, General Integrated Analytical Triangulation program (GIANT) user's guide: Rockville, Maryland, NOAA Technical Report NOS 126 CGS 11, 66 p.

Evenden, G.I., 1990, Cartographic projection procedures for the UNIX-environment - a users manual: U.S. Geological Survey Open-File Report 90-284, 63 p.

Evenden, G.I., 1991, Notes on a method to transform digitized coordinates to geographic coordinates: U.S. Geological Survey Open-File Report 91-17, 5 p.

FEMA (FEDERAL EMERGENCY MANAGEMENT AGENCY), 1989, Hazard mitigation opportunities in Puerto Rico: Interagency Hazard Mitigation Report, FEMA-DR-

842-PR, October 1989, 28 p.
Golden, J.H., 1990, Meteorological data from Hurricane Hugo: Proceedings, 22nd Joint UJNR Panel Meeting-Wind and Seismic Effects, May 14-18, 1990.
Grove, K.A., and Trumbull, J.V.A., 1978, Surficial geologic maps and data on three potential offshore sand sources on the insular shelf of Puerto Rico: U.S. Geological Survey Miscellaneous Field Studies Map MF-1017.
Hubbard, D.K., Parsons, K.M., Bythell, J.C., and Walker, N.D., 1991, The effects of Hurricane Hugo on reefs and associated environments of St. Croix, U.S. Virgin Islands — a preliminary assessment: Journal of Coastal Research Special Issue No. 8, p. 33-48.
Johnson, H.P., and Helferty, Maryann, 1990, The geological interpretation of side-scan sonar: Reviews of Geophysics, v. 28, no. 4, p 381-389.
Kaye, C.A., 1959, Shoreline features and Quaternary shoreline changes, Puerto Rico: U.S. Geological Survey Professional Paper 317-B, p. 49-140.
Knowlton, N.A., Land, J.C., Rooney, M.C., Clifford, P., 1981, Evidence for delayed mortality in hurricane-damaged Jamaican staghorn corals: Nature, v. 294, p. 251.
Knowlton, N.A., Weil, E.A., Weight, L.A., and Gusman, H.M., 1992, Sibling species in *Montastrea annularis*, coral bleaching, and the coral climate record: Science, v. 255, p. 330-333.
Leatherman, S.P., 1983, Shoreline mapping: a comparison of techniques: Shore and Beach, v. 51, no. 7, p. 28-33.
Leatherman, S.P., and Clow, J.B., 1983, UMD shoreline mapping project: IEEE Geoscience and Remote Sensing Society Newsletter, v. 22, p. 5-8.
Lessios, H.A., Robertson, D.R., and Cubit, J.D., 1984, Spread of *Diadema* mass mortalities through the Caribbean: Science, v. 226, p. 335-337.
Malinverno, A., Edwards, M., and Ryan, W.B.F., 1990, Processing of SeaMARC swath sonar data: IEEE (Institute of Electrical and Electronic Engineers) Journal of Oceanic Engineering, v. 15, p. 14-23.
McBride, R.A., 1989, Accurate computer mapping of coastal change: Bayou Lafourche shoreline, Louisiana, USA, in Magoon, O.T., ed., Coastal Zone '89, New York, ASCE, p. 707-719.
Monroe, W.H., 1977, Geologic map of the Carolina Quadrangle, Puerto Rico: U.S. Geological Survey Miscellaneous Investigation Series, Map I-1054, scale 1:20,000.
NOAA (NATIONAL OCEANIC AND ATMOSPHERIC ADMINISTRATION), 1989, Hurricane Hugo, effects on water levels and storm surge recorded at NOAA/National Ocean Service Water Level Stations: Unpublished Data Report.
NOAA (NATIONAL OCEANIC AND ATMOSPHERIC ADMINISTRATION), 1990, Hurricane Hugo, September 10-22, 1989, Natural disaster survey report: U.S. Department of Commerce, National Oceanic and Atmospheric Administration, National Weather Service, SIlver Springs, MD, 61 p.
NRC (NATIONAL RESEARCH COUNCIL), 1990, Managing coastal erosion: National Academy Press, Washington. D.C., 182 p.
Pease, M.H., and Monroe, W.H., 1977, Geologic map of the San Juan Quadrangle, Puerto Rico: U.S. Geological Survey Miscellaneous Investigations Series, Map I-1010, scale 1:20,000.
Pilkey, O.H., Bush, D.M., and Rodriguez, R.W., 1987, Bottom sediment types of the northern insular shelf of Puerto Rico: Punta Penon to Punta Salinas: U.S.

Geological Survey Miscellaneous Investigations Map I-1861.
Poppe, L.J., Eliason, A.H., and Fredricks, J.J., 1985, APSAS—an automated particle size analysis system: U.S. Geological Survey Circular 963, p. 1-77.
Reed, T.B., and Hussong, D., 1989, Digital image processing techniques for enhancement and classification of SeaMARC II side scan sonar imagery. Journal of Geophysical Research, v. 94, p. 7469-7490.
Rodriguez, R.W., 1979, Origin, evolution and morphology of the shoal Escollo de Arenas, Vieques, Puerto Rico, and its potential as a sand resource: Unpublished Masters thesis, University of North Carolina at Chapel Hill, 71 p.
Rodriguez, R.W., and Trias, J.L., 1989, Map showing characteristics of the Escollo de Arenas sand and gravel deposit, Vieques island, Puerto Rico: U.S. Geological Survey Miscellaneous Field Studies Map MF-2108.
Rodriguez, R.W., and Webb, R.M.T., and Bush, D.M., 1993, Impact of hurricane Hugo on Coastal Resources of Puerto Rico: Journal of Coastal Research (in press).
Rodriguez, R.W., Webb, R.M.T., Bush, D.M., and Scanlon, K.M., 1992, Marine geologic map of the north insular shelf of Puerto Rico: Rio Bayamon to Rio Grande de Loiza: U.S. Geological Survey Miscellaneous Investigation Map (in press).
Rodgers, C.S., McLain, L.N., and Tobias, C.R., 1990, Effects of Hurricane Hugo (1989) on a coral reef in St. John, USVI: unpublished report to Virgin Islands National Park.
Schwab, W.C., Danforth, W.W., Scanlon, K.M., and Masson, D.G., 1991, A giant submarine slope failure on the northern insular slope of Puerto Rico: Marine Geology, v. 96, p. 237-246.
Shinn, E.A., 1976, Coral reef recovery in Florida and the Persian Gulf: Environmental Geology, v. 1, p. 241-254.
Stafford, D.B., and Langfelder, J.A., 1971, Air photo survey of coastal erosion: Photogrammetric Engineering, v. 37, p. 565-575.
Sykes, L.R., McCan, W.R., and Kafka, A.L., 1982, Motion of the Caribbean plate during the last 7 million years and implications for earlier Cenozoic movements: Journal of Geophysical Research, v. 87, p. 10656-10676.
Trias, J.L., 1990, Maps showing characteristics of the Isabela offshore sand deposit, northwestern Puerto Rico: U.S. Geological Survey Miscellaneous Field Studies Map, MF-2136.
Trias, J.L., and Carlo, Milton, 1992, Description of 19 beach profile stations along the San Juan Metropolitan area, Puerto Rico: Presentation of preliminary data, February 1991 to January 1992: U.S. Geological Survey Open-File Report 92-347, 70 p.